1-2016

Size and chemistry selective membranes from block polymer templates

Ryan A. Mulvenna
Purdue University

Graduate School Form
30 Updated 12/26/2015

PURDUE UNIVERSITY
GRADUATE SCHOOL
Thesis/Dissertation Acceptance

This is to certify that the thesis/dissertation prepared

By Ryan Andrew Mulvenna

Entitled
SIZE AND CHEMISTRY SELECTIVE MEMBRANES FROM BLOCK POLYMER TEMPLATES

For the degree of Doctor of Philosophy

Is approved by the final examining committee:

Byan W. Boudouris
Chair

William A. Phillip

You-Yeon Won

Michael Harris

To the best of my knowledge and as understood by the student in the Thesis/Dissertation Agreement, Publication Delay, and Certification Disclaimer (Graduate School Form 32), this thesis/dissertation adheres to the provisions of Purdue University's "Policy of Integrity in Research" and the use of copyright material.

Approved by Major Professor(s): Byan W. Boudouris

Approved by: John Morgan 1/26/2016
Head of the Departmental Graduate Program Date

SIZE AND CHEMISTRY SELECTIVE MEMBRANES FROM BLOCK POLYMER TEMPLATES

A Dissertation

Submitted to the Faculty

of

Purdue University

by

Ryan A. Mulvenna

In Partial Fulfillment of the

Requirements for the Degree

of

Doctor of Philosophy

May 2016

Purdue University

West Lafayette, Indiana

"To those who I have lost, and to those who I love..."

ACKNOWLEDGEMENTS

I would like to deeply thank my advisor, Professor Bryan Boudouris for his steady hand and his involvement in my development. You demonstrate what it takes to be successful every day. I hope to emulate this upon my graduation. I thank you deeply for your training and your sound counsel when I have needed it the most.

I would like to also thank Professor James Litster for his help in getting me to Purdue, as well as your counsel. I am eternally grateful that you got me here for this once in a lifetime experience. Thank you. All the best for your travels to the UK, mate.

Next I would like to thank Lizbeth Rostro (Ph.D.) and Aditya Baradwaj (soon to be Ph.D.) for being one of the 'first three' with me. I could not have asked anyone better to work with in the lab startup environment, and I truly wish you all the best with your future endeavors.

I would like to next especially thank the Notre Dame WATER team (Prof. Bill Phillip, Jacob Weidman, and Chris Zhang) for being a wonderful and productive team with us. We could not have done this without you, and I hope we still continue to surge forward with our collaboration far into the future!

I would also like to thank Rafael Prato for your help and friendship when you were in the POWER lab. I was sad to see you go, but I hope your travels to Europe get you to where you want to be in life. You deserve it.

Thank you also Dr. Steve Gaik for your presence in the POWER lab. Our group really needed a senior research figure in our fledgling lab. You were a great mentor and example of professionalism, and a role model. Thank you for all of you help.

For all of those that I have mentored, thank you for your help! Thank you Sara Berger, Ryan Pitzer, and especially Alec Bokhart and Christian White. It was wonderful to work with you two in the Bindley, and I had a smile on my face everyday because of it!

I would also like to say thank you to Prof. Cliff Johnston and Prof Hilka Kentämaa for diversifying my skillset to enhanced oil recovery. It has been a very pleasant experience. I would also like to especially thank Dr. Rituraj Borgohain and Dr. Barbara Cohen for their camaraderie, help, and friendship while working in Bindley.

Jessica, Holly, Seung, Adam, Ned, Martha, Jenny and Darby: thank you for your time and camaraderie in the POWER lab over these past several years! We have formed a great team.

I would like to say a humongous thank you for my family. The past few years have been difficult over such an enormous distance, but thank you for your love and support Mum and Dad and I am looking forward to seeing you both again soon!

Last, but certainly not the least, is Amber. Thank you for being my rock over these past few years. I quite figuratively would not have been here now without you. Thank you for tolerating me when I have been late or I've had late nights. I would not and could not have done this without you, and words cannot show you how lucky I am to have you.

TABLE OF CONTENTS

Page

Page

Page

LIST OF TABLES

LIST OF FIGURES

Figure Page

LIST OF SCHEMES

ABSTRACT

Mulvenna, Ryan A. Ph.D., Purdue University, May 2016. Size and Chemistry Selective Membranes from Block Polymer Templates. Major Professor: Bryan Boudouris.

The use of block polymers continues to gain attention with their myriad applications in industry for advanced applications in biology, medicine, electronics, and separations. The ability of block polymers to self assemble into ordered states on the nanometer level makes these materials suitable for applications that mandate structural order on this scale. By tuning the chemistry of these block domains, we may explore their utilization for advanced separations.

In this dossier, we detail the efforts into the controlled radical polymerization of polyisoprene-*b*-polystyrene-*b*-poly(*N*,*N*-dimethylacrylamide) (PI-PS-PDMA) via. a facile reversible addition-fragmentation chain transfer (RAFT) mechanism. For this high molecular weight block polymer synthesis, it was experimentally established that rate retardation occurred during the addition of the PS and PDMA domains. Utilizing *ab initio* methods, it was determined that this rate retardation may be attributed to slow intermediate radical termination.

Utilizing a scalable self-assembly and non-solvent induced phase separation (SNIPS) technique, casting a solution of PI-PS-PDMA as a convectively drying thin film before quenching in water affords an anisotropic, size-selective membrane template.

Scanning electron microscopy imaging of these films yielded a pore density on the order of 10^{13} pores m^{-2} with pore sizes down to less than 1 nm, pushing the observed limits of size separation observed using block polymer membranes.

Upon fashioning PI-PS-PDMA into membrane devices, the PDMA interior may be deprotected to a polyacrylic acid (PAA) functionality. Facile amidation chemistry of these deprotected PI-PS-P(Acrylate) templates to PI-PS-PAA membranes demonstrates these devices are versatile in their tunable capacity for size and chemistry separation of target analytes (*e.g.*, small molecules and heavy metal salts).

By incorporation of acrylate block chemistries into a PI-PS support, the potential for low pore sizes for separation of salts and small molecules using block polymers are possible. By integrating the tunable block polymer chemistry to enable chemical tuning of pores, precise chemo-selective control may be made for targeted elution of analytes and fouling resistant membranes for advanced reverse osmosis (RO) and small molecule purification for application in industry.

CHAPTER 1. INTRODUCTION

The first instance of the syntheses of block polymers was reported by Szwarc in 1956.[1, 2] Utilizing anionic polymerization, new classes of solvent and melt processable block polymers (*e.g.* polystyrene-*b*-polybutadiene-*b*-polystyrene (SBS) and polystyrene-*b*-polyisoprene-*b*-polystyrene (SIS)) thermoplastic elastomers quickly garnered impact in the chemical and materials industry as a facile mechanical and processable substitute for natural rubber. By utilizing the nanostructured ordering of block polymers from the melt and/or solution state, one such recent application of block polymers are in their use as separation devices. In the seminal work by Peinemann,[3] block polymer membranes of anionically synthesized polystyrene-*b*-poly(4-vinyl pyridine) (SV) were established as highly size selective membranes for targeted filtration applications.[4] Their anisotropic, high-flux architecture consists of pore walls lined with the poly(4-vinyl pyridine) moiety were subsequently demonstrated in both the diblock polymer (SV) and triblock polymer polyisoprene-*b*-polystyrene-*b*-poly(4-vinyl pyridine) (ISV) membrane system. However, their use to facilitate (sub)nanometer size and chemistry selective separations are limited by their poor mechanical strength and pore functionalization chemistry of poly(4-vinyl pyridine).

Over the course of these last few decades, alternate polymerization techniques for creating different block polymer chemistries has greatly expanded. With the advent of nitroxide mediated polymerization in the 1970's and 1980's,[5, 6] as well as the advent of

atom-transfer radical polymerization (ATRP)[7] in 1995 and reversible addition-fragmentation chain transfer (RAFT)[8] polymerization in 1998, new facile routes of block polymer synthesis have become available. With such facile chemistry available, different polymer chemistries may be created to create mechanically robust materials with facile tunable chemistry for size as well as chemistry targeted separation of analytes.

1.1 Thesis Overview

The motivation for this work focuses on creating new facily synthesized block polymer materials as architectures for size as well as chemistry specific separation. This work will focus on synthesizing, characterizing, and determining the structure-property relationships for chemically tunable block polymer materials for anisotropic membranes. The incorporation of a mechanically robust thermoplastic polyisoprene-*b*-polystyrene (IS) backbone. Combined with a chemically tunable block (polyacrylate), the triblock polymers polyisoprene-*b*-polystyrene-*b*-polyacrylate (ISAcrylate) are cast as films using the self-assembly and non-solvent induced phase separation (SNIPS) method. Upon fabrication of ISAcrylate membranes, facile deprotection of the polyacrylate pore wall lining to polyisoprene-*b*-polystyrene-*b*-poly(acrylic acid) (ISA) porous templates are made. Using carboxylic acid chemistry, the pore walls that consist of polyacrylic acid may be refunctionalized utilizing dicarbimmide (Steglich amidation)[9] chemistry to any desired functionality for selective screening, absorption or permeation of a target analyte.

Chapter 2 focuses on the current state of block polymers for application to membrane separation devices. Block polymerization techniques will be discussed, as well

as their application into creating block polymer membranes. The techniques and classes of membranes are discussed, as well as their formation mechanism.

Chapter 3 has been published as “Polymerization Rate Considerations for High Molecular Weight Polyisoprene-*b*-Polystyrene-*b*-Poly(*N*,*N*-dimethylacrylamide) Triblock Polymers Synthesized Via Sequential Reversible Addition-Fragmentation Chain Transfer (RAFT) Reactions", by Ryan A. Mulvenna, Rafael A. Prato, William A. Phillip, and Bryan W. Boudouris, *Macromol. Chem. Phys.* **2015**, *216*, 1831−1840. Here, a kinetic study of the synthesis of polyisoprene-*b*-polystyrene-*b*-poly(*N*,*N*-dimethylacrylamide) (PI-PS-PDMA) triblock polymers were performed to elucidate the reaction conditions necessary for block polymer membrane material candidates of total molecular weight (M_n) between $40 < M_n < 150$ kDa. During the course of the PS and PDMA block additions, it was found that rate retardation occurred during these syntheses steps. Utilizing *ab initio* methods, it was determined that this rate retardation may be attributed to slow intermediate radical termination to precisely predict and tune the block size and composition for viable (PI-PS-PDMA) block polymer membrane material candidate screening.

Chapter 4 has been published as “Tunable Nanoporous Membranes with Chemically-Tailored Pore Walls from Triblock Polymer Templates", by Ryan A. Mulvenna, Jacob L. Weidman, Benxin Jing, John A. Pople, Yingxi Zhu, Bryan W. Boudouris, and William A. Phillip, *J. Membr. Sci.* **2014,** *470*, 246–256. Here, a synthesized PI-PS-PDMA block polymer of ~ 70 kDa with a hexagonal close-packed (HCP) solid state geometry is cast using a non-solvent induced phase separation (SNIPS)

technique. The resulting anisotropic template consists of 10^{13} pores m^{-2}, which upon reaction of this template affords PAA lined pores with pore sizes down to less than 1 nm.

Chapter 5 relates to chemically tunable block polymer membranes for target analyte purification in collaboration with Jacob Weidman. This work establishes the chemical tunability of PI-PS-PAcrylates by refunctionalizing the deprotected polyacrylate wall from PAA using amidation chemistry. By selectively tuning the pore chemistry with a heteroatom group, greater control may be made in the selective elution and capture of a target analyte. More specifically, we look at the functionalization of a self-assembled and deprotected PI-PS-PAA template to a alcohol, thiol, and amine functionalities using a ethyl/phenyl amine linking group. The chemical tunability of the nanoporous template is subsequently demonstrated in preliminary adsorption testing with the highly selective adsorption of (heavy) metals (*i.e.*, copper and lead) over the adsorption of copper and magnesium in both homogenous and competitive adsorption testing.

Chapter 6 discusses to the synthesis and casting of block polymer membranes with facile deprotection chemistry for RO applications in collaboration with Jacob Weidman and Chris Zhang. This work builds upon previous studies into utilizing chemically tunable PI-PS-PDMA block polymer membranes by interchanging the active PDMA domain for a polyacrylate protecting group that is labile under milder deprotection conditions. The milder deprotection conditions enables parent block polymers of lower molecular weight (~ 40 - 60 kDa) to access lower pore sizes into the (sub) nanometer regime for separation of small molecules and salts for high performance RO applications without degradation under harsher, high temperature conditions.

Chapter 7 contains ongoing and future work concerning novel block polymer material architectures. Specifically, incorporation of chemistry selective block polymer membrane architectures into multi-component separation networks, as well as new polymer architectures with a reactive thermoplastic support layer for functionalization into potential candidates for size, chemistry, and anti-fouling block polymer membrane templates.

1.2 References

1. Szwarc, M. *Nature* **1956**, 178, 1168.

2. Szwarc, M.; Levy, M.; Milkovich, R. *J. Am. Chem. Soc.* **1956**, 78, 2656.

3. Peinemann, K.-V.; Abetz, V.; Simon, P. F. W. *Nat. Mater.* **2007**, 6, 992.

4. Phillip, W. A.; Dorin, R. M.; Werner, J.; Hoek, E. M. V.; Wiesner, U.; Elimelech, M. *Nano Lett.* **2011**, 11, 2892.

5. D. H. Solomon; E. Rizzardo; Cacioli, P. *US patent 4,581,429*, **1986**.

6. Rizzardo, E.; Solomon, D. H. *Aust. J. Chem.* **2012**, 65, 945.

7. Wang, J.-S.; Matyjaszewski, K. *J. Am. Chem. Soc.* **1995**, 117, 5614.

8. Chiefari, J.; Chong, Y.; Ercole, F.; Krstina, J.; Jeffery, J.; Le, T. P.; Mayadunne, R. T.; Meijs, G. F.; Moad, C. L.; Moad, G. *Macromolecules* **1998**, 31, 5559.

9. Neises, B.; Steglich, W. *Angew. Chem., Int. Ed. Engl.* **1978**, 17, 522.

CHAPTER 2: BLOCK POLYMERS FOR MEMBRANES

2.1 Overview

In modern industry, efficient separation is the cornerstone for profitability of any product.[1] Of the variety of methods available for efficient separation, the use of membranes is an attractive option. Consisting on no moving parts, these low energy consuming, high reliability devices are a viable process alternative in the separation of a target compound.[1-4]

In industry, two size separation regimes are of particular interest. First, the ultrafiltration regime with separation scales on the order of 10 to 100 nm are of high import for separating macromolecules such as high value therapeutic proteins.[2] Second, the nanofiltration regime with separation scales on the order of 0.5 to 2 nm are size-selectively permeable to small molecules and salts for potential application to fine chemical purification and salt rejection.[1, 3-8] Membranes with nano and ultra pore sizes can be fabricated from a variety of different materials including inorganics, such as aluminum oxide or zeolites, and organic materials, including myriad polymers.[1] Composite membranes, which incorporate inorganic entities within polymeric matrices, also are explored commonly in the hopes of combining the selectivity of inorganic structures with the mechanical robustness of polymeric materials.[9, 10] However, the versatility and ease of processing[11] with polymeric systems is ideal for membrane fabrication.[1]

Two common processes used to fabricate porous polymeric membranes are: 1) phase separation techniques, which result in highly porous membranes, and 2) the high-energy bombardment of dense films to produce track-etched membranes that contain a low density of pores with a monodisperse size.[1, 4] Current UF and NF membranes are stymied from certain applications due to the tradeoff between high flux and high size selectivity and the deleterious effects of fouling.[12, 13]

The phase inversion (Loeb-Sourirjan)[14] class of membranes have distinct performance and fabrication advantages over other membrane architectures. Phase inversion membranes have a high-flux performance advantage due to their anisotropic architecture consisting of a thin selective surface layer of pores that taper into a macroporous 'gutter' support (Figures 2.1a and 2.1b). The tapered porous structure facilitates stymied size selectivity at a high permeate flux and low pressure drop.[14-19] The fabrication advantage of phase inversion membranes arises from its facile capacity for manufacturing by continuous casting of polymer film on a support before controlled drying and quenching create the anisotropic architecture for large scale fabrication (Figures 2.1b and 2.2).[1]

In contrast, track-etched membranes consisting of monolithic porous channels (Figure 2.1c) benefit from sharp values size/molecular weight cut-off (MWCO) for more precise-sized elutions. However, the monolithic structure suffers from low flux due to low pore area density. In addition, high pressure drops occur because of the monolithic pore shape across the membrane film, making this technique’s application to industry

limited.[20-22] As a result, there is a compromise of a commercial membranes performance between high size selectivity and high flux.[23, 24]

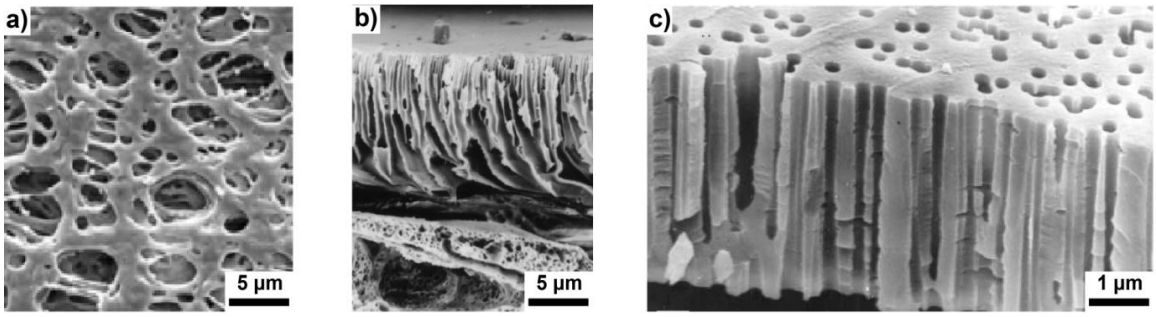

Figure 2.1. SEM images of membranes formed via. the phase inversion method of a polysulphone homopolymer from (a) top view and (b) side view perspective. (c) Profile picture of a monolithic etching a dense polycarbonate film with an Ar^{+} track creating cylindrical low dispersity pores.[20]

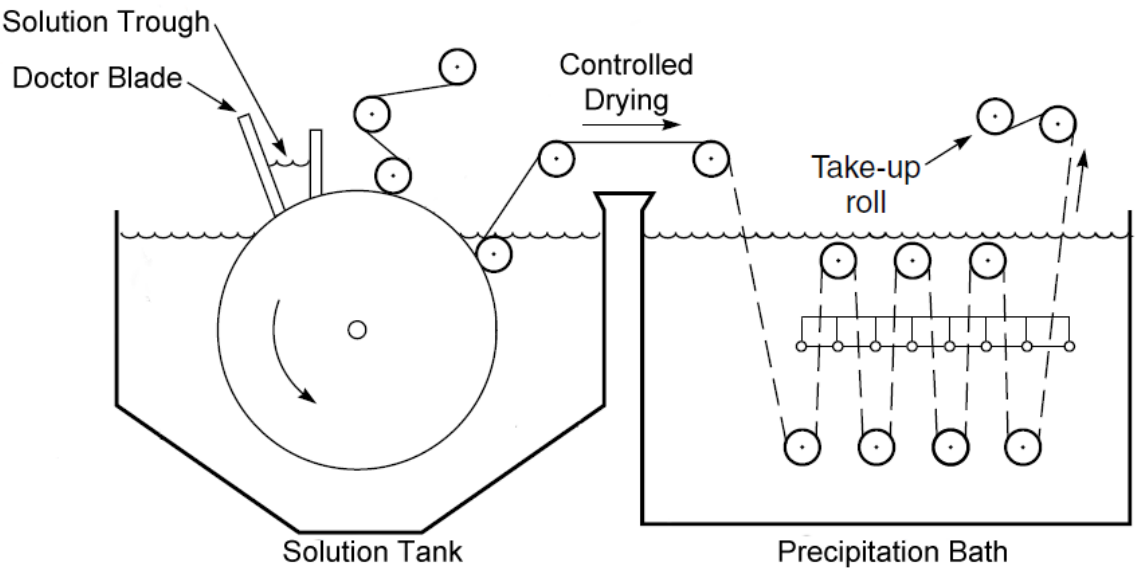

Figure 2.2. Schematic of the scalable method of continuous roll-to-roll fabrication of phase inversion membranes cast from a thin homopolymer solution film.[1] Reproduced from Figure 3.16 in Reference 1.

As a result of the random pore generation on the immediate surface, mixed homopolymer mixtures forming phase inversion membranes have distributed sizes of tapered pores. The limited chemistry of the polymers greatly restricts their ability for tailored separation. As such, generating architectures that have monodisperse pore sizes that retain high permeation flow rates while adding tailorable pore wall chemistry to increase fouling resistance or to perform chemically-selective separations is an attractive measure for advancing the utilization of membrane separation technology in industry.[25]

2.2 Block Polymer Self-Assembly

One such method to control the geometry of feature formation for polymers is to utilize the self-assembly properties of block polymers. Depending on the monomer(s) reactivity, stoichiometry, and reaction mechanism, a variety of polymer architectures are possible (Figure 2.3).[26-30]

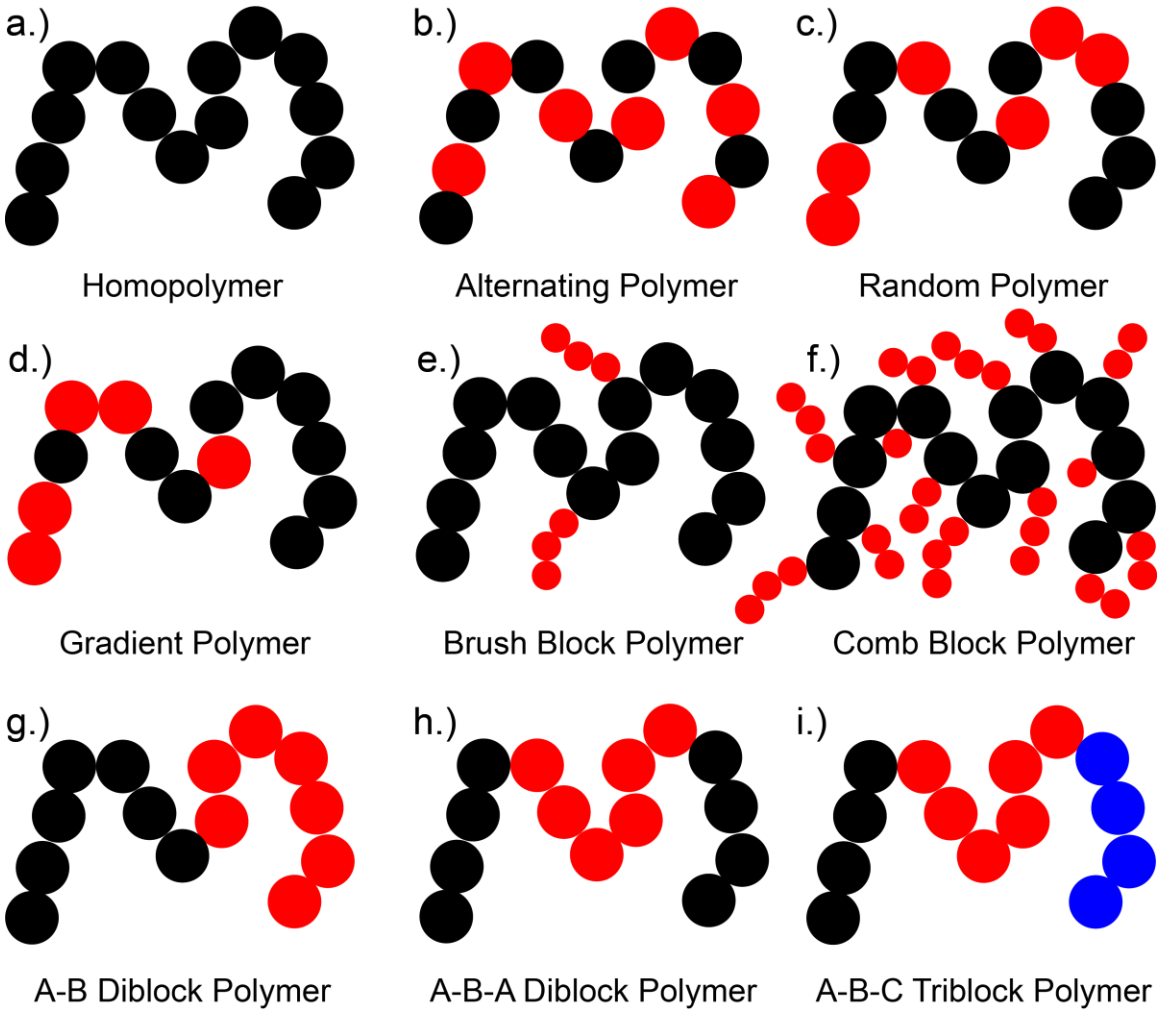

Figure 2.3. Schematic examples of common mixed linear (block) and grafted type polymers, where the black, red and blue represent chemically distinct units.

As shown in Figures 2.3g - 2.3i, by joining chemically-dissimilar polymer chain segments allows the individual intramolecular blocks are able to microphase separate into chemically distinct domains with length scales on the order of nanometers.[26-30] Microphase separation phenomenon in block polymers occurs due to the chemical dissimilarity between each of the chemically dissimilar domains when the polymer is labile in either a concentrated solution or in the melt state. This occurs as a result of thermodynamic minimization of its energy interaction between a chemically dissimilar intramolecular block. By modeling this thermodynamic phenomena using self-consistent field theory (SCFT),[31] creating an ordered structure at thermodynamic equilibrium in the melt state (Figure 2.4a). Similarly, intermolecular block interactions between neighboring block copolymers of similar size creates ordered repetition of nanostructure.[13,15-17,26, 32-37] Microphase separation can only occur if the product of the length of the block copolymer (N) and the chemical dissimilarity χ is sufficiently high at a given temperature (*i.e.* $\chi N \geq 10$). If χN is not sufficiently large, separation is incoherent, making the diblock system disordered in its spatial composition (Figure 2.4a).[38] As a constraint of the fractional volume (f) of the block(s) and the overall block size (N), a variety of ordered, micro-phase separated architectures with features on the order of nanometers are accessible (Figure 2.4b).[26]

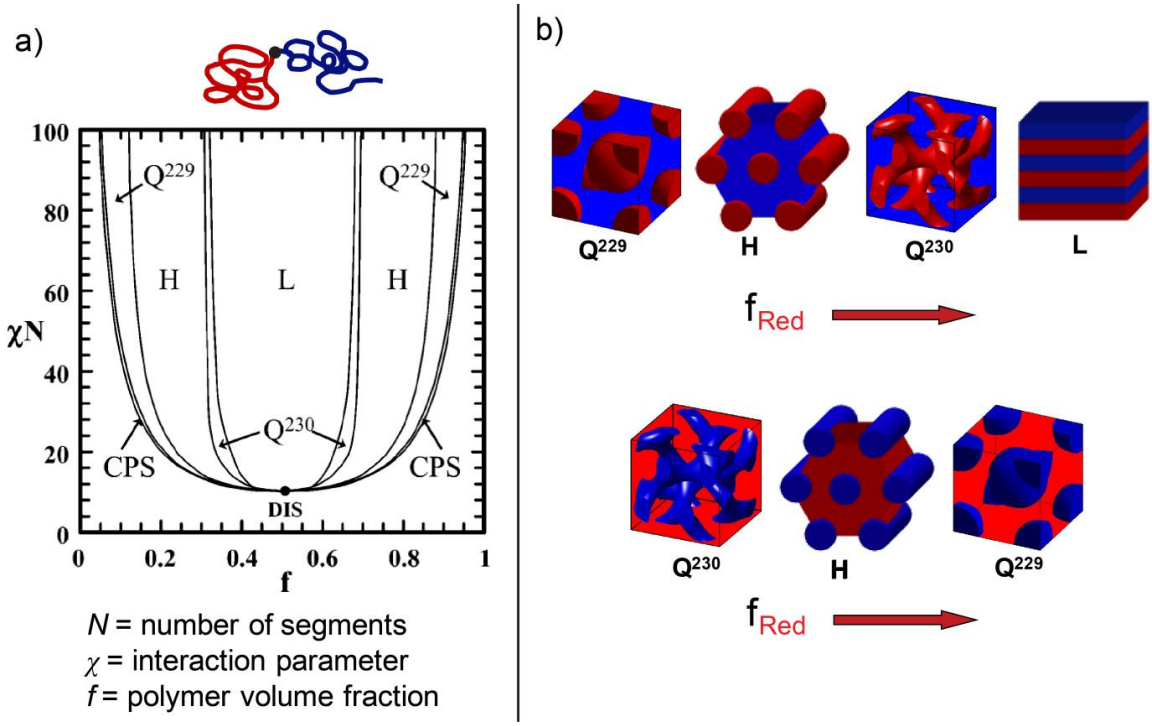

Figure 2.4. (a) Simulated microphase diagram of a linear diblock copolymer (the independent variable f denotes the fraction of the red phase). CPS represents close-packed (face centered cubic) spheres, Q^{229} represents body-centered spheres, H represents hexagonally close packed, Q^{230} represents the gyroid phase, and L represents lamellae.[39] (b) The microphase structure of the diblock system at a given χN. With increasing fraction of the red block (horizontally across (a)), the microstructure of the diblock changes.[27] Figures reproduced from Reference 26.

The aforementioned block polymer structures have also been observed experimentally in the solution and the solid state in predicted fashion by changing the fraction and the length of block polymer chain(s) in a variety of different block chemistry combinations.[40-43] By increasing the number of domains with different chemistries, a greater control of their physiochemical properties and self-assembled geometries may be made to enable increasingly advanced materials for myriad applications.[26, 27, 44]

2.3 Block Polymer Synthesis

The synthetic procedure for block polymer synthesis relies on a chain growth mechanism. To an activated initiator (Equation 2.1), a controlled addition of units creates a chain of length i (Equation 2.2). As a prerequisite for block polymerization, termination between two propagating chains (Equation 2.3) is required to be minimized to inhibit termination.

$$I \rightarrow I^* \qquad (2.1)$$

$$I^* + M \rightarrow IM^* \xrightarrow{M} IMM^* \rightarrow\rightarrow\rightarrow A_i^* \qquad (2.2)$$

$$A_i^* + A_j^* \rightarrow A_{i+j} \qquad (2.3)$$

Upon successful creation of the active chain A_i^* (Equation 2.2), the polymer chain with its reactive terminus may be 1) directly used in a one pot synthesis by addition of another monomer identity B to form a block polymer of A-B (*e.g.* anionic polymerization), or 2) the active chain A_i^* may be first isolated as a stable intermediate by cooling and purifying the reaction to yield A_i . From this, the polymer A_i may be used as a 'macroinitiator' in the presence of B to yield a A-B block polymer (*e.g*, controlled radical polymerizations such as NMP, ATRP, or RAFT).

As a result of minimizing chain termination, a low polymer chain dispersity, ($Đ$ < 1.2), of the blocks and the composite polymer are typically achieved. The value of $Đ$ is

the ratio of the second moment divided by the first moment of the mean molecular weight of the chain (Equation 2.4).

$$Đ = \frac{M_w}{M_n} = \frac{\sum_i x_i M_i^2}{\left(\sum_i x_i M_i\right)^2} \qquad (2.4)$$

In practice, the most common synthetic methods for block polymerization utilize either an ionic terminus intermediate from an organic/organometallic initiator (*e.g,*. anionic/cationic polymerization, Equation 2.5 and 2.6. respectively) or a radical terminus intermediate from a thermal/UV initiator (*i.e.*, NMP, ATRP, or RAFT, Equation 2.7).[35]

$$M - L \xrightarrow{A_n} \left[LA_{n-1}A^- \right] M^+ \xrightarrow{H^+} A_n \qquad (2.5)$$

$$R - X + MX \xrightarrow{A_n} \left[RA_{n-1}A^+ \right] X^- \xrightarrow{OH^-} A_n \qquad (2.6)$$

$$\begin{array}{ccccccc} & \xrightarrow{\Delta/UV} & & \xrightarrow{A_i} & & \xrightarrow{A_{n-i}} & \\ I & \rightarrow & I^\bullet & \rightarrow & A_i^\bullet & \leftrightarrow & A_n^\bullet \\ & & & & T\updownarrow & & T\updownarrow \\ & & & & A_i\mathrm{T} & & A_nT \end{array} \qquad (2.7)$$

In both the anionic and cationic methods (Equations 2.5 and 2.6), addition of another purified monomer in an inert solvent environment to the intermediate polymer ion complex will enable additional block addition to the anionic/cationic intermediate. To terminate the anionic/cationic polymerization, quenching with a Brønsted-Lowry acid or

base respectfully will terminate the reaction. For a controlled free radical polymerization, a reversible, degenerative chain transfer agent (T) is utilized during the course of chain propagation to inhibit undesirable side reactions between the radical termini (*i.e.*, via. homolytic recombination and chain transfer). To terminate the controlled polymerization, cooling the reaction mixture to recover the polymer with a stable and regenerable terminus is possible. The stable terminus (Figure 2.5) enables the product to be subsequently used as a macroinitiator in the presence of a radical source to enable chain extension and chemically dissimilar monomer addition for the facile generation of block polymers.

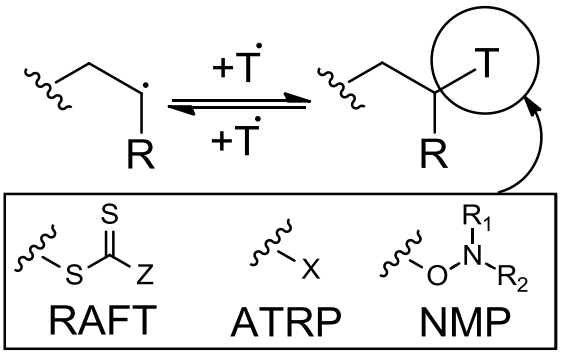

Figure 2.5. Generalized structures of commonly utilized radical termini (T) utilized in controlled radical polymerization. The RAFT polymerization method utilizes a thiocarbonylthio derivative (the Z group controls the stability of the conjugate thio-radical group),[45] the ATRP method utilizes a halogen in a reversible metal redox cycle,[46] and the NMP method utilizes a tertiary stabilized alkoxyamine[47] to enable controlled radical polymerization for low dispersity block polymer synthesis.

While both ionic and controlled free radical polymerization mechanisms are capable of generating block polymers with low *Đ*, the high reactivity of carbanions and carbocations make them particularly vulnerable to trace contamination. In addition, the charge propagating mechanism for chain growth makes the ionic site vulnerable to reaction with protic and electron withdrawing groups.[35, 48-51] In contrast, controlled radical polymerization mechanisms are significantly more tolerant to functional groups.[52, 53] As a result, block polymer architectures for advanced material applications with larger diversities of (tunable) chemical functionality may be synthesized.

2.4 Block Polymers for Membranes

One technique for templating ordered porous polymer structures is by the use of block polymers.[48, 54-56] Nanometer scale porous features in block polymers may be facilitated by casting from solvent and quenching in a non-solvent to generate porous films.[57-59] Alternatively, equilibrated self-assembled block polymer patterns may be used as a selective resist for etching monolithic structures.[60-62]

In the establishing work of this field, Peinemann[59] demonstrated that the self-assembly of block polymers from solution serve as a means to template the creation of isotropic sized pores for targeted size-selective anisotropic membrane templates. More specifically, by utilizing the existing phase inversion method to achieve an isotropic template,[14] a solution of a block polymer is cast as a thin film (Figure 2.6a). Controlled evaporation of the drying film creates a thin concentrated layer of polymer at the surface (Figure 2.6b). Appropriate selection of the solvent and evaporation time enables the

nucleation of lyophillic monolith domains (shown as blue blocks) at the incident surface (part 1 in Figure 2.6c). Arresting the self-assembly and vitrifying the structure by quenching into a non-solvent bath (part 2 in Figure 2.6c). sets the perpendicular lyophillic features. The subsequent exchange of the remaining casting solvent with the non-solvent bath causes the lypohillic features to contract, resulting in the creation of monolithic cylinders de-swell and contract, forming tapered pores (part 3 Figure 2.6c). For the film below the concentrated surface, (Figure 2.6d) the dilute block polymer solution undergoes macrophase separation with the non-solvent bath, creating a highly macroporous support layer. The resulting structure consists of tapered low dispersity sized pores selectively lined with a polymer block on anisotropic membrane support to facilitate a low hydraulic resistance for high permeation rate capacity. As a result of the self-assembly of block polymers from solution to template anisotropic architectures, this block polymer membrane casting method is referred to as a self-assembly and non-solvent induced phase separation (SNIPS) process.[35, 48-51, 63-66]

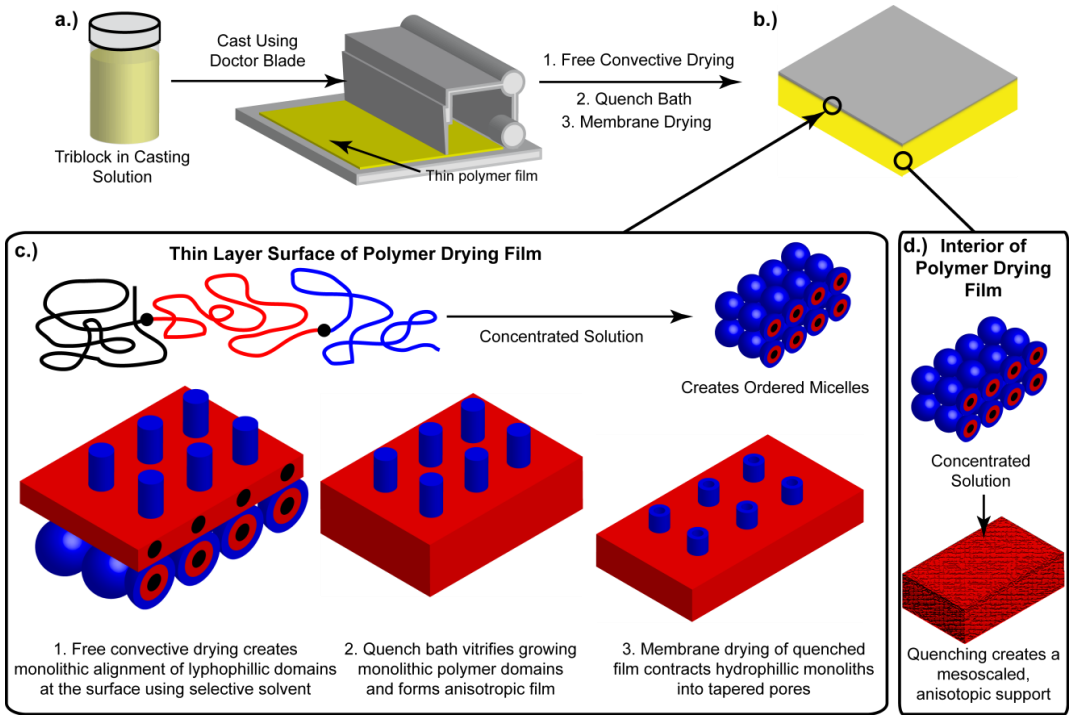

Figure 2.6. (a) SNIPS Casting of a block polymer selective solvent, the solution is cast as a thin sheet. (b) Controlled evaporation at the surface of the film is creates a thin concentrated layer of polymer at the surface. (c) An expanded view of the concentrated layer at the surface creating ordered micelles 1. Microphase separation templates the nucleation of perpendicular cylinders into the interior of the film during the drying process. 2. Perpendicular cylinder growth is halted by quenching the film. 3. Subsequent drying of the film contracts the monolithic block domains, creating a thin layer of low dispersity tapered pores. (d) During the casting process, the sudden quenching of film with the concentrated underlayer undergoes rapid macrophase separation, giving rise to the anisotropic membrane architecture.[63-66]

In the heavily-studied SNIPS process of utilizing polystyrene-*b*-poly(vinyl pyridine) (PS-PVP) and polyisoprene-*b*-polystyrene-*b*-poly(4-vinyl pyridine) (PI-PS-P4VP)[48, 57, 58, 67, 68] block polymers (Figure 2.7a), the tapered pore walls of the resulting membranes consist of the lyophillic PVP functionality when cast from solution of

dioxane and tetrahydrofuran (Figure 2.7b).[69] While the PVP amine is capable of functionalization, their tunable size and chemistry separation potential of this system is hindered due to the generation of the positive quaternary center (Figure 2.7c) with pore sizes restricted to greater than 7 nm.[64, 70, 71] In addition, the PI-PS-P4VP system relies on synthetically challenging anionically-controlled polymerization mechanisms that require cryogenic temperatures, *in situ* solvent exchange procedures, and stringent *non aura* conditions for successful synthesis on any scale.[52, 65]

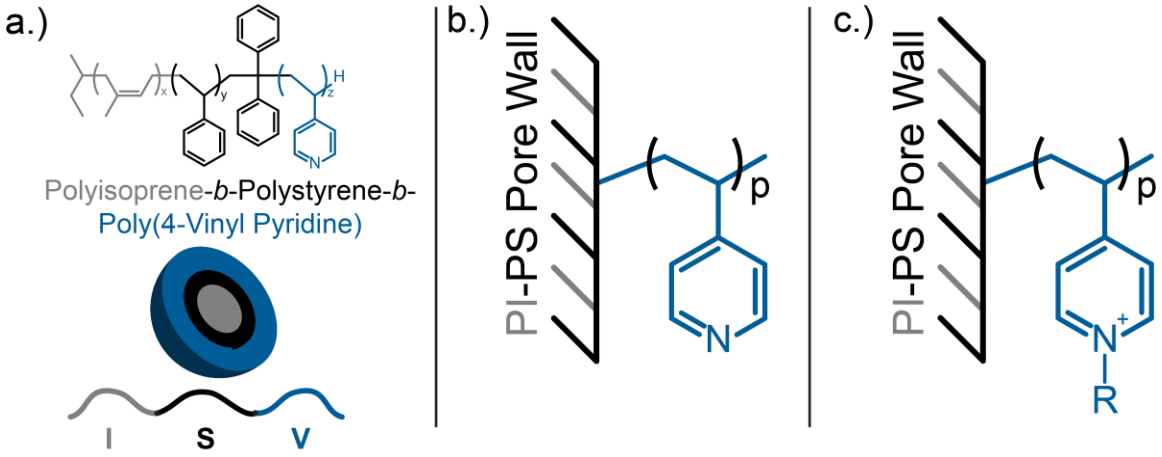

Figure 2.7. (a) Diblock or triblock polymer structure (pictured) consisting of poly(4-vinyl pyridine) domain and polyisoprene-*b*-polystyrene/polystyrene are most commonly used in templating block polymer anisotropic membranes.[65] (b) The interior of the pore walls are lined with the poly(4-vinyl pyridine) moiety.[65] (c) Functionalization of poly(4-vinyl pyridine) moiety.via. quaternerization is possible to facilitate size as well as chemistry selectivity. Such chemical inter-tunability can serve as a viable template for the targeted elution of materials with similar size on the basis of chemical functionality.[65, 72]

2.5 References

1. Baker, R. W. *Membrane Technology and Applications*. 2nd ed.; J. Wiley: Chichester ; New York, **2004**.

2. Zydney, A. L. *High Performance Ultrafiltration Membranes: Pore Geometry and Charge Effects.* Elsevier: Amsterdam, **2011**; Vol. 14, 333.

3. Hilal, N.; Al-Zoubi, H.; Darwish, N. A.; Mohamma, A. W.; Arabi, M. A. *Desalination* **2004**, 170, 281.

4. Zeman, L. J.; Zydney, A. L. *Microfiltration and Ultrafiltration: Principles and Applications.* Marcel Dekker Inc.: New York, **1996**.

5. Mimoune, S.; Belazzougui, R. E.; Amrani, F. *Desalination* **2007**, 217, 251.

6. Shinde, M. H.; Kulkarni, S. S.; Musale, D. A.; Joshi, S. G. *J. Membr. Sci.* **1999**, 162, 9.

7. Wickramasinghe, S. R.; Stump, E. D.; Grzenia, D. L.; Husson, S. M.; Pellegrino, J. *J. Membr. Sci.* **2010**, 365, 160.

8. Warkiani, M. E.; Bhagat, A. A. S.; Khoo, B. L.; Han, J.; Lim, C. T.; Gong, H. Q.; Fane, A. G. *ACS Nano* **2013**, 7, 1882.

9. Miller, S. J.; Koros, W. J.; Vu, D. Q. *Catalysis* **2007**, 170B, 1590.

10. Lind, M. L.; Ghosh, A. K.; Jawor, A.; Huang, X. F.; Hou, W.; Yang, Y.; Hoek, E. M. V. *Langmuir* **2009**, 25, 10139.

11. Curtin, D. E.; Robert D. Lousenberg; Timothy J. Henry; Paul C. Tangeman; Monica E. Tisack *J. Power Sources* **2002**, 131, 41.

12. Mehta, A.; Zydney, A. L. *J. Membr. Sci.* **2005**, 249, 245.

13. Geise, G. M.; Park, H. B.; Sagle, A. C.; Freeman, B. D.; McGrath, J. E. *J. Membr. Sci.* **2011**, 369, 130.

14. Loeb, S.; Sourirajan, S. *Adv. Chem. Series* **1962**, 38.

15. Millipore, E. Millipore Express® PLUS Membrane Filters Catalogue. http://www.millipore.com/catalogue/module.do?id=C2997 (accessed 08/08/12).

16. Guerrier, B.; Bouchard, C.; Allain, C.; Bénard, C. *AlChE J.* **1998**, 44, 791.

17. Ho, W. S. W.; Sirkar, K. K. *Membrane Handbook.* Kluwer Academic Publishing: Boston, **2001**; 954.

18. Baker, R. W.; Lokhandwala, K. *Ind. Eng. Chem. Res.* **2008**, 47, 2109.

19. He, Y.; Cussler, E. L. J. *J. Membr. Sci.* **1992**, 68.

20. Apel, P. *Rad. Meas.* **2001**, 34, 559.

21. Pepy, G.; Boesecke, P.; Kuklin, A.; Manceau, E.; Schiedt, B.; Siwy, Z.; Toulemondeg, M.; Trautmanne, C. *J. Appl. Crystallogr.* **2007**, 40, 388.

22. Spohr, R. *Rad. Meas.* **2005**, 20.

23. Fissell, W. H.; Dubnisheva, A.; Eldridge, A. N.; Fleischman, A. J.; Zydney, A. L.; Roy, S. *J. Membr. Sci.* **2009**, 326, 58.

24. Han, J.; Fu, J.; Schoch, R. B. *Lab on a Chip* **2008**, 8, 23.

25. Zhang, Y.; Sargent, J. L.; Boudouris, B. W.; Phillip, W. A. *J. Appl. Polym. Sci.* **2015**, 132, 41683.

26. Bates, F. S. *MRS Bulletin* **2005**, 30, 525.

27. Bates, F. S.; Fredrickson, G. H. *Physics Today* **1999**, 52, 32.

28. Leibler, L. *Macromolecules* **1980**, 13, 1602.

29. Matsen, M.; Bates, F. S. *Macromolecules* **1996**, 29, 1091.

30. Zhang, L.; Eisenberg, A. *Science* **1995**, 268, 1728.

31. Tang, C.; Lennon, E. M.; Fredrickson, G. H.; Kramer, E. J.; Hawker, C. J. *Science* **2008**, 322, 429.

32. Shefelbine, T. A.; Vigild, M. E.; Matsen, M. W.; D. A. Hajduk, M. A. H.; Cussler, E. L.; Bates, F. S. *J. Am. Chem. Soc.* **1999**, 121, 8457.

33. Hiemenz, P. C.; Lodge, T. P. *Polymer Chemistry 2nd ed.* Boca Raton, FL: **2007**.

34. Gennes, P.-G. d. *Scaling Concepts in Polymer Physics*. Cornell University: **1979**.

35. Hadjichristidis, N.; Pispas, S.; Floudas, G. *Block Copolymers: Synthetic Strategies, Physical Properties, and Applications*. Wiley: **2002**.

36. Hamley, I. *The Physics of Block Copolymers*. Oxford Science: **1999**.

37. Hamley, I. *Nanotechnology* **2003**, 14, 39.

38. Khandpur, A. K.; Foerster, S.; Bates, F. S.; Hamley, I. W.; Ryan, A. J.; Bras, W.; Almdal, K.; Mortensen, K. *Macromolecules* **1995**, 28, 8796.

39. Cochran, E. W.; Garcia-Cervera, C. J.; Fredrickson, G. H. *Macromolecules* **2006**, 39, 2449.

40. Yu, K.; Eisenberg, A. *Macromolecules* **1998**, 31, 3509.

41. Zhu, L.; Cheng, S. Z.; Huang, P.; Ge, Q.; Quirk, R. P.; Thomas, E. L.; Lotz, B.; Hsiao, B. S.; Yeh, F.; Liu, L. *Adv. Mat.* **2002**, 14, 31.

42. Li, M.; Ober, C. K. *Materials Today* **2006**, 9, 30.

43. Zhu, L.; Huang, P.; Chen, W. Y.; Ge, Q.; Quirk, R. P.; Cheng, S. Z.; Thomas, E. L.; Lotz, B.; Hsiao, B. S.; Yeh, F. *Macromolecules* **2002**, 35, 3553.

44. Lodge, T. P. *Macromolecular Chem. Phys.* **2003**, 204, 265.

45. Moad, G.; Rizzardo, E.; Thang, S. H. *Polymer* **2008**, 49, 1079.

46. Matyjaszewski, K. *Macromolecules* **2012**, 45, 4015.

47. Matyjaszewski, K.; Xia, J. *Chem. Rev.* **2001**, 101, 2921.

48. Phillip, W. A.; Dorin, R. M.; Werner, J.; Hoek, E. M. V.; Wiesner, U.; Elimelech, M. *Nano Lett.* **2011**, 11, 2892.

49. Hsieh, H.; Quirk, R. P. *Anionic polymerization: principles and practical applications*. CRC Press: **1996**.

50. Szwarc, M. *Living polymers and mechanisms of anionic polymerization*. Springer: **1983**.

51. Hadjichristidis, N.; Iatrou, H.; Pispas, S.; Pitsikalis, M. *J. Polym. Sci., Part A: Polym. Chem.* **2000**, 38, 3211.

52. Hawker, C. J.; Wooley, K. L. *Science* **2005**, 309, 1200.

53. Coessens, V.; Pintauer, T.; Matyjaszewski, K. *Prog. Polym. Sci.* **2001**, 26, 337.

54. Jackson, E. A.; Hillmyer, M. A. *ACS Nano* **2010**, 4, 3548.

55. Phillip, W. A.; O'Neill, B.; Rodwogin, M.; Hillmyer, M. A.; Cussler, E. L. *ACS Appl. Mater. Interfaces* **2010**, 2, 847.

56. Yang, S. Y.; Park, J.; Yoon, J.; Ree, M.; Jang, S. K.; Kim, J. K. *Adv. Funct. Mater.* **2008**, 18, 1371.

57. Jung, A.; Filiz, V.; Rangou, S.; Buhr, K.; Merten, P.; Hahn, J.; Clodt, J.; Abetz, C.; Abetz, V. *Macromol. Rapid Commun.* **2013**, 34, 610.

58. Pendergast, M. T. M.; Dorin, R. M.; Phillip, W. A.; Wiesner, U.; Hoek, E. M. V. *J. Membr. Sci.* **2013**, 444, 461.

59. Peinemann, K.-V.; Abetz, V.; Simon, P. F. W. *Nat. Mater.* **2007**, 6, 992.

60. Yang, S. Y.; Ryu, I.; Kim, H. Y.; Kim, J. K.; Jang, S. K.; Russell, T. P. *Adv. Mat.* **2006**, 18, 709.

61. Jackson, E. A.; Lee, Y.; Hillmyer, M. A. *Macromolecules* **2013**, 46, 1484.

62. Phillip, W. A.; Rzayev, J.; Hillmyer, M. A.; Cussler, E. L. *J. Membr. Sci.* **2006**, 286, 144.

63. Marques, D. S.; Vainio, U.; Chaparro, N. M.; Calo, V. M.; Bezahd, A. R.; Pitera, J. W.; Peinemann, K.-V.; Nunes, S. P. *Soft Matter* **2013**, 9, 5557.

64. Dorin, R. M.; Sai, H.; Wiesner, U. *Chem. of Mat.* **2014**, 26, 339.

65. Phillip, W. A.; Dorin, R. M.; Werner, J.; Hoek, E. M. V.; Wiesner, U.; Elimelech, M. *Nano Lett* **2011**, 11, 2892.

66. Phillip, W. A.; Hillmyer, M. A.; Cussler, E. L. *Macromolecules* **2010**, 43, 7763.

67. Jung, A.; Rangou, S.; Abetz, C.; Filiz, V.; Abetz, V. *Macromol. Mater. Eng.* **2012**, 297, 790.

68. Nunes, S. P.; Behzad, A. R.; Hooghan, B.; Sougrat, R.; Karunakaran, M.; Pradeep, N.; Vainio, U.; Peinemann, K. V. *ACS Nano* **2011**, 5, 3516.

69. Clodt, J. I.; Filiz, V.; Rangou, S.; Buhr, K.; Abetz, C.; Höche, D.; Hahn, J.; Jung, A.; Abetz, V. *Adv. Funct. Mater.* **2012**, 23, 731.

70. Dorin, R. M.; Phillip, W. A.; Sai, H.; Werner, J.; Elimelech, M.; Wiesner, U. *Polymer* **2014**, 55, 347.

71. Fritzmann, C.; Löwenberg, J.; Wintgens, T.; Melin, T. *Desalination* **2007**, 216, 1.

72. Odian, G. *Principles of Polymerization*. Wiley: **2004**.

CHAPTER 3. POLYMERIZATION RATE CONSIDERATIONS FOR HIGH MOLECULAR WEIGHT POLYISOPRENE-B-POLYSTYRENE-B-POLY(N,N-DIMETHYLACRYLAMIDE) TRIBLOCK POLYMERS SYNTHESIZED VIA SEQUENTIAL REVERSIBLE ADDITION-FRAGMENTATION CHAIN TRANSFER (RAFT) REACTIONS

3.1 Overview

The reversible addition-fragmentation chain transfer (RAFT) polymerization mechanism is a powerful technique for synthesizing functional block polymers for myriad applications. Most kinetic studies regarding the RAFT mechanism have focused on low molecular weight homopolymer and block polymer syntheses using a dithiobenzoate chain transfer agent (CTA). Here, we evaluate the polymerization kinetics for a high molecular weight A-B-C triblock polymer system, polyisoprene-*b*-polystyrene-*b*-poly(*N*,*N*-dimethylacrylamide) (PI-PS-PDMA), using a trithiocarbonate agent for application of these types of polymers. In addition, we establish that the PS and PDMA block additions exhibit polymerization rate retardation, which is due to slow chain fragmentation of the CTA, as demonstrated by the magnitudes of the equilibrium constants for both the styrene and *N*,*N*-dimethylacrylamide reactions, as calculated using *ab initio* modeling. This elucidation of the nature of the controlled RAFT mechanism provides a critical handle for the more precise design and control of other next-generation

high molecular weight block polymer systems that are polymerized using the RAFT mechanism.

3.2 Introduction

Recent advancements regarding reversible addition-fragmentation chain transfer (RAFT) polymerization schemes[1-3] have afforded opportunities for the controlled and ready syntheses of homopolymers and block polymers with a large number of pendant group functionalities.[4-6] The use and versatility of these facile RAFT reactions have enabled the development of highly-tailored, nanostructured materials with applications extending into many areas of technological relevance (*e.g.*, electronic materials,[7-9] drug delivery,[10, 11] and separations devices).[12-16] In combination with modeling of the RAFT kinetic parameters (Scheme 3.1) using *ab initio* numerical methods[17, 18] and reaction engineering modeling,[19-21] a solid grasp on RAFT polymerization rate considerations have been developed in previous studies.[22-26] However, almost all of these implementations and RAFT kinetic mechanism studies have called for the syntheses and utilization of relatively low molecular weight (< 30 kg mol^{-1}) block polymer or homopolymer materials. Conversely, many emerging applications require the utilization of block polymers with higher overall molecular weights in order to generate larger domain sizes and to allow for optimization of the nanostructural and mechanical properties of the materials.[16, 27-30] Recent important efforts have demonstrated that the syntheses of high molecular weight, low dispersity multiblock polymers through chain extension reactions are possible via RAFT polymerization schemes.[27, 31, 32] On the other

hand, limited work has been performed where RAFT polymerization mechanisms are implemented to generate chemically-dissimilar, high molecular weight linear block polymer materials for chemically-tailored, nanostructured devices.

We have shown that A-B-C triblock polymers of relatively high molecular weight (~60 kg mol^{-1}) can be synthesized using a RAFT-mediated scheme. After synthesis, these triblock polymers can be cast into nanofiltration membranes with tailored pore chemistries using a combination of block polymer self-assembly in solution and a non-solvent induced phase separation (SNIPS) casting technique.[27] The scalable SNIPS technique creates asymmetric films with a high density of pores of nearly-uniform pore size. This high density array of uniform pores facilitates the creation of separation devices with a combination of high flux and high separation selectivity.[33, 34] In order to generate high flux, highly selective devices, the successful self-assembly of the block polymer precursor utilized in the SNIPS process is critical. In particular, the fabrication of ordered, nanostructured, and mechanically-robust thin films is only observed if: (1) the total molecular weight of the block polymer is relatively high ($\geq$ 40 kg mol^{-1}); (2) the molecular weight distribution of the block polymer is relatively narrow ($Đ \leq 1.5$); and (3) the composition of the block polymer is held within a relatively tight window with respect to the volume fractions of the three constituent moieties. However, upon proper control of molecular weight, dispersity, and composition of the triblock polymer, the pore size may be tuned by varying total molecular weight[27, 35] for targeted nanofiltration and ultrafiltration applications.[36-42] As such, it is critical to evaluate the mechanism and practical limitations of high molecular weight A-B-C triblock polymers using the RAFT

polymerization mechanism (Scheme 3.1)[18, 22, 23, 43-47] such that these multifunctional macromolecules can be synthesized in a predictable and reproducible manner.

Scheme 3.1. Mechanism of a thermally-initiated RAFT polymerization scheme, which incorporates the different postulated fundamental steps of the RAFT polymerization with respective first order constants.[18, 22, 23, 43-47]

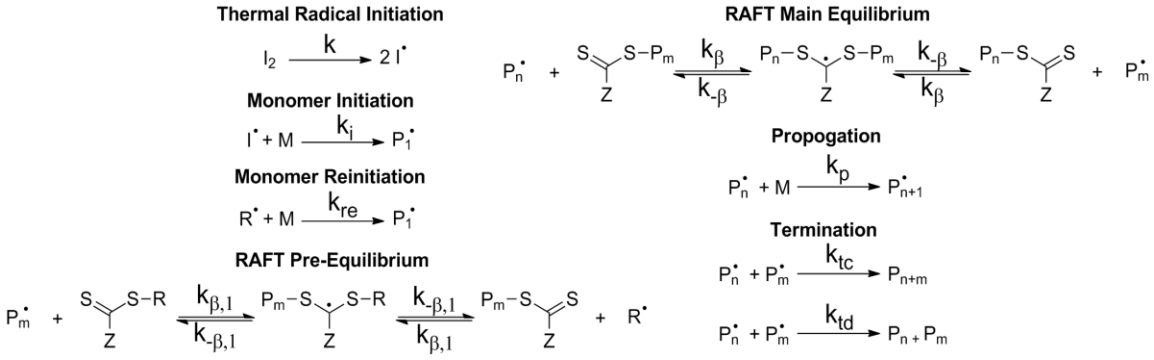

Depending on the identity of the monomer and the chain transfer agent (CTA) used (Scheme 3.1),[1, 18, 22, 48] the reaction may encounter regimes of low conversions of monomer during the preliminary stages of a RAFT polymerization (*i.e.*, polymerization lag). Furthermore, the RAFT-mediated polymerization can result in a decreased rate of polymerization with increasing CTA concentration (*i.e.*, rate retardation can be observed). Previously, it has been postulated that rate retardation may originate from: (1) a slow CTA initiation step (Scheme 3.2a);[49-51] (2) slow intermediate radical fragmentation (Scheme 3.2b);[52-55] intermediate radical termination (IRT) (Scheme 3.2c);[56] a composite model of slow intermediate fragmentation and intermediate radical termination (Scheme 3.2d);[44] or self-termination (Scheme 3.2e).[43] These postulated

mechanisms surrounding rate retardation have been narrowed to be either from (1) a slow intermediate radical fragmentation or (2) an intermediate radical termination mechanism.[25, 57] The use of novel experimental techniques, including electron paramagnetic resonance (EPR) spectroscopy acquired during the polymerization reaction,[49, 54, 55, 58-61] and *ab initio* numerical methods[17, 18] in combination with reaction engineering modeling[19-21] have been used to determine reaction kinetic and equilibrium parameters of the RAFT mechanism (Scheme 3.1) that cannot be determined from experimental conversion-time data alone. Of these parameters, the value of the chain fragmentation constant (K) is of prime import. This calculated value may be used to help validate that a slow intermediate fragmentation mechanism is responsible for rate retardation.[19-21, 25, 57]

While experimental studies on a slow intermediate radical fragmentation and the IRT model have continued to prove, disprove, or counter each other, such studies primarily have been performed on homopolymerization systems of low total molecular weight using dithiobenzoate agents.[43, 44, 49-56] By expansion of the kinetic analyses associated with RAFT reaction schemes to higher molecular weight and block polymerizations using a different class of chain transfer agent, we combine experimental results with *ab initio* methods[17, 18] to afford further insights into the rate retardation mechanism in a RAFT polymerization system.

Scheme 3.2. Postulated mechanistic origins of a) polymerization lag and b) through e) rate retardation and termination in the RAFT polymerization mechanism.

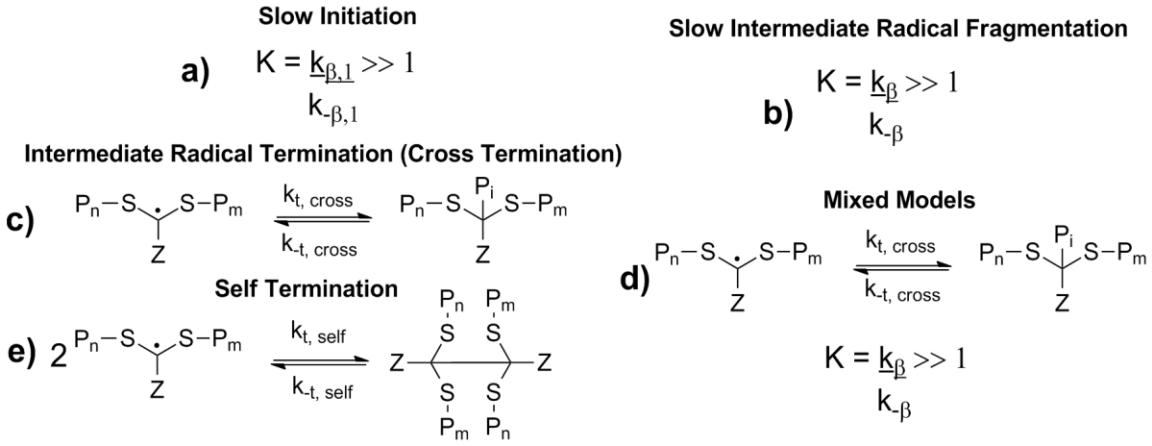

Here, we report the rates of polymerizations for the synthesis of each moiety of a high molecular weight A-B-C triblock polymer, polyisoprene-*b*-polystyrene-*b*-poly(*N*,*N*-dimethylacrylamide) (PI-PS-PDMA), utilizing a trithiocarbonate chain transfer agent. These block polymers were generated through sequential polymerization and macroinitiation (of the second and third blocks) according to the RAFT polymerization schemes shown in Scheme 3.3. By modeling the controlled polymerization,[25, 57] we quantify the fundamental reaction parameters for each polymerization using experimental data and *ab initio* numerical methods.[17, 18] In this way, we may also provide a clear pathway by which to tune the molecular weight of each moiety of the triblock polymer in a systematic manner.

Scheme 3.3. Synthesis and nomenclature of the polyisoprene-*b*-polystyrene-*b*-poly(*N*,*N*-dimethylacrylamide) (PI-PS-PDMA) triblock polymers.

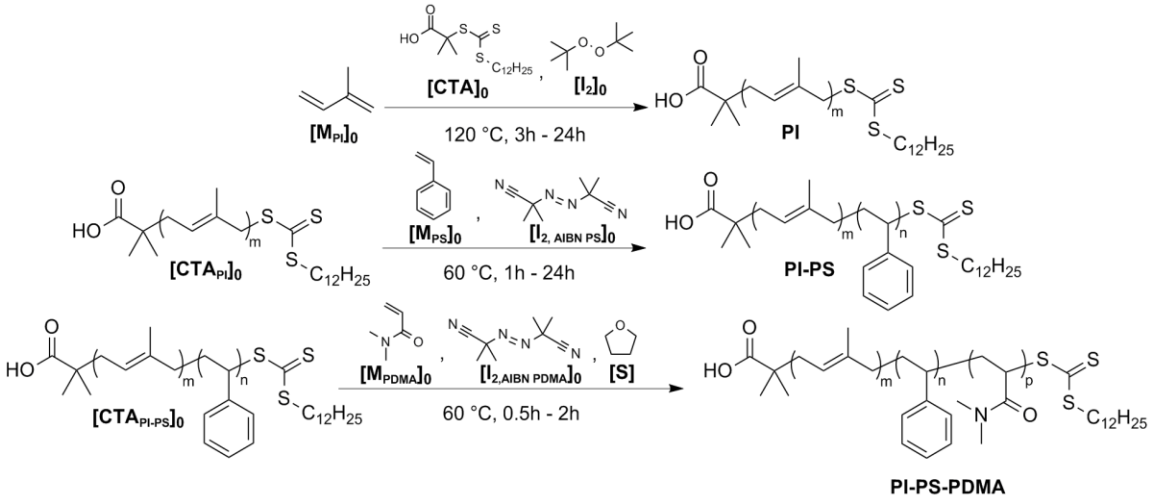

3.3 Results and Discussion

By performing a series of experimental polymerizations of each of the moieties of the triblock polymer, the effective, overall kinetic parameters were quantified (*i.e.*, the effective first order rate constant (k_{eff}) was calculated). Unfortunately, a large number of the intrinsic kinetic parameters define a postulated RAFT mechanism (as shown in Scheme 3.1). As such, the system degree of freedom is underspecified. In order to fully specify the system, a series of assumptions, exceptions, and/or measurement techniques must be used to define these kinetic parameters as they cannot be determined from experiment or from existing literature.[17, 18] For modeling of the experimental data, the mechanism chosen for rate retardation (Scheme 3.2), where applicable, is used in conjunction with the RAFT mechanism in Scheme 3.1. To simplify the expression, it is assumed, based on previous studies, that the electron donating (Z) group and the reinitiating (R·) substituent groups (Scheme 3.1) are optimal choices for the classes of

monomers to be block polymerized.[27, 62, 63] Therefore, the first order monomer initiation, re-initiation and propagation order rate constants may be considered to be equal (*i.e.*, $k_i = k_{re} = k_p$)[3, 64] without significantly affecting the calculated parameters on the RAFT block polymerization study. In addition, due to the observed absence of irreversibly terminated chains for each block polymerization sequence, the corresponding termination rates from chain transfer and disproportionation may be neglected (*i.e.* k_{tc} and $k_{td} \approx 0$).[3, 64]

The combination of these reactions creates a system of differential equations for modeling the chain length as a function of time.[20, 32, 52, 57, 65, 66] The RAFT equilibrium constant (K) values were computationally-predicted by calculating the ΔH_0 and ΔS_0 values between the RAFT adducts and the fragmented species in Scheme 3.1 using Gaussian 03 software.[17, 18] Calculations for accurately determining the zero point energy level were performed at a successively higher level of theory. Starting from a structure optimized using a B3-LYP/6-31G level of theory, the vibrational energies upon solution were checked. Next, a scan in steps of 10° over the entire 360° possible for the bond rotations to the trithiocarbonate groups were performed to validate that a globally-optimized structure has been obtained. Subsequent application of a higher RMP2/6-311 level of theory was used to calculate the ΔH_0 and ΔS_0 energy levels of the RAFT adducts and the fragmented species accurately. In turn, these parameters were used to obtain the K parameters using *ab initio* numerical methods.[17, 18, 67] By calculating the *ab initio*-determined equilibrium constant K values[17, 18] for each block polymerization (Table 3.1), it is possible to determine the origin of experimentally-observed kinetic rate-retardation. That is, it is possible to connect thermodynamic theory to kinetic practice in the following manner. High values of K (*i.e.*, $\geq 10^6$ mol L^{-1} observed in dithiobenzoate

mediated RAFT polymerizations)[19-21] indicate that a long half-life of RAFT adduct existence occurs (see the RAFT main equilibrium in Scheme 3.1).[52-55] This, therefore, suggests that a slow intermediate radical fragmentation mechanism is responsible for rate retardation.[52-55] Consequently, by combining this computational modeling and the experimental data from RAFT polymerization species (Scheme 3.1) as a system of explicit kinetic equations, complete quantification of the kinetics of a polymerization can be made for precise tuning of high molecular weight block polymers for tailored, nanostructured materials.

Table 3.1. The thermodynamic values and equilibrium constants at 120 °C for the PI synthesis and at 60 °C for the PI-PS and PI-PS-PDMA block polymerization using the RMP2/6-311+G(3df,2p)//B3-LYP/6-31G(d) *ab initio* method. The procedure and assumptions of these calculated values are referenced from previous literature.[17, 18]

Synthesis	ΔH_0 (kJ mol^{-1})	ΔS_0 (J mol^{-1} K^{-1})	ΔG_0 (kJ mol^{-1})	K (L mol^{-1})
PI	-69.1	-120	-29.1	3.7×10^4
PI-PS	-89.0	-118	-50.0	6.2×10^7
PI-PS-PDMA	-75.0	-109	-38.7	1.2×10^6

Previously, the kinetic parameters of the RAFT-mediated polymerization of isoprene using the 2-(dodecylthiocarbonothioylthio)-2-methylpropanoic acid chain transfer agent have been well-established by the Wooley group for polymers with molecular weights of less than 20 kg mol^{-1}, and the Perrier group has extended this analysis for low molecular weight polyisoprene (PI) samples to other chain transfer agent

chemical functionalities.[62, 63] However, the RAFT-mediated polymerization of isoprene with larger targeted molecular weights and low dispersity values has not been evaluated. Here, we elucidate the polymerization rates for higher molecular weight PI samples. For simplicity of modeling, the timescales of all reactions were chosen to ensure the establishment of steady-state pseudo-first order growth for all polymerization trials (*i.e.* there is a linear first order conversion plot with respect to time) at constant monomer concentrations. Additionally, for all studies, the specified molar ratio of the CTA functionality to the radical initiator (or macroinitiator, in the case of the diblock polymer and triblock polymer syntheses) is constant for each polymerization reaction. This allowed for controlled molecular weight targeting of the block polymers at low dispersity, and it allowed for us to observe the effect of the rate of polymerization as a function of the monomer to CTA ratio.

As expected, the controlled nature of the PI synthesis was maintained (Figure 3.1)[62, 63] for reaction times up to 24 h even at the larger PI chain lengths synthesized in this study. In the neat polymerization of isoprene, decreasing concentrations of chain transfer agent and initiator resulted in a decrease in the rate of polymerization (Figure 3.1d) (*i.e.* no rate retardation was observed). The conversion of isoprene largely becomes independent of the monomer to chain transfer agent concentration ratio at high $[M_{PI}]_0$:$[CTA]_0$ values (*i.e.*, near 2920:1) (Figure 3.1a). Over the PI concentrations and reaction times studied, a monotonic decrease of dispersity to values as low as 1.27 was recorded at a lowest $[M_{PI}]_0$:$[CTA]_0$ ratio of 730:1 after 24 hours (Figure 3.4). As the $[M_{PI}]_0$:$[CTA]_0$ ratio was increased to synthesize higher molecular weights of PI, successively higher values of dispersity were recorded at each time interval.

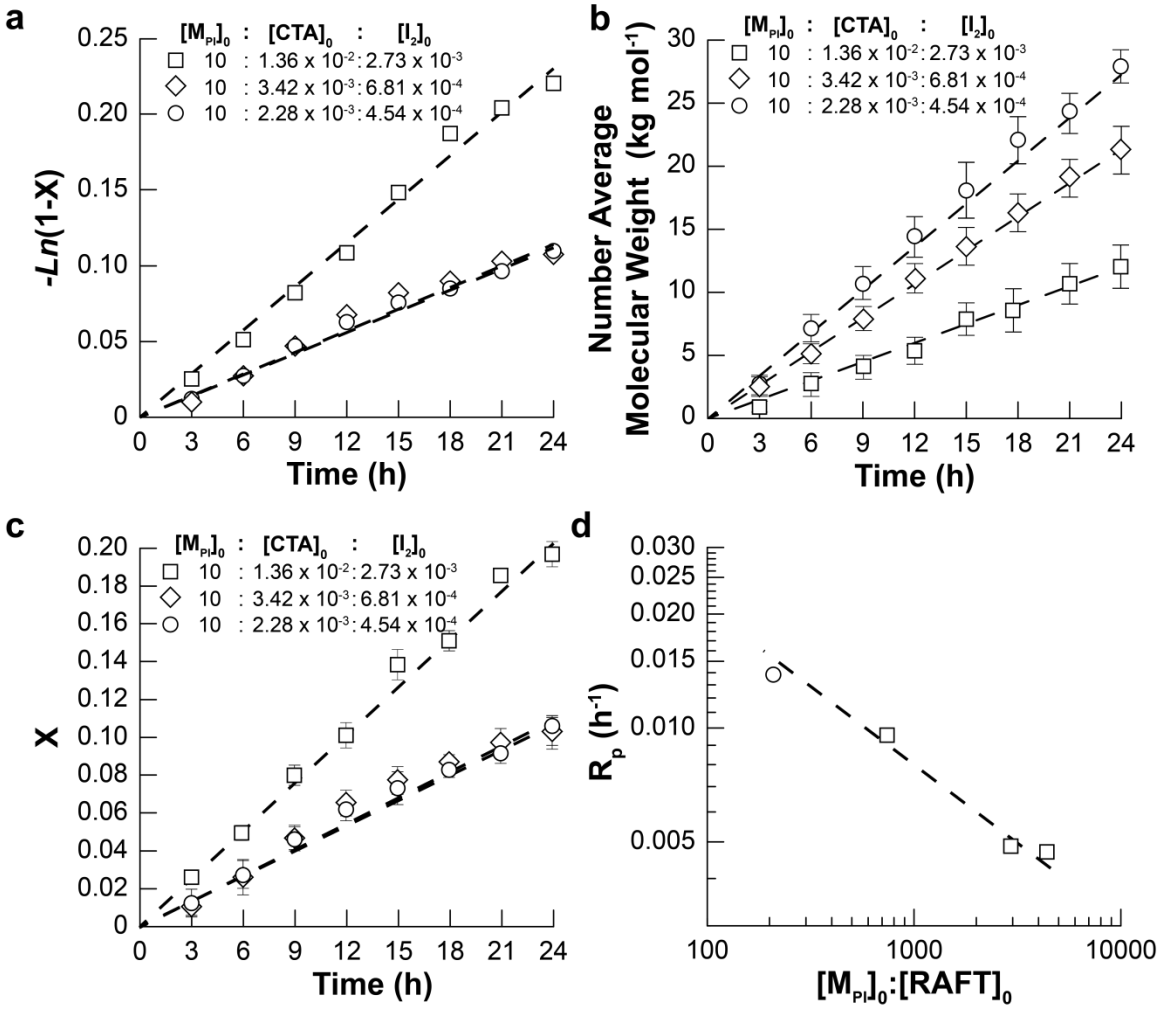

Figure 3.1. (a) Conversion of isoprene versus time at various concentrations of chain transfer agent and initiator (in mol L^{-1}). (b) Number average molecular weight of polyisoprene versus time at various concentrations of chain transfer agent and initiator. The dashed curves represent the fits from the linear regressions determined from the data in Figure 3.1a. (c) First order kinetic plot of isoprene conversion versus time at various concentrations of chain transfer agent and initiator. The dashed curves represent the best fits modeled using the reaction scheme shown in Scheme 3.1 (d) The rates of polymerization determined by the gradients of first order plot of conversion in (a), as well as the R_p value determined from the kinetic trials presented by the Wooley group.[63] The dashed line represents the power law curve of best fit for R_p values determined from our kinetic trials (squares only).

The RAFT-mediated polymerization of isoprene does not show rate retardation or a lag in the polymerization rate. Therefore, the use of additional reaction pathways/constraints outlined in Scheme 3.1 does not apply to the PI synthesis reaction scheme. To provide a quantitative model of the rate of PI polymerization, an *ab initio* calculation[17, 18] was performed to computationally predict the chain transfer constant (*K*) and to specify the system constants for solving high molecular weight, low dispersity reaction modeling (Figure 1c).

A low calculated value of 3.7×10^4 mol L^{-1} (Table 3.1) demonstrates that main RAFT equilibrium favors the dissociated (instead of the RAFT adduct) state.[20, 21, 66] As such, the polymerization rate relates to degenerative chain transfer kinetics (*i.e.*, $R_p \propto ([I_2]_0)^{\frac{1}{2}}$).[68] By normalizing the isoprene polymerization rate by the square root of initiator concentration (Figure 3.5), the constant values (~ 6 $mol^{-1/2}$ $L^{1/2}$ h^{-1}) calculated at each monomer to chain transfer agent ratio asserts that RAFT isoprene polymerization behaves as degenerative chain transfer radical polymerization with no observed rate retardation.

The second of the two primary components in this triblock polymer system is one that allows for the incorporation of a high glass transition temperature domain. This polystyrene domain serves to impart structural integrity to the otherwise rubbery (at room temperature) PI component of the PI-PS diblock polymer in practical applications. Here, we have synthesized the PS block through the initiation of styrene from the PI macroinitiator in a neat polymerization reaction. Gelation of this bulk polymerization can be avoided by limiting the styrene conversion to < 20% (Figure 2a), which allows for the

synthesis of varying molecular weights of the PI-PS diblock polymer. All of these reactions resulted in diblock polymers with narrow molecular weight distributions ($Đ$ ~1.3, Figure 3.6). In this polymerization reaction, there was a delay between the start of the reaction and the beginning of chain growth (*i.e.*, ~3 h, Figure 3.7) that was independent of the styrene concentration. This delay time is indicative of a polymerization lag from slow initiation of the styrene monomers from the PI-based macroinitiator chains (see Scheme 3.2a).[49-51] As expected, however, the controlled nature of the PI-PS synthesis was maintained, even at high PI-PS chain lengths synthesized in this study. In addition, the molecular weights of the polymers grew linearly with reaction time past this lag time (Figures 2a and b), indicating a controlled, steady-state living polymerization where the dispersity values decreased with polymerization time (Figure 3.8).

For the neat PI-PS kinetic polymerization study, rate retardation occurs (Figure 2). As such, further incorporation of rate retardation mechanisms (Scheme 3.2) are required to account for this retardation behavior. The PS block addition in this study is performed at relatively low conversions where a very small concentration of polymer chains are present in mixture; therefore, it is unlikely that a self- or cross-termination mechanism is responsible for rate retardation (*i.e.* Schemes 3.2c to 3.3e). This is firstly due to the entropic effects from a large steric barrier generated by the long macroinitiator PI-RAFT chain. This barrier would shield any reaction of the RAFT adduct with an incoming large polymer chain, making reaction of the radical site highly unlikely.[69] Secondly, contrived conditions of high concentrations of initiator are required for self- and cross-termination to occur, and these conditions were not used in this study.[43] This

reasoning is supported by the failure to see any star polymer formation experimentally in the size-exclusion chromatography (SEC) traces of the PI-PS diblock copolymers (Figure 3.8). Therefore, by reasonable deduction, the only remaining probable cause of rate retardation of the PS block addition to PI-RAFT may be attributed to slow intermediate fragmentation (Scheme 3.2b).[52-55] To explain the concept of slow intermediate fragmentation as the cause of rate retardation in the PS block addition, *ab initio* theory was applied[17, 18] to determine the *K* value of this polymerization. A large value of 6.2×10^7 mol L^{-1} (Table 3.1) for PI-PS-RAFT polymerization was calculated (*i.e.*, in comparison to dithiobenzoate RAFT polymerization study *K* values of ~10^6 mol L^{-1}). This larger value demonstrates that the main RAFT equilibrium favors the adduct state over the fragmented, dissociated state to allow for chain growth.[20, 21, 66] Thus, with a high proportion of propagating chains existing as protected adducts due to slow intermediate fragmentation, the propagation of the PS block addition to a PI macroinitiator at a degenerative chain transfer rate is inhibited. This, therefore, mechanistically explains why rate retardation in PS block addition to PI is observed.[52-55]

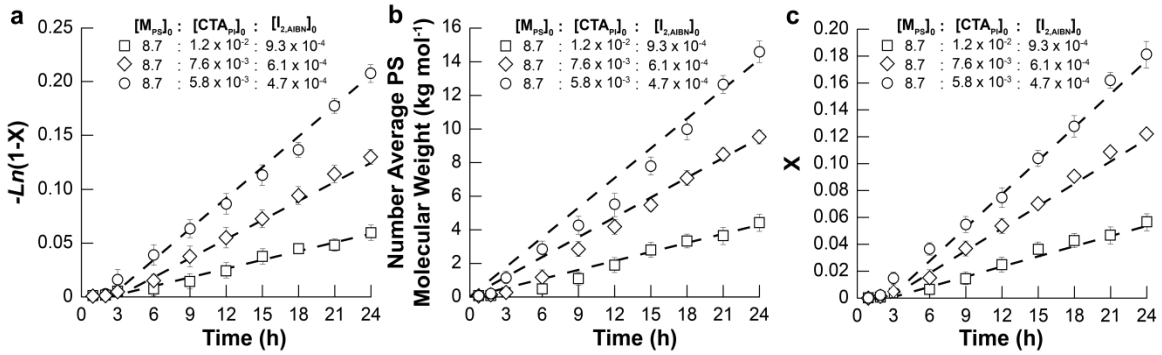

Figure 3.2. (a) First order kinetic plot of neat styrene conversion versus time at various concentrations of PI-RAFT-based (9.5 kg mol^{-1}, $Đ$ = 1.5) chain transfer agent and initiator (the numerical values have units of mol L^{-1}). The dashed lines represent the best fits of the linear regressions used in determining an effective rate of polymerization (R_p) at each monomer concentration. The straight line of this plot indicates the establishment of steady-state radical concentration over the time scale of this study to simplify the modeling of the kinetic analyses. (b) Molecular weight of polystyrene versus time at various ratios of monomer to PI-RAFT-based macroinitiator chain transfer agent (*i.e.*, $[M_{PS}]_0$:$[CTA_{PI}]_0$ ratio). The dashed curves represent the fits from the linear regression from Figure 2a. (c) First order kinetic plot of styrene conversion versus time at various concentrations of PI-RAFT macroinitiator and initiator. The equilibrium constant used was $K_{PS} = 6.2 \times 10^7$ for each CTA concentration.

The third moiety of the triblock polymer is PDMA, which provides a means by which to manipulate the chemical functionality of the triblock polymer before or after deposition of the material into a thin film.[27, 70] By limiting the conversion of the *N*,*N*-dimethylacrylamide to < 20%, high molecular weight PDMA blocks (of up to 75 kg mol^{-1}) may be added to PI-PS-RAFT macroinitiators with the resulting triblock possessing dispersity values of less than 1.5. In this polymerization reaction, there was a concentration-independent delay between the start of the reaction and the beginning of

chain growth (*i.e.*, ~1 h, see Figure 3). This lag behavior and the rapid polymerization rates are consistent with previous literature on the initiation and growth of homopolymer polyacrylamides and polyacrylates from the 2-(dodecylthiocarbonothioylthio)-2-methylpropanoic acid chemical functionality.[71] This delay time, similarly observed for PS block addition, is also indicative of possible polymerization lag from slow initiation (Scheme 3.2a).[49-51] The controlled nature of the PI-PS-PDMA triblock synthesis was maintained over the course of the study (2 h). For polymerization times up to 2 h, no increase of dispersity was observed (Figure 3.9).

In a finding analogous to the neat PI-PS diblock polymer polymerization study, rate retardation also was observed during PDMA block addition to the PI-PS-RAFT macroinitiator in solution when tetrahydrofuran (THF) was used as the solvent. As this is a dilute polymerization using a high molecular weight PI-PS-based macroinitiator, the coordination and reaction of a large radical polymer chain with a large RAFT macroinitiator adduct is unlikely.[69] Therefore, it is improbable that rate retardation is due to intermediate radical termination (Schemes 3.2c and 3.2d). In addition, the absence of any increase in dispersity of PI-PS-PDMA during the polymerization (Figure 3.9) indicated no occurrence of cross-termination reactions (Scheme 3.2e).

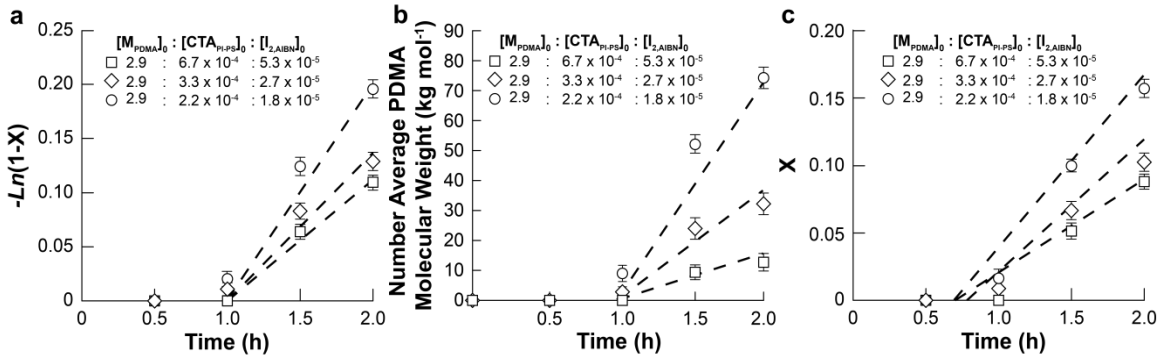

Figure 3.3. (a) The first order kinetic plot of *N*,*N*-dimethylacrylamide conversion versus time at various concentrations of PI-PS-RAFT macroinitiator (12.8 kg mol^{-1}-33.2 kg mol^{-1}, $Đ$ = 1.4) and the radical source. The dashed lines represent the best fits of the linear regression used in determining an effective rate of polymerization (R_p) at each monomer ratio. The straight line of this plot indicates the establishment of steady state radical concentration over the time scale of this study that simplifies the modeling of the kinetic analyses. (b) Molecular weight of poly(N,N-dimethylacrylamide) versus time at various ratios of monomer to PI-PS-RAFT-based macroinitiator chain transfer agent (*i.e.*, $[M_{PDMA}]_0$:$[CTA_{PI\text{-}PS}]_0$ ratio). The dashed curves represent the fits from the linear regression determined in (a). (c) First order kinetic plot of *N*,*N*-dimethylacrylamide conversion versus time at various concentrations of PI-PS-RAFT macroinitiator and initiator. The dashed lines represent the best fits using the reaction scheme shown in Scheme 3.1 and Scheme 3.2b.

Therefore, by elimination of all other mechanistic reasons for rate retardation, the only remaining probable cause of rate retardation of PDMA block addition to PI-PS-RAFT may be attributed to slow intermediate fragmentation (Scheme 3.2b).[52-55] Upon application of *ab initio* theory[17, 18] to determine the *K* value of PDMA block addition for accurate modeling of controlled high molecular weight PDMA addition (Figure 3), a value of 1.2 × 10^6 mol L^{-1} (Table 3.1) for the PI-PS-PDMA polymerization was

calculated. As the magnitude of this value is consistent with slow fragmentation dithiobenzoate RAFT agent values (*i.e.*, with $K \sim O(10^6)$ and above), a large proportion of radical chains exist in the adduct state over fragmented, dissociated state for chain growth.[20, 21, 66] Because a majority of propagating PI-PS/PI-PS-PDMA macroinitiator radical chains exist as protected adducts, the PDMA block addition exhibits rate retardation.[52-55]

3.4 Conclusion

In summary, we have monitored the rates of polymerizations at each step of three chemically-dissimilar RAFT-mediated block polymerizations of PI-PS-PDMA. To facilitate self-assembly using the SNIPS casting technique, the dispersity of the PI-PS-PDMA block polymer must be less than 1.5. As such, using these reaction conditions, we establish that there is an upper molecular weight limit of 30 kg mol^{-1} for the PI moiety of the triblock polymer using this polymerization scheme. Rate retardation is observed in the PS and PDMA block addition reactions. This occurred due to the high values of the RAFT chain equilibrium constants ($\geq 10^6$) observed for PS addition to a PI-RAFT macroinitiator ($K_{PS} = 6.2 \times 10^7$) as well as PDMA addition to a PI-PS-RAFT macroinitiator ($K_{PDMA} = 1.2 \times 10^6$). Furthermore, it has been demonstrated that, by simple tuning of the CTA and the initiator concentration, it is possible to achieve controlled high molecular weights and low dispersity values for these PI-PS-PDMA block polymers. The usage of *ab initio* methods in a trithiocarbonate block polymerization system gave further credence to a slow fragmentation mechanism being responsible for observed rate

retardation in PI-PS and PI-PS-PDMA RAFT block polymerizations. Finally, the elucidation of high molecular weight RAFT block polymerization kinetics with sufficiently low dispersity demonstrates the great utility of this facile polymerization technique to create well-defined block polymers that can be utilized in advanced separation applications.

3.5 Acknowledgements

Portions of this work by W.A.P. were made possible with support from the Army Research Office (ARO) through the Polymer Chemistry Program (Award Number: W911NF-14-1-0229, Program Manager: Dr. Dawanne Poree). The work of R.A.M. and R.A.P. was supported by the National Science Foundation (NSF) through the Nanomanufacturing Program (Award Number: 1436255, Program Manager: Dr. Khershed Cooper). We appreciatively acknowledge this support. B.W.B. thankfully acknowledges support from the Ralph W. and Grace M. Showalter Research Trust Award at Purdue University.

3.6 Supporting Information

3.6.1 Materials and General Procedures

All chemicals were used as received from Sigma-Aldrich unless otherwise noted. Isoprene, styrene, and *N*,*N*-dimethylacrylamide (DMA) were purified by passage through a basic alumina (Fisher Scientific) column prior to use. ^{1}H NMR spectra were measured

on a Bruker DRX500 spectrometer using a ~1 wt% polymer solution in deuterated chloroform. Size exclusion chromatography (SEC) data were collected on a Hewlett-Packard 1260 Infinity series equipped with a Hewlett-Packard G1362A refractive index (RI) detector and three PLgel 5 μm MIXED-C columns. The mobile phase was comprised of tetrahydrofuran (THF) at 35 °C at a flow rate of 1 mL min^{-1}. The SEC was calibrated using polystyrene standards (Agilent Easi Cal) with molecular weights ranging from 1 kg mol^{-1} to 200 kg mol^{-1}.

3.6.2 Polyisoprene Synthesis

The controlled polymerization of isoprene using a RAFT-mediated mechanism has been described in detail previously, and only modifications of monomer to RAFT initiator ratios have been made in order to facilitate the growth of high molecular weight polymers.[27, 72-74] In an example reaction, 15 mL (0.15 mol) of purified isoprene were mixed with 74.5 mg of 2-(dodecylthiocarbonothioylthio)-2-methylpropanoic acid (0.20 mmol) and 7.51 μL of *tert*-butyl peroxide (0.04 mmol). The contents were injected into an argon-purged 25 mL high pressure reaction vessel containing a Teflon-coated stir bar. The vessel underwent four freeze-pump-thaw cycles prior to being refilled with argon and placed in a stirred oil bath at 120 ºC for a predetermined period of time. After the reaction, the mixture was cooled in a water bath and the residual isoprene monomer was removed under vacuum. The remaining solids were dissolved in tetrahydrofuran (THF), and the polymer was precipitated three times into methanol before being dried under vacuum overnight.

3.6.3 Polyisoprene-*b*-Polystyrene Synthesis

The PI-PS diblock copolymer was synthesized through the macroinitiation of the PI chain using a RAFT-mediated polymerization reaction.[27, 72] Here, we detail an example reaction for the synthesis of PI-PS grown from a PI macroinitiator (9.5 kg mol^{-1}, $Đ$ = 1.5). Specifically, 0.4 g (0.04 mmol) of PI macroinitiator were mixed with 7 mL (0.06 mol) of purified styrene and 0.55 mg (3.3 μmol) of azobisisobutyronitrile (AIBN). The mixture was charged into a sealed 100 mL round bottom flask containing a Teflon-coated stir bar. The vessel underwent four freeze-pump-thaw cycles prior to being refilled with argon and placed in a stirred oil bath at 60 ºC. Aliquots (~0.25 mL) were taken once every 3 h under a purge of argon gas using a purged, airtight syringe. All aliquots were precipitated from THF three times into methanol and dried under vacuum overnight.

3.6.4 Polyisoprene-*b*-Polystyrene-*b*-Poly(*N*,*N*-Dimethylacrylamide) Synthesis

The PI-PS-PDMA triblock polymer was synthesized through the macroinitiation of the PI-PS block polymer using a RAFT-mediated polymerization reaction. In a representative reaction, 1 g (0.02 mmol) of the PI-PS macroinitiator was mixed with 10.2 mL (0.10 mol) of purified DMA monomer, 0.23 mg (1.6 μmol) of azobisisobutyronitrile (AIBN), and 23.5 mL of THF. The mixture was then charged into a 100 mL round bottom flask containing a Teflon-coated stir bar and under an argon blanket. The vessel underwent four freeze-pump-thaw cycles prior to being refilled with argon and placed in a stirred oil bath at 60 ºC for a predetermined period of time. After the reaction, the mixture was cooled in a water bath and the residual *N*,*N*-dimethylacrylamide monomer

and THF were removed under vacuum. The remaining solids were then dissolved in THF, and precipitated three times into a mixture of cold hexanes before being dried under vacuum overnight.

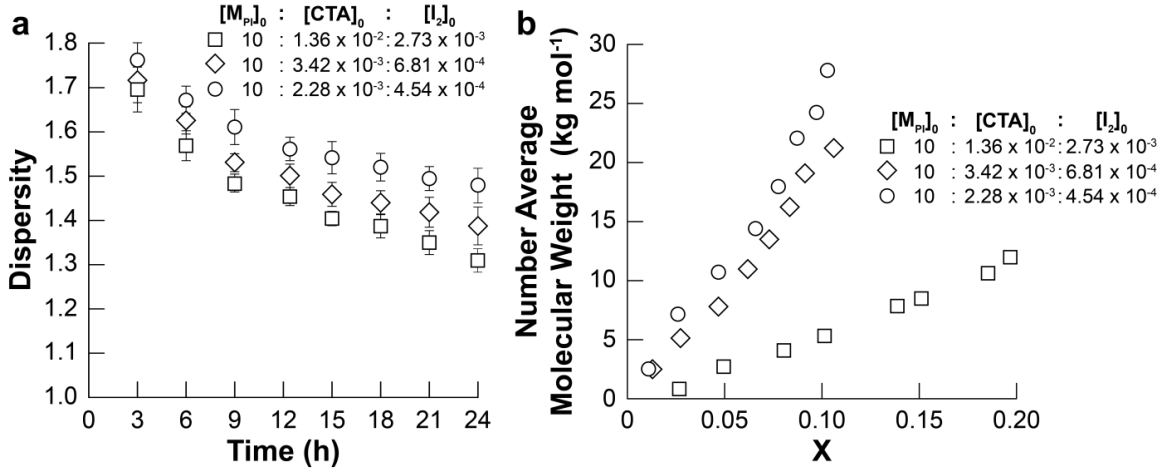

Figure 3.4. (a) The dispersity values of the PI macromolecules as a function of reaction time. The data points in each plot denote the average values of each experimental condition and the error bars represent the range of the maximum and minimum values found over 2 repeat reactions (*i.e.*, 3 total reactions). The numbers of each curve refer to the different initial molar ratio conditions used. (b) Plot of the average PI molecular weight versus the corresponding conversion over the different amounts of $[CTA]_0$ and $[I_2]_0$ used. The high degree of linearity of this plot at different chain transfer agent and initiator concentrations suggests successful controlled radical polymerization of PI homopolymer of variable high molecular weight utilizing a RAFT mediated mechanism.

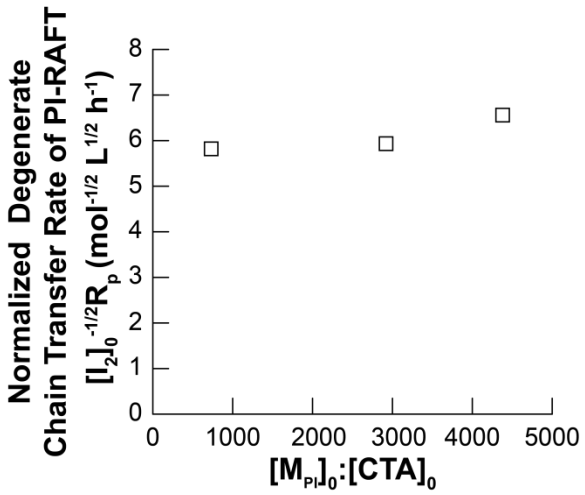

Figure 3.5. Reaction rates of the PI kinetic studies (R_p) divided by the square root of their respective initial *tert*-butyl peroxide initiator ($[I_2]_0$) as a function of the monomer to RAFT chain transfer agent ($[M_{PI}]_0$:$[CTA]_0$). As $R_p \propto [I_2]_0^{1/2}$ in a degenerative chain transfer reaction, the approximately equal values of the plotted $R_p [I_2]_0^{-1/2}$ versus $[M_{PI}]_0$:$[CTA]_0$ ratio indicate that the PI polymerization kinetically proceeds via a degenerative chain transfer reaction with no observed rate retardation.

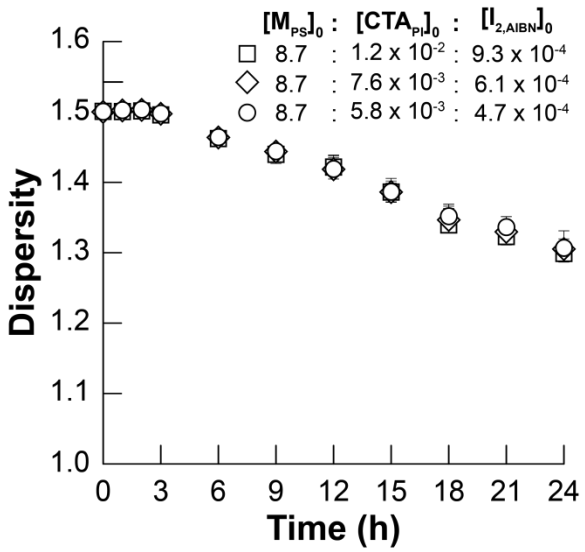

Figure 3.6. The corresponding dispersity values of the PI-PS macromolecules as a function of reaction time. The data points in each plot denote the average values of each experimental condition and the error bars represent the range of the maximum and minimum values found over 2 repeat reactions. The numbers of each curve refer to the different initial molar ratio conditions used.

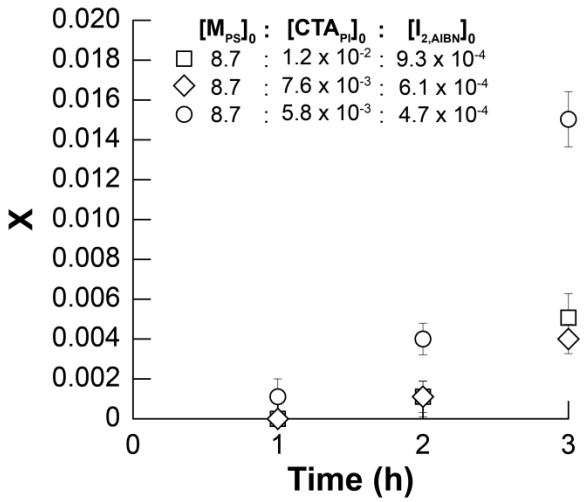

Figure 3.7. Conversion of a PS block grown from a PI macroinitiator (9.5 kg mol^{-1}, $Đ$ = 1.5) versus time during the early stages of polymerization (1 - 3 h). The data points in each plot denote the average values of each experimental condition and the error bars represent the range of the maximum and minimum values found over 2 repeat reactions. The numbers of each curve refer to the different initial molar ratio conditions used.

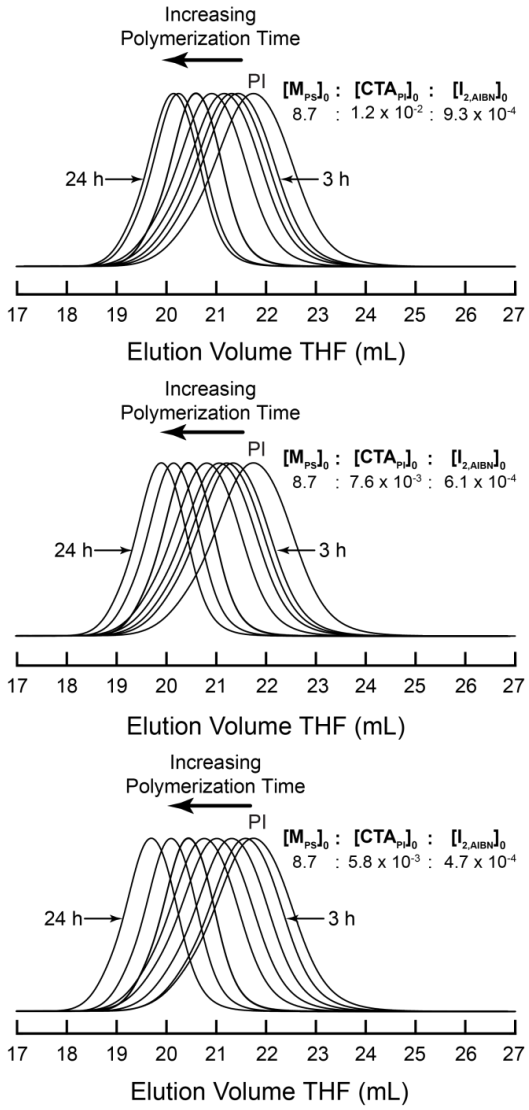

Figure 3.8. SEC traces for PI-PS diblock samples grown from a PI macroinitiator using a RAFT-mediated mechanism. The curves in the figure, from the right to the left, represent SEC traces of PI macroinitiator starting material and the PI-PS diblock, respectively, taken at each 3 h time intervals (*i.e.*, from 3 h to 24 h). As expected, the molecular weight of the polymer increases with increasing reaction time. The numbers in each figure refer to: the molar ratio of styrene monomer ($[M_{PS}]_0$) to the molar ratio of PI RAFT macroinitiator chain transfer agent ($[CTA_{PI}]_0$) to the molar ratio of initiator ($[I_{2,AIBN}]_0$).

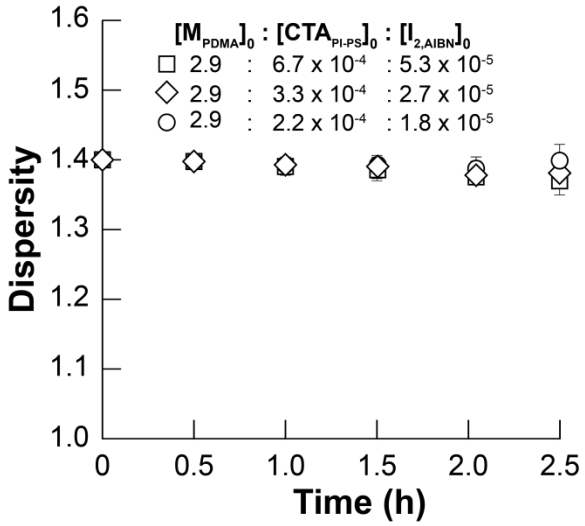

Figure 3.9. The corresponding dispersity values of the PI-PS-PDMA macromolecules as a function of reaction time. The data points in each plot denote the average values of each experimental condition and the error bars represent the range of the maximum and minimum values found over 2 repeat reactions. The numbers of each curve refer to the different initial molar ratio conditions used.

3.7 References

1. Chiefari, J.; Chong, Y.; Ercole, F.; Krstina, J.; Jeffery, J.; Le, T. P.; Mayadunne, R. T.; Meijs, G. F.; Moad, C. L.; Moad, G. *Macromolecules* **1998**, 31, 5559.

2. Mayadunne, R. T.; Rizzardo, E.; Chiefari, J.; Chong, Y. K.; Moad, G.; Thang, S. H. *Macromolecules* **1999**, 32, 6977.

3. Barner-Kowollik, C. *Handbook of RAFT Polymerization*. John Wiley & Sons: **2008**.

4. Braunecker, W. A.; Matyjaszewski, K. *Prog. Polym. Sci.* **2007**, 32, 93.

5. York, A. W.; Kirkland, S. E.; McCormick, C. L. *Adv. Drug Delivery Rev.* **2008**, 60, 1018.

6. Hawker, C. J.; Wooley, K. L. *Science* **2005**, 309, 1200.

7. Iovu, M. C.; Craley, C. R.; Jeffries-El, M.; Krankowski, A. B.; Zhang, R.; Kowalewski, T.; McCullough, R. D. *Macromolecules* **2007**, 40, 4733.

8. Rostro, L.; Baradwaj, A. G.; Boudouris, B. W. *ACS Appl. Mater. Interfaces* **2013**, 5, 9896.

9. Moad, G.; Chen, M.; Haussler, M.; Postma, A.; Rizzardo, E.; Thang, S. H. *Polym. Chem.* **2011**, 2, 492.

10. Stenzel, M. H. *Chem. Commun.* **2008**, 3486.

11. Oh, J. K.; Drumright, R.; Siegwart, D. J.; Matyjaszewski, K. *Prog. Polym. Sci.* **2008**, 33, 448.

12. Gaucher, G.; Dufresne, M.-H.; Sant, V. P.; Kang, N.; Maysinger, D.; Leroux, J.-C. *J. Membr. Sci.* **2005**, 109, 169.

13. Segalman, R. A. *Mater. Sci. Eng., R* **2005**, 48, 191.

14. Kim, H.; Park, S.; Hinsberg, W. D. *Chem. Rev.* **2009**, 110, 146.

15. Jeong, B.; Gutowska, A. *Trends Biotechnol.* **2002**, 20, 305.

16. Ikkala, O.; ten Brinke, G. *Science* **2002**, 295, 2407.

17. Coote, M. L.; Radom, L. *J. Am. Chem. Soc.* **2003**, 125, 1490.

18. Feldermann, A.; Coote, M. L.; Stenzel, M. H.; Davis, T. P.; Barner-Kowollik, C. *J. Am. Chem. Soc.* **2004**, 126, 15915.

19. Karniadakis, G.; Sherwin, S. *Spectral/hp element methods for computational fluid dynamics*. Oxford University Press: **2013**.

20. Wulkow, M. *Macromol. React. Eng.* **2008**, 2, 461.

21. Wulkow, M. *Macromol. Theory Simul.* **1996**, 5, 393.

22. Barner-Kowollik, C.; Buback, M.; Charleux, B.; Coote, M. L.; Drache, M.; Fukuda, T.; Goto, A.; Klumperman, B.; Lowe, A. B.; McLeary, J. B.; Moad, G.; Monteiro, M. J.; Sanderson, R. D.; Tonge, M. P.; Vana, P. *J. Polym. Sci., Part A: Polym. Chem.* **2006**, 44, 5809.

23. Moad, G. *Macromol. Chem. Phys.* **2014**, 215, 9.

24. Moad, G.; Rizzardo, E.; Thang, S. H. *Aust. J. Chem.* **2009**, 62, 1402.

25. Moad, G.; Rizzardo, E.; Thang, S. H. *Aust. J. Chem.* **2012**, 65, 985.

26. Moad, G.; Rizzardo, E.; Thang, S. H. *Aust. J. Chem.* **2006**, 59, 669.

27. Mulvenna, R. A.; Weidman, J. L.; Jing, B.; Pople, J. A.; Zhu, Y.; Boudouris, B. W.; Phillip, W. A. *J. Membr. Sci.* **2014**, 470, 246.

28. Kim, E.; Ahn, H.; Park, S.; Lee, H.; Lee, M.; Lee, S.; Kim, T.; Kwak, E.-A.; Lee, J. H.; Lei, X.; Huh, J.; Bang, J.; Lee, B.; Ryu, D. Y. *ACS Nano* **2013**, 7, 1952.

29. Yoon, J.; Lee, W.; Thomas, E. L. *Adv. Mat.* **2006**, 18, 2691.

30. Runge, M. B.; Bowden, N. B. *J. Am. Chem. Soc.* **2007**, 129, 10551.

31. Rzayev, J.; Penelle, J. *Angewandte Chemie* **2004**, 116, 1723.

32. Zetterlund, P. B.; Gody, G.; Perrier, S. *Macromol. Theory Simul.* **2014**, 23, 331.

33. Sidney, L.; Srinivasa, S. *Sea Water Demineralization by Means of an Osmotic Membrane*. American Chemical Society: **1963**; Vol. 38, 117.

34. Zhang, Y.; Sargent, J. L.; Boudouris, B. W.; Phillip, W. A. *J. Appl. Polym. Sci.* **2015**, 132, 41683.

35. Dorin, R. M.; Phillip, W. A.; Sai, H.; Werner, J.; Elimelech, M.; Wiesner, U. *Polymer* **2014**, 55, 347.

36. Phillip, W. A.; Rzayev, J.; Hillmyer, M. A.; Cussler, E. L. *J. Membr. Sci.* **2006**, 286, 144.

37. Qiu, X.; Yu, H.; Karunakaran, M.; Pradeep, N.; Nunes, S. P.; Peinemann, K.-V. *ACS Nano* **2012**, 7, 768.

38. Hahn, J.; Clodt, J. I.; Filiz, V.; Abetz, V. *RSC Adv.* **2014**, 4, 10252.

39. Lee, K. P.; Arnot, T. C.; Mattia, D. *J. Membr. Sci.* **2011**, 370, 1.

40. Petersen, R. J. *J. Membr. Sci.* **1993**, 83, 81.

41. Hong, S.; Elimelech, M. *J. Membr. Sci.* **1997**, 132, 159.

42. Marshall, A.; Munro, P.; Trägårdh, G. *Desalination* **1993**, 91, 65.

43. Kwak, Y.; Goto, A.; Fukuda, T. *Macromolecules* **2004**, 37, 1219.

44. Konkolewicz, D.; Hawkett, B. S.; Gray-Weale, A.; Perrier, S. *J. Polym. Sci., Part A: Polym. Chem.* **2009**, 47, 3455.

45. Junkers, T.; Barner-Kowollik, C.; Coote, M. L. *Macromol. Rapid Commun.* **2011**, 32, 1891.

46. Ting, S. R. S.; Davis, T. P.; Zetterlund, P. B. *Macromolecules* **2011**, 44, 4187.

47. Calitz, F. M.; McLeary, J. B.; McKenzie, J. M.; Tonge, M. P.; Klumperman, B.; Sanderson, R. D. *Macromolecules* **2003**, 36, 9687.

48. Semsarilar, M.; Perrier, S. *Nat. Chem.* **2010**, 2, 811.

49. McLeary, J.; Calitz, F.; McKenzie, J.; Tonge, M.; Sanderson, R.; Klumperman, B. *Macromolecules* **2004**, 37, 2383.

50. McLeary, J.; Calitz, F.; McKenzie, J.; Tonge, M.; Sanderson, R.; Klumperman, B. *Macromolecules* **2005**, 38, 3151.

51. van den Dungen, E. T. A.; Matahwa, H.; McLeary, J. B.; Sanderson, R. D.; Klumperman, B. *J. Polym. Sci., Part A: Polym. Chem.* **2008**, 46, 2500.

52. Barner-Kowollik, C.; Coote, M. L.; Davis, T. P.; Radom, L.; Vana, P. *J. Polym. Sci., Part A: Polym. Chem.* **2003**, 41, 2828.

53. Vana, P.; Davis, T. P.; Barner-Kowollik, C. *Macromol. Theory Simul.* **2002**, 11, 823.

54. Junkers, T.; Delaittre, G.; Chapman, R.; Günzler, F.; Chernikova, E.; Barner-Kowollik, C. *Macromol. Rapid Commun.* **2012**, 33, 984.

55. Ranieri, K.; Delaittre, G.; Barner-Kowollik, C.; Junkers, T. *Macromol. Rapid Commun.* **2014**, 35, 2023.

56. Monteiro, M. J.; de Brouwer, H. *Macromolecules* **2001**, 34, 349.

57. Konkolewicz, D.; Hawkett, B. S.; Gray-Weale, A.; Perrier, S. *Macromolecules* **2008**, 41, 6400.

58. Chernikova, E.; Golubev, V.; Filippov, A.; Lin, C. Y.; Coote, M. L. *Polym. Chem.* **2010**, 1, 1437.

59. Schilli, C.; Lanzendörfer, M. G.; Müller, A. H. *Macromolecules* **2002**, 35, 6819.

60. Buback, M.; Junkers, T.; Vana, P. *Macromol. Rapid Commun.* **2005**, 26, 796.

61. Hawthorne, D. G.; Moad, G.; Rizzardo, E.; Thang, S. H. *Macromolecules* **1999**, 32, 5457.

62. Jitchum, V.; Perrier, S. *Macromolecules* **2007**, 40, 1408.

63. Germack, D. S.; Wooley, K. L. *J. Polym. Sci., Part A: Polym. Chem.* **2007**, 45, 4100.

64. Moad, G.; Solomon, D. H. *The Chemistry of Radical Polymerization*. Elsevier: **2006**.

65. Monteiro, M. J. *J. Chem. Phys.* **2005**, 43, 5643.

66. Wulkow, M.; Busch, M.; Davis, T. P.; Barner-Kowollik, C. *J. Polym. Sci., Part A: Polym. Chem.* **2004**, 42, 1441.

67. Coote, M. L.; Radom, L. *Macromolecules* **2004**, 37, 590.

68. Hiemenz, P. C.; Lodge, T. P. *Polymer Chemistry 2nd ed.* CRC Press: **2007**.

69. Vana, P. In *Kinetic aspects of RAFT polymerization*, Macromol. Symp., Wiley Online Library: **2007**; 71.

70. Rzayev, J.; Hillmyer, M. A. *J. Am. Chem. Soc.* **2005**, 127, 13373.

71. Perrier, S.; Barner-Kowollik, C.; Quinn, J. F.; Vana, P.; Davis, T. P. *Macromolecules* **2002**, 35, 8300.

72. Germack, D. S.; Wooley, K. L. *J. Polym. Sci., Part A: Polym. Chem.* **2007**, 45, 4100.

73. Germack, D. S.; Harrisson, S.; Brown, G. O.; Wooley, K. L. *J. Polym. Sci., Part A: Polym. Chem.* **2006**, 44, 5218.

74. Jitchum, V.; Perrier, S. *Macromolecules* **2007**, 40, 1408.

CHAPTER 4. TUNABLE NANOPOROUS MEMBRANES WITH CHEMICALLY-TAILORED PORE WALLS FROM TRIBLOCK POLYMER TEMPLATES

4.1 Overview

Membranes derived from self-assembled block polymers have shown promise as highly selective and highly permeable filters, but the complex synthetic routes and limited pore functionalities of existing systems need to be improved if these materials are to serve as a platform for the next generation of nanostructured membranes. Here, the facile synthesis of a polyisoprene-*b*-polystyrene-*b*-poly(*N*,*N*-dimethylacrylamide) (PI-PS-PDMA) triblock polymer using a controlled reversible addition-fragmentation chain transfer (RAFT) polymerization mechanism is reported. This material is then processed into a membrane using a self-assembly and non-solvent induced phase separation (SNIPS) technique, which creates an asymmetric, porous structure consisting of a selective layer that contains a high density of PDMA-lined pores (9.4×10^{13} pores m^{-2}) with an average diameter of 8.1 nm, as determined using solute rejection tests. Solvent flow experiments demonstrate that the PI-PS-PDMA membrane has a pH-independent permeability of 6 L m^{-2} h^{-1} bar^{-1}. The PDMA moiety lining the pore walls is converted, through simple hydrolysis in the solid state, to yield a poly(acrylic acid)-lined (PAA-lined) structure. The permeability of the PI-PS-PAA membrane is pH-dependent, and

ranges from 0.6 L m^{-2} h^{-1} bar^{-1} for solutions with a pH greater than 4 to 16 L m^{-2} h^{-1} bar^{-1} for a solution at pH 1. Solute rejection tests demonstrated a pore size of 2.6 nm for the PI-PS-PAA membrane, which is the smallest pore size reported to date for membranes fabricated from self-assembled block polymers. The facile synthesis of the PI-PS-PDMA material, the scalable SNIPS membrane fabrication protocol, and the simple conversion chemistry of the pore functionality demonstrate that these nanostructured membranes are a strong platform for applications within the range of water purification, pharmaceutical separations, sensors, and drug delivery.

4.2 Introduction

Ultrafiltration [1] (~10-100 nm pore size) and nanofiltration [2] (~0.5-2 nm in pore size) membranes are widely-used to effect size-selective separations in the water treatment and pharmaceutical industries [3, 4]. For example, metals [5], bacteria [6], and viruses [7] have been separated selectively from aqueous solutions using ultrafiltration (UF) and nanofiltration (NF) membranes [3]. Furthermore, UF and NF membranes have been used to mediate mass transfer in drug delivery, micropatterning, biological sensing, and immobilization applications [8]. As such, controlling the material compositions and nanostructures of these technology platforms is of prime import. Furthermore, the versatility and ease of processing [9] associated with polymeric systems make them the standard material for membrane fabrication [3].

While commercial membranes are dominated by homopolymer material systems, block polymer-based membranes are emerging as a technology that could be applicable

in a number of scenarios [10-13]. The utilization of these designer macromolecules enables the microphase-separated domains of the block polymer to template pore formation. Previously, this has occurred using either: 1) non-solvent induced phase separation techniques to generate anisotropic membranes [14-16] or 2) the self-assembly of block polymers into ordered nanostructures and the subsequent removal of one of the phases through selective etching techniques to yield monolithic structures [17-19]. In the phase inversion methodologies, porous channels form as the lyophilic shells of micelles contract during the casting process. This leaves the volumes previously occupied by the solvent-loving moieties as open pores [20-22]. Monolithic membrane pores are produced by the selective etching of specific well-ordered nanoscale domains [12, 17, 23]. In both processes, the resulting membranes have highly uniform pore sizes. However, use of the self-assembly and non-solvent induced phase separation (SNIPS) technique has been favored over monolithic templates recently due the ability to fabricate membranes with thinner selective layers, which result in higher fluxes without compromising size selectivity [11, 14-16, 21, 24].

Previous efforts to fabricate block polymer membranes via the SNIPS methodology have resulted in a limited number of pore functionalities. The heavily-studied polystyrene-*b*-poly(vinyl pyridine) (PS-PVP) and polyisoprene-*b*-polystyrene-*b*-poly(4-vinyl pyridine) (PI-PS-P4VP) [11, 14-16, 21, 24] systems are hindered by the limited chemical group conversion of the PVP functionality [24], which resides on the pore wall. In addition, the PI-PS-P4VP system relies on anionically-controlled polymerization mechanisms that can require low temperatures (–78 ºC), *in situ* solvent exchange procedures [11], and highly stringent *non aura* conditions. As such, a critical need exists for

a methodology that enables the large-scale production of block polymers such that nanostructured membranes can be generated that allow for: 1) high selectivity, 2) high flux, 3) straightforward materials syntheses, and 4) generation of tailored pore functionalities.

Here, we report the facile synthesis of a polyisoprene-*b*-polystyrene-*b*-poly(*N*,*N*-dimethylacrylamide) (PI-PS-PDMA) triblock polymer using a controlled reversible addition-fragmentation chain transfer polymerization mechanism. Subsequently, the PI-PS-PDMA is cast into a functional membrane with an ordered, yet asymmetric, nanostructure using a self-assembly and non-solvent induced phase separation process. This particular triblock polymer is selected because the combination of the PI and PS domains provide mechanical integrity to the membrane while the PDMA domain allows for the pore walls of the membrane to have specific, and easily-tailored, chemical functionality [11, 25, 26]. The structure of this tapered nanoporous thin film allows for a sharp size-selective cut-off down to ~1 nm in pore size while retaining a relatively high flux. The PDMA moiety of the triblock polymer lines the pore walls of the membrane, and we demonstrate that it can be converted, through simple hydrolysis in the solid state, to yield a poly(acrylic acid)-lined (PAA-lined) structure. This acrylic acid functionality allows for a size selectivity that is at the lower bound of block polymer-based separations, and it has been shown to be a robust platform to add any number of chemistries to the membrane walls [27]. This combination of these unique features enable these membranes to be used as a readily-fabricated platform for high flux, high performance nanoscale applications.

4.3 Results and Discussion.

Controlled radical (*e.g.*, RAFT) polymerization enables any existing free radical polymerization, which dominates the current polymer synthesis marketplace, to be retrofitted for the facile synthesis of block polymers by the simple addition of a RAFT (or any other living free radical controlling) agent. For this reason, the PI-PS-PDMA triblock polymer used in this work was synthesized using a RAFT-mediated polymerization mechanism. A combination of ^{1}H NMR spectroscopy and size exclusion chromatography (SEC) indicated the synthesis of a relatively low dispersity, high molecular weight triblock polymer. The PI, PS, and PDMA blocks had ^{1}H NMR-determined molecular weights of 14.2 kDa, 31.1 kDa and 23.3 kDa, respectively (Figure 4.1a). This corresponds to a volume fraction of 24%, 46% and 30%, respectively (based on the following values of the homopolymer densities at 25 °C: ρ_{PI} = 0.92 g cm^{-3}, ρ_{PS} = 1.06 g cm^{-3}, and ρ_{PDMA} = 1.21 g cm^{-3}) [28]. The PI-PS-PDMA had a dispersity (*Đ*) value of 1.3, based on polystyrene standards, and showed a clean shift in SEC elution times as the molecular weight increased after successive additions of the PS and PDMA blocks (Figure 4.1b).

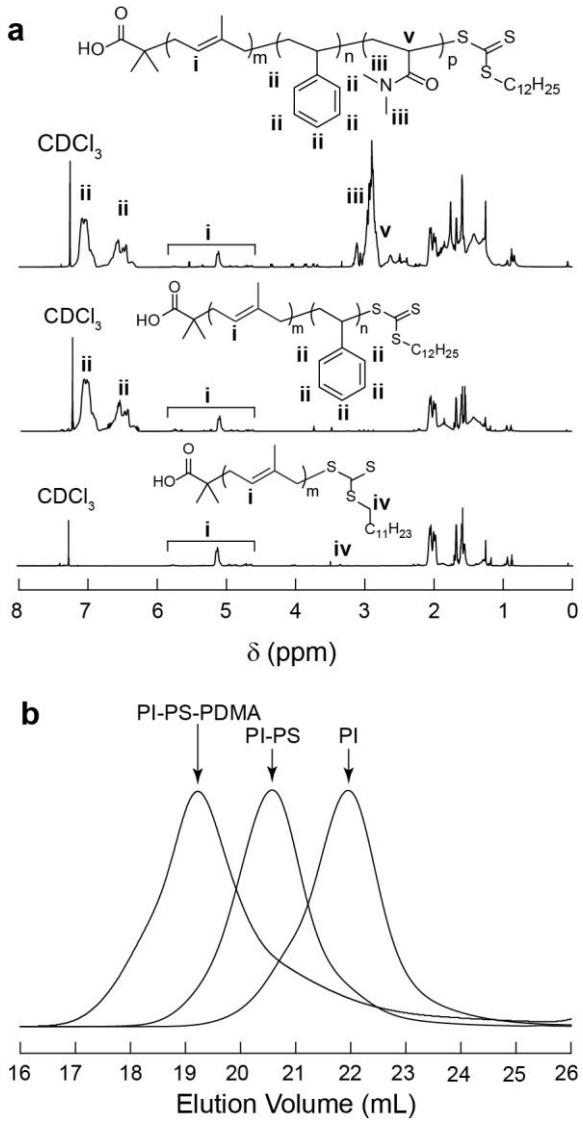

Figure 4.1. (a) ^{1}H NMR spectra of the PI (lower) and PI-PS (middle) precursors and the PI-PS-PDMA triblock polymer (upper). Characteristic peaks from each moiety are labeled to highlight the relative composition the triblock polymer. (b) SEC traces of the triblock polymer series with THF as the mobile phase at a flow rate of 1 mL min^{-1}. The clean shift (*i.e.*, no trailing or coupling signals) indicates the ability of the PI homopolymer and the PI-PS diblock copolymer to serve as macroinitiating agents for the synthesis of the PI-PS-PDMA triblock polymer.

This specific triblock polymer composition was targeted because prior work that used self-assembled block polymers as templates for the nanostructure of porous membranes suggested that a hexagonally close-packed (HCP) geometry in the powder state is conducive to the formation of high quality membranes [11, 29]. SAXS analyses of the pressed powder PI-PS-PDMA sample were consistent with the HCP morphology with peaks shown at 1, √3, √4, √7 and √9 multiples of the principal reflection, q^* (Figure 4.2a).

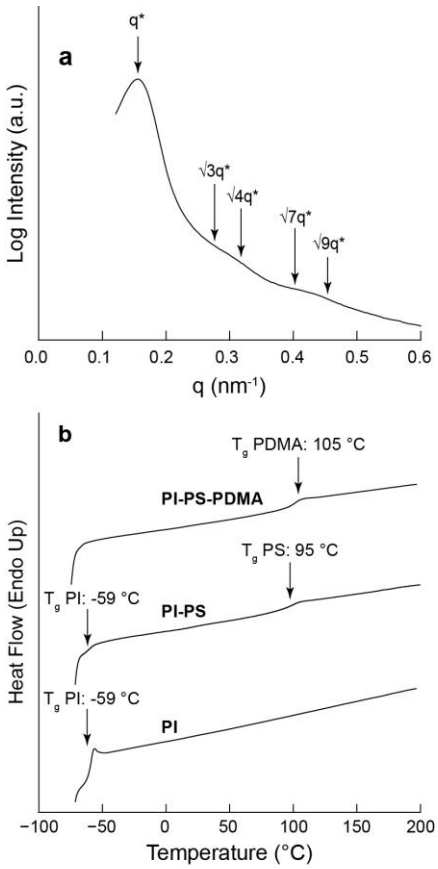

Figure 4.2. (a) Small-angle x-ray scattering (SAXS) data of the bulk PI-PS-PDMA powder. Note that the principle reflection (q^* = 0.151 nm^{-1}) indicates a solid state domain spacing of ~42 nm. The listed reflections suggest a hexagonally-packed structure for the PI-PS-PDMA powder in the solid state. (b) The second heating scan of DSC traces of the PI and PI-PS precursor samples and the PI-PS-PDMA triblock polymer. The glass transition temperature (T_g) values for each domain in these samples corresponds well with the glass transition temperature values measured for equivalently-sized homopolymer analogs. Discrete glass transition temperatures in the triblock polymers were not observed readily due to the close proximity of the glass transition temperatures of PS and PDMA.

The triblock polymer, PI-PS-PDMA, was synthesized instead of a diblock copolymer analog, PS-PDMA, because incorporating the rubbery, low T_g PI block (DSC traces are provided in Figure 4.2b) improves the mechanical response of the ultimate membrane. Tensile testing conducted using the bulk PI-PS-PDMA material (Figure 4.3) supports this hypothesis. Specifically, the mechanical toughness of the PI-PS-PDMA sample is consistent with the toughness of PI-PS-P4VP triblock polymers studied in prior work that demonstrated the advantages of moving from diblock to multiblock systems when fabricating nanostructured porous materials [11].

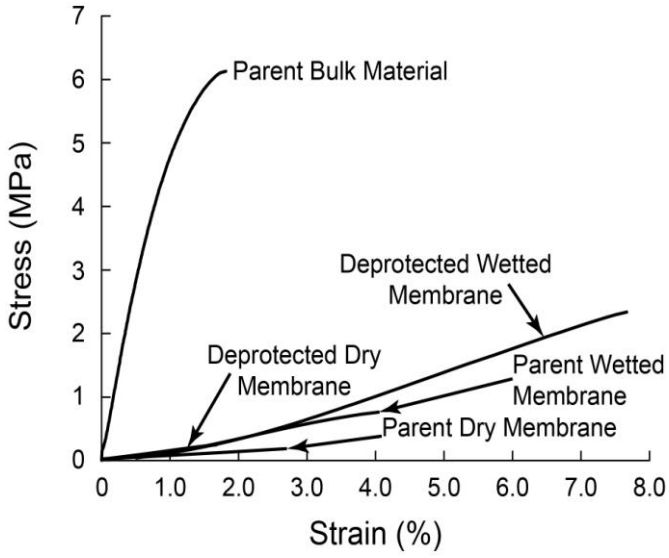

Figure 4.3. Stress-strain curves of the bulk material and of cast membranes. The parent bulk material, composed of PI-PS-PDMA, has a toughness of 6.7 kJ m^{-3}. The parent membrane, has a toughness of 2.4 kJ m^{-3} (dry) state and 1.7 kJ m^{-3} (wet). The PI-PS-PAA membrane, has a toughness of 1.7 kJ m^{-3} (dry) and 9.6 kJ m^{-3} (wet), respectively. The significant increase in toughness of the membranes in the wetted state may be attributed to the serendipitous feature of crosslinking of PI domains in the presence of strong acids for prolonged periods at elevated temperatures while converting from PDMA to PAA .

Asymmetric membranes were fabricated from the PI-PS-PDMA triblock polymer using the SNIPS technique described above. The anisotropic structures of the membranes produced by the SNIPS method are displayed in the cross-sectional SEM micrographs shown in Figure 4.4. These micrographs indicate that the total membrane thickness (~40 – 50 μm) consists of two sections, a denser top (selective) layer and a more porous underlying (gutter) layer. The ~10-micrometer-thick dense layer is situated at the top of the micrograph, which corresponds to the surface of the membrane that was exposed to the atmosphere during solvent evaporation. The triblock polymer concentration in this region increases significantly during the evaporation step causing the block polymer to self-assemble and template the nanostructure of the membrane in this upper region. A micrograph of the top surface of the parent membrane shows an average of 9.4×10^{13} pores m^{-2} with an average pore diameter of 53 nm and a standard deviation of 20 nm (Figure 4.5a). Below the dense layer, the membrane quickly opens into macrovoids that are characteristic of membranes formed via phase inversion [30], rather than block polymer self-assembly. Due to the relatively large sizes of these voids, this underlying layer provides minimal resistance to flow while providing mechanical support to the selective layer, which increases the durability of the membrane.

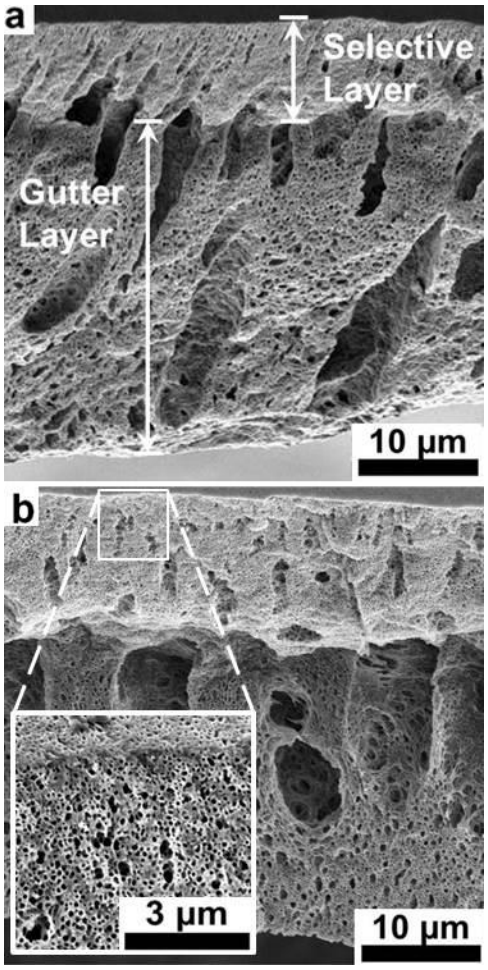

Figure 4.4. Cross-sectional SEM micrographs of the triblock polymer membranes. The asymmetric structure of the (a) parent PI-PS-PDMA and (b) deprotected PI-PS-PAA membranes consist of a selective layer and a gutter layer, which contains microscopic voids. In the inset of (b), a higher magnification micrograph of the PI-PS-PAA top-surface-cross-section interface shows the structure of the ~10 µm active layer as it opens into the microporous support layer.

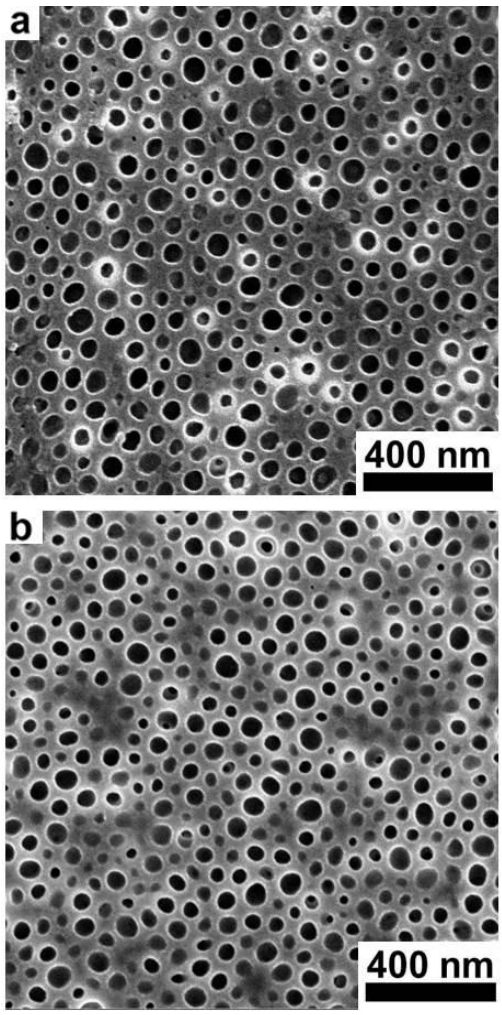

Figure 4.5. SEM micrographs of the top surface of the block polymer-derived membranes. (a) The active layer surface of the PI-PS-PDMA parent membrane that was cast from a 15% (by weight) polymer solution in a 70/30 (w/w) mixture of dioxane and tetrahydrofuran as solvent with a 75 s evaporation time (b) The active layer surface of a converted PI-PS-PAA membrane. This membrane is produced by soaking a parent membrane in a 6 M hydrochloric acid solution for 48 hours at 85°C. Note that the structural features of both surfaces are approximately the same despite the chemical treatment used.

The hydraulic permeability of the parent membrane was determined by measuring the water flux at applied pressures ranging from 5 to 40 psi. The water flux vs. applied pressure data were fit with a linear equation, whose slope is equal to the hydraulic permeability [3]. In Figure 4.6, the blue squares represent the hydraulic permeability of the parent membrane for feed solutions of pH 2.5, 5.5, and 10.5. Over this pH range, the hydraulic permeability of the parent membrane was constant at a value of ~6 L m^{-2} h^{-1} bar^{-1}. This indicates that the PDMA groups (pKa = 7.3) lining the pore walls are not affected by the pH of the solution [31].

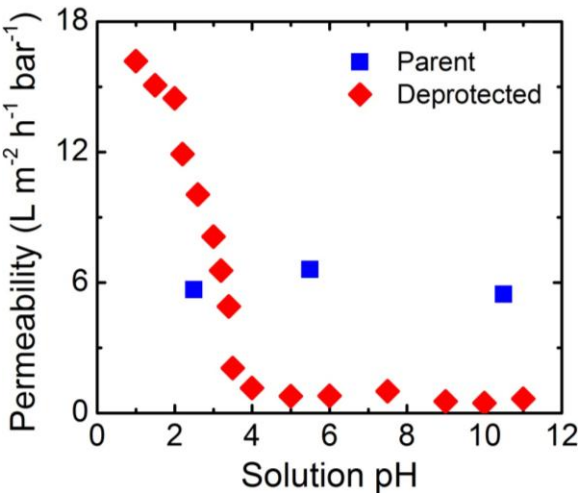

Figure 4.6. Hydraulic permeabilities of the parent (*i.e.*, PDMA-functionalized) and deprotected (*i.e.*, PAA-functionalized) membranes plotted vs. solution pH. For pH values ranging from 2-11, the parent membrane had a constant hydraulic permeability of 6 L m^{-2} h^{-1} bar^{-1}. The PI-PS-PAA membrane had a permeability of 0.6 L m^{-2} h^{-1} bar^{-1} from pH 4-12. Below pH 4, the permeability of the PI-PS-PAA membrane increased monotonically; reaching a permeability of 16 L m^{-2} h^{-1} bar^{-1} at pH 1.

Molecular weight cutoff tests were performed on the parent membrane to probe its ability to reject molecules based on differences in solute size. In these experiments, the membrane was challenged with solutions containing PEO molecules ranging in molecular weight from 1.1 to 10 kDa. Using literature data for the intrinsic viscosity and diffusion coefficients of PEO, the hydrodynamic radii were calculated to range from 0.75 to 3.0 nm.[32, 33] Percent rejection values were calculated by comparing the concentration of PEO in the solution that permeated the membrane to the concentration of PEO in the initial feed solution. The results of the solute rejection experiments are represented by the blue squares in Figure 4.7; a MWCO curve (*i.e.*, solute rejection plotted against molecular weight of the solute) is also provided in Figure 4.8. During these experiments, the feed solutions were stirred at 400 rpm to produce mass transfer coefficients, k, on the order of 1.0×10^{-5} m s^{-1} [4], while the water flux, J_w, during the MWCO tests was equal to 7.9×10^{-7} m s^{-1}. Because this results in a J_w/k value around 0.13, which is significantly lower than the suggested limit where concentration polarization becomes severe, the presented results are solely a function of the ability of the triblock polymer membrane to separate solutes based on size [4, 34].

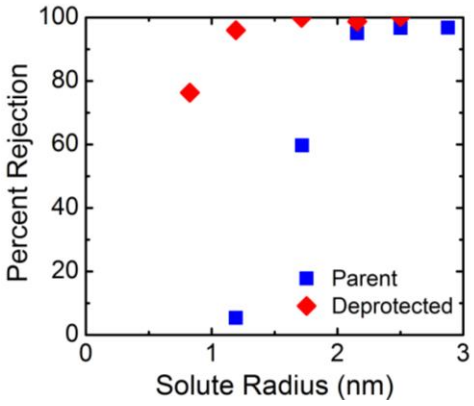

Figure 4.7. Solute rejection curves for the parent and deprotected (*i.e.*, PAA-functionalized) membranes were generated using solutions that contained polyethylene oxide (PEO) molecules as model solutes of known size. PEO molecular weights of 1.1, 2.1, 4.0, 6.0, 7.8, and 10.0 kDa were used. The percent rejection was determined by taking the ratio of the PEO concentration in the permeate to the 1 g L^{-1} feed.

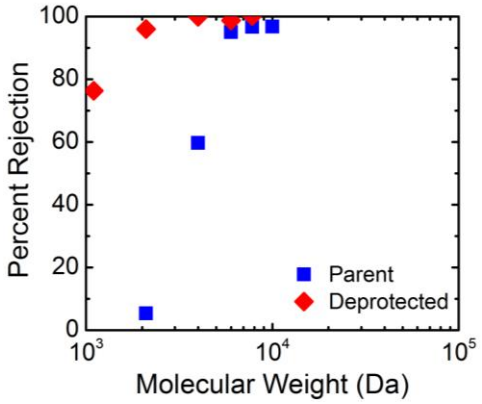

Figure 4.8. Molecular weight cut-off (MWCO) curves for the parent and deprotected membranes shown in Figure 4.4. Here, they are plotted against molecular weight of solute molecules. The solutions contained polyethylene oxide (PEO) molecules of 1.1, 2.1, 4.0, 6.0, 7.8, and 10.0 kDa molecular weights. The percent rejection was determined by taking the ratio of the PEO concentration in the permeate to the 1 g L^{-1} feed.

For the parent membrane, solutes with a hydrodynamic radius greater than 2.2 nm, (*i.e.*, the 6.0 kDa PEO molecule) were almost completely rejected. Molecules with hydrodynamic radii smaller than 1.2 nm (*i.e.*, the 2.1 kDa PEO sample) permeate through the membrane with little (~4%) rejection. The 4.0 kDa PEO sample, which has a hydrodynamic radius equal to 1.7 nm, was only partially rejected (60% rejection). This point of datum, in conjunction with established theories for size-selective separations, was used to estimate the pore size of the parent membrane at 8.1 nm in diameter [35].

It is noted that there is a significant disagreement in the reported pore size of the parent membrane between that calculated from MWCO data (8.1 nm) in the wetted state and that observed in SEM micrographs (53 nm) in the dried state (Figure 4.5). This may be attributed to the swelling of the PDMA domains in a wetted environment [28, 36]. The average number of repeat units in a linear PDMA block with molecular weight of 23.3 kDa can be approximated as N_{PDMA} = 235. In the upper limit that the chains are fully extended with a carbon-carbon bond length (l) of 1.4 Å, the PDMA chain length as a rigid rod (*i.e.*, neglecting any geometrical constraints associated with bond angles) $L = 2 N l$ would be 65.8 nm.[37] Therefore, the pore would be closed completely if the chains were extended fully (131.6 nm) from both sides of the pore. However, due to the balance between the enthalpy of solvent-repeat unit mixing and the entropy associated with chain stretching, it is known that the length of moderate-density, surface-grafted polymer brush chains will scale as $N^{0.6}$, if the polymer brush is in a good solvent [38, 39]. This scaling behavior changes when the polymer brush is confined to a nanoscale cylinder. Specifically, computational models predict that, for relatively large polymers in the moderate brush density regime, the size of the polymer brush will scale with $N^{0.8}$ in a

good solvent [40, 41]. Using the scaling from computations, the extended PDMA brush within the pore would be ~22 nm long. Therefore, the effective pore diameter for the membrane in the wetted state (*i.e.*, the pore size calculated from MWCO tests) would be 44 nm smaller relative to the dry state (*i.e.*, the pore size determined using the SEM images)

In order to probe this hypothesis experimentally, the structure of the PI-PS-PDMA membrane was characterized in the solvated state by wetting the pores of the membrane with the hydrophilic ionic liquid, 1,3-dimethylimidazolium bis(trifluoromethyl)sulfonylimide ([mmim][Tf_2N]). Because the vapor pressure of [mmim][Tf_2N] approaches zero, its evaporation rate in the vacuum environment of the SEM is negligible, which enables the conformation of solvated PDMA brushes to be observed using electron microscopy. In the solvated state, the PDMA brushes extend toward the center of the pore reducing the effective pore diameter (Figure 4.9). In some cases, it appears that the extended PDMA chains span the pore width and form mushroom-like structures. This extension of the PDMA brushes into the pores of the membrane also provides a rationalization for the very sharp MWCO reported in Figure 4.8 despite the spread in pore sizes observed in Figure 4.5.

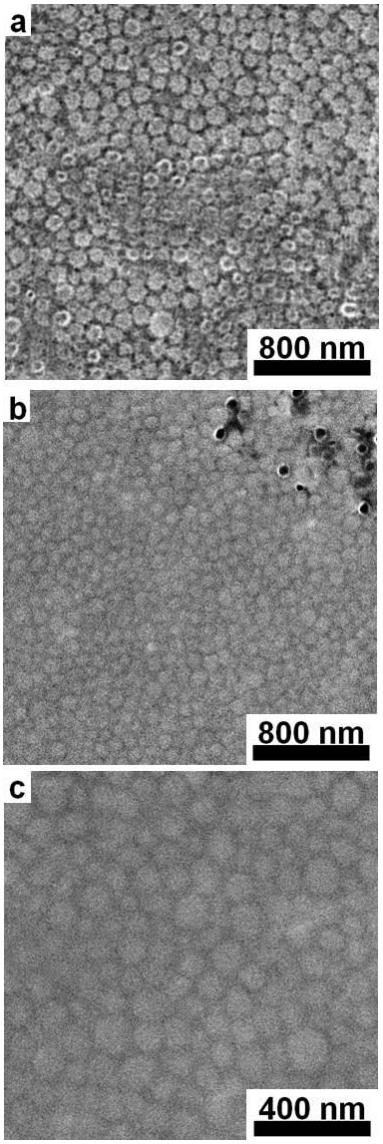

Figure 4.9. SEM micrographs of triblock polymer membranes wet with the ionic liquid 1,3-dimethylimidazolium bis(trifluoromethyl)sulfonylamide ([mmim][Tf_2N]). (a) The top surface of the PI-PS-PDMA membrane contains a combination of open pores and mushroom-like structures due to the swelling of the PDMA chains in [mmim][Tf_2N]. (b) Pores are not visible on the top surface of the PI-PS-PAA due to the swelling of the PAA chains in [mmim][Tf_2N]. (c) A higher magnification micrograph of the top surface of the PI-PS-PAA membranes.

While the tight molecular weight cutoff of the PI-PS-PDMA-based membrane is useful, the conversion of the pore walls to a specific functionality will be of utility in the production of fouling-resistant and/or chemically selective membranes. Specifically, based on the relative quality of the casting solvents for the three blocks of the block polymer and the difference in pore size determined between the dry and wet states, we hypothesize that the parent membrane contains PDMA-lined nanopores that provide the ability to tailor the chemical functionally of the membrane post fabrication. Taking advantage of this useful property requires the conversion of the PDMA block to the carboxylic acid derivative, poly(acrylic acid) (PAA); previously, it has been shown that PAA can be used as a versatile platform for functional group conversion to a variety of different moieties [26].

The conversion of the PDMA moiety to PAA was performed via submersion of the parent membrane in an aqueous 6 M HCl solution. No appreciable conversion of PDMA to PAA was observed at temperatures below 60 ºC; however, a high degree of conversion was observed at a solution temperature of 85 ºC, in agreement with previous reports [26]. Deprotection of the poly(*N*,*N*-dimethylacrylamide) groups to poly(acrylic acid) groups (PAA) was monitored by the decreasing intensity of the characteristic carbonyl stretch from the PDMA peak (labeled a in Figure 4.10) and the simultaneous increase in the characteristic carbonyl stretch from PAA peak (labeled b in Figure 4.10). The disappearance of the characteristic carbonyl stretch from the PDMA demonstrates the complete conversion of the DMA group occurs after 48 hours of exposure (Figure 4.10).[26]

No discernible degradation of the membrane matrix occurred during the deprotection stage. This is supported by mechanical testing of the PDMA-functionalized and PAA-functionalized membranes (Figure 4.3), which demonstrates that the toughness of the PAA-functionalized membrane is slightly larger than that of the PDMA-functionalized membrane. This serendipitous increase in toughness may be attributed to crosslinking within the PI domains that occurs when the membrane is exposed to a strong acid at elevated temperatures while converting from PDMA to PAA .

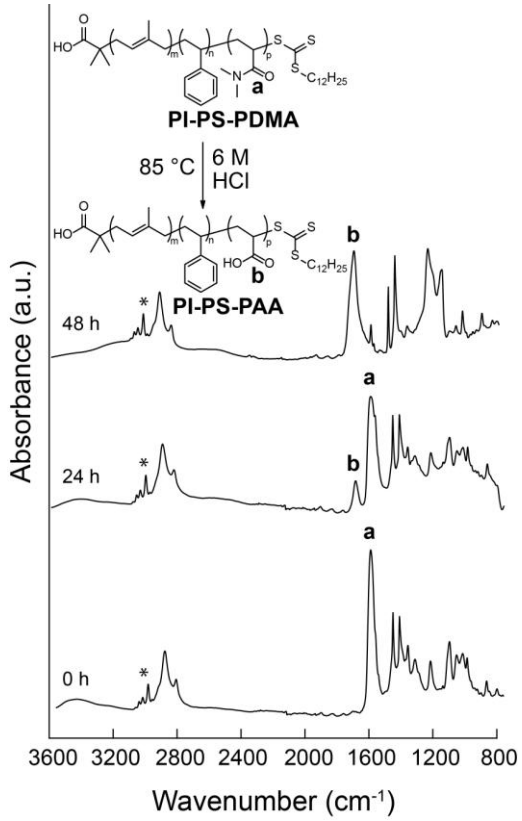

Figure 4.10. Attenuated Total Reflectance Fourier Transform Infrared Spectroscopy (ATR-FTIR) monitoring the conversion of the pore walls from PDMA to PAA by suspension of the cast membrane in a 6 M HCl solution at 85 °C as a function of time. The signal at ~1600 cm^{-1} corresponds to the characteristic carbonyl stretch from the PDMA peak labeled a while the absorption at ~1700 cm^{-1} corresponds to characteristic carbonyl stretch from PAA peak labeled b. As shown in the uppermost spectrum, peak a deceases with time as PDMA is converted to PAA, where the reaction nears full conversion at a reaction time of 48 h. The relative intensities are standardized using the characteristic aromatic C-H stretches (*) of the un-reactive polystyrene domain between 3100-3000 cm^{-1}.

Figures 4.4b and 4.5b show SEM micrographs of the membrane cross-section and top surface, respectively, following the exposure to 6 M HCl at an elevated temperature

for 48 hrs. In the dried state, the structure of this converted membrane has the same characteristic features as that of the parent membrane. Furthermore, the porosity, average pore size, and pore density on the surface of the PAA-lined membrane were estimated, and their values were found to be within 4% of the values reported for the parent membrane. The data above demonstrate that the PDMA block has been converted to the PAA block in the solid state successfully and the nanostructure of the asymmetric triblock polymer membrane in the dry state is not altered significantly by the deprotection protocol.

Following the conversion to PAA, the hydraulic permeability of the membrane was determined over a pH range between 1 and 12. These data are represented by the red diamonds in Figure 4.6. The permeability of the membrane remained low (~0.6 L m^{-2} h^{-1} bar^{-1}) as the pH of the feed solution was decreased from pH 12.0 down to 4.0. At pH 3.5, there was a sharp increase in permeability. As the pH was decreased further, the permeability continued to increase and exceeded that of the parent membrane around pH 3.0. The permeability did not plateau with further decreases in pH, and the maximum determined permeability was over 16 L m^{-2} h^{-1} bar^{-1} at a pH of 1.0, which is comparable to high flux commercial nanofiltration membranes [42, 43].

It is hypothesized that the dependence of the permeability on pH is due to the extension and contraction of the PAA chains lining the walls of the pores in the membrane. At high pH, the deprotonated PAA is negatively charged, which causes the PAA chains to extend into the open pores. Because the deprotonated PAA chains contain negative charges that repel each other, the PAA brushes extend farther into the pores of

the membrane than the neutrally-charged PDMA brushes of the parent membrane, which results in a lower permeability. As the solutions tested become more acidic, and pH decreases, the PAA is protonated. The neutrally-charged polymer chains are able to collapse back, in part, toward the pore wall. This increases the effective diameter of the pores, which results in higher permeabilities [44]. A similar observation has been made for membranes containing poly(4-vinyl pyridine) [45, 46].

The pH-responsive nature of the PI-PS-PAA membrane is verified by tapping-mode atomic force microscopy (AFM), which demonstrates that the swelling characteristics of the membrane in water exhibit a clear weak polyacid behavior. Using a liquid cell attachment, the surface morphology of a PI-PS-PAA membrane was observed under several different solution pHs (Figure 4.11). In Figure 4.11a, the top surface of a PI-PS-PAA membrane in the dry state has a high density of clearly defined pores with sharp edges. The density of pores is ~ 9.0×10^{-13} pores m^{-2}, which is consistent with the SEM results in Figure 4.3. It is noted that the pores observed by AFM possess V-shaped edges, which is possibly a result of the pyramidal shape of the AFM tip used. By section analysis (NanoScope Analysis), the average depth of the pores in the dry state is ~30 nm.

In an acidic solution (pH = 2.98), the surface of the membrane displays a swollen morphology (Figure 4.11b). The pores of the membrane can still be observed but show a lower depth (~19 nm) and lower slope of the pore edge than the dry membrane. When the pH is increased to pH = 6.88, no pores are observed by AFM (Figure 4.11c). Instead, a blurred featureless surface, which is similar to the morphology of fully swollen polymer brushes, is observed. This blurred featureless surface is consistent with SEM micrographs of the top surface of the PI-PS-PAA membrane when the PAA brushes that line the pore

wall are solvated by [mmim][Tf_2N] (Figure 4.9b). This behavior supports the hypothesis that the pH-responsive nature of the membrane is a result of the PAA brushes lining the pore surface. With increasing pH, the charge fraction of PAA chains increases and the chains expand into the bulk solution to minimize electrostatic repulsion, and as a result the pore diameter and slope of the pore edge are reduced.

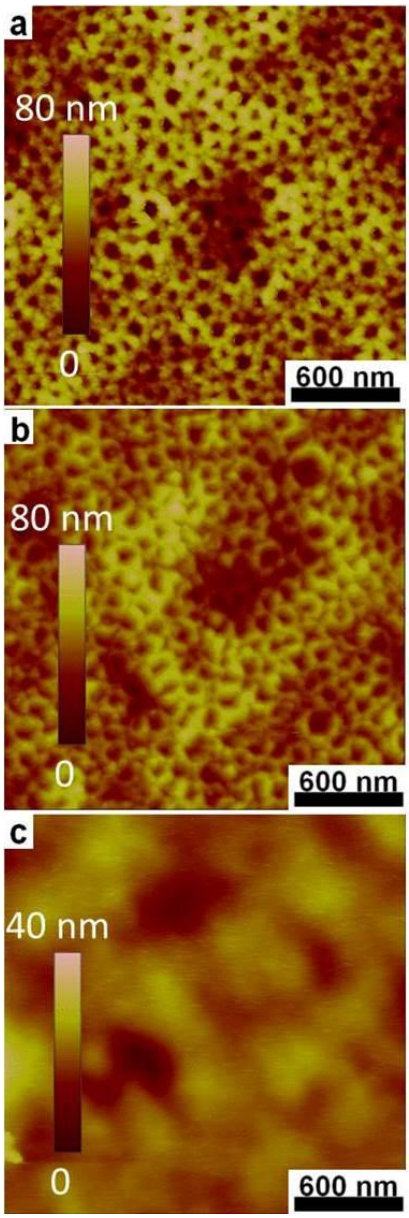

Figure 4.11. AFM micrographs of a PI-PS-PAA membrane in various environments. (a) Well-defined pores are noticeable on the surface of the dry membrane. (b) In a 50 mM acetic acid solution (pH = 2.98), the PAA brushes swell partially, which reduces the effective pore size. (c) In 50 mM ammonium acetate solution (pH = 6.88), the PAA brushes have swollen significantly, and there are no longer AFM-detectable pores on the surface.

A molecular weight cutoff experiment after conversion of PDMA to PAA was performed and resulted in the curve shown by the red diamonds shown in Figure 4.7 and Figure 4.8. This experiment was performed in deionized water (pH = 5.5) where the PAA chains that line the pore walls are expected to extend into the pores, constricting flow. The curve shows nearly complete rejection for solutes with characteristic radii above 1.25 nm, and moderate rejection (~76%) for solutes that are 0.8 nm in radius. This curve has shifted to the left of the parent curve, again suggesting that the pore size of the PAA-lined membrane is smaller than the parent membrane. Based on the theory for size-selective transport [35], the pore diameter of the converted membrane is calculated to be 2.6 nm in diameter, compared to 8.1 nm for the parent membrane. This PI-PS-PAA membrane retains its high selectivity after deprotection and is able to perform size-selective separations for solutions containing particles with hydrodynamic radii of ~1 nm. This is in the extreme lower limit of pore sizes for membranes based on block polymers; in fact, it is the smallest diameter reported for nanoporous films originating from block polymer templates. As such, this membrane architecture presents a new paradigm in block polymer based separations. Furthermore, the ability of tunable pore functionality makes this carboxylic acid-functionalized membrane analog a highly versatile and powerful platform for nanoscale separations.

4.4 Conclusion

These results demonstrate the ability to use a PI-PS-PDMA triblock polymer, synthesized via the easily-controlled RAFT polymerization mechanism, as a templating

agent for the nanostructure of asymmetric, porous membranes that are produced using the SNIPS technique. Furthermore, the PDMA block that lines the pore walls of the membrane can be converted cleanly by simply soaking the membrane in an HCl solution to yield PAA-lined pores. This enables the pore functionality to be chemically-tailored without degradation of the membrane nanostructure. Additionally, the high densities of well-defined pores in these membranes are capable of producing size selective separations for solutes as small as 8 nm in the as-synthesized PI-PS-PDMA state and 2 nm in diameter after conversion to the PI-PS-PAA state. The unique combination of properties provided by the PI-PS-PDMA material will enable next-generation membranes that meet the process demands of multiple high value separations (*e.g.*, water purification, biopharmaceuticals separations) to be designed and produced in a simple and facile manner.

4.5 Acknowledgements

We gratefully acknowledge support from the Ralph W. and Grace M. Showalter Research Trust Award at Purdue University. Portions of this work were made possible with support from the Indiana Clinical and Translational Sciences Institute funded, in part by Grant Number TR000006 (Project Manager: Dr. Thomas Sors) from the National Institutes of Health, National Center for Advancing Translational Sciences, Clinical and Translational Sciences Award through the Collaboration in Translational Research (CTR) Pilot Program. Portions of this research were carried out at the Stanford Synchrotron Radiation Lightsource, a Directorate of SLAC National Accelerator and an Office of

Science User Facility operated for the U.S. Department of Energy Office of Science by Stanford University. Portions of this research were also performed with the equipment from the Center for Environmental Science and Technology (CEST) at Notre Dame and Notre Dame Integrated Imaging Facility (NDIIF).

4.6 Supplementary Information

4.6.1 Materials and Methods.

The ^{1}H NMR spectra were measured on a Bruker DRX500 spectrometer using a ~1% polymer solution (by weight) in deuterated chloroform (Sigma-Aldrich). Size exclusion chromatography (SEC) data were collected on a Hewlett-Packard 1260 Infinity series equipped with a Hewlett-Packard G1362A refractive index (RI) detector and three PLgel 5 μm MIXED-C columns. The mobile phase consisted of tetrahydrofuran (THF) at 35 °C fed at a flow rate of 1 mL min^{-1}. The SEC was calibrated using polystyrene standards (Agilent Easi Cal) with molecular weights ranging from 1 kg mol^{-1} to 200 kg mol^{-1}. Differential scanning calorimetry (DSC) data were collected using a TA Instruments Q20 Series differential scanning calorimeter. The samples were initially heated to 200 °C, held isothermally for 10 minutes before being cooled to –75 °C under a nitrogen gas purge. The data shown are from the final scan from –75 °C to 200 °C at a heating rate of 10 °C min^{-1}. Attenuated total internal reflectance-Fourier transform infrared (ATR-FTIR) spectroscopic measurements were acquired using a Thermo-Nicolet Nexus FTIR equipped with a diamond substrate. Under a constant purge of nitrogen, the ATR-FTIR data were collected in 32 scans in the range of 4500 - 800 cm^{-1} using a

deuterated triglycine sulfate (DTGS) KBr detector and KBr beam splitter. Small angle x-ray scattering (SAXS) measurements of the polymer powder, containing ~1% (by weight) butylated hydroxytoluene (BHT), were prepared by pressing a 2-mm-thick polymer disc into a washer using a Carver press. The powder sample was then annealed at 180 °C for 24 h under vacuum and then cooled to room temperature. SAXS experiments were conducted at beamline 1-4 of the Stanford Synchrotron Radiation Lightsource (SSRL).

All chemicals were purchased from Sigma-Aldrich unless otherwise noted. Degassed, inhibitor free tetrahydrofuran (THF) (Sigma-Aldrich) was purified by passage through an alumina column (Innovative Technology). Isoprene, styrene, and *N*,*N*-dimethylacrylamide were purified by passage through a basic alumina (Fisher Scientific) column prior to use. A Millipore water purification system (Milli Q Advantage A10, Millipore Corporation, Bilerica, MA) provided deionized water, which was used as the non-solvent during membrane fabrication, in preparing solutions for permeability and solute rejection tests, and for rinsing the test cell at the conclusion of an experiment.

4.6.2 Polymer Synthesis and Characterization

As shown in Scheme 4.1, a reversible addition-fragmentation chain transfer (RAFT) polymerization mechanism was utilized for the synthesis of the PI-PS-PDMA triblock polymer used in this work.

Scheme 4.1. Synthesis of the polyisoprene-*b*-polystyrene-*b*-poly(*N,N*-dimethylacrylamide) (PI-PS-PDMA) triblock polymer.

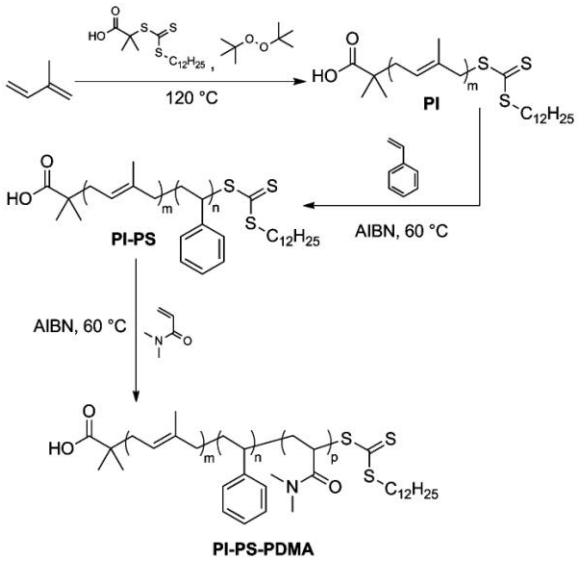

A RAFT-mediated polymerization mechanism was utilized for the synthesis of polyisoprene [47]. The polymerization was performed in a 25 mL vacuum flame-dried reaction flask containing a Teflon-coated magnetic stir bar. 15 mL (0.15 mol) of isoprene, 24.2 mg (0.07 mmol) of 2-(dodecylthiocarbonothioylthio)-2-methylpropanoic acid (chain transfer agent) and 2.5 μL (0.01 mmol) of *tert*-butyl peroxide were added to the reaction flask. Once the solids were dissolved completely in the solution, four freeze-pump-thaw cycles were performed. Next, the reaction flask was refilled with argon and the reaction was heated to 120 °C. The solution in the reaction flask was stirred at 120 °C for 40 hours. The mixture was cooled to room temperature, precipitated in methanol three times, and the product (PI) dried under vacuum for 24 hours (M_n = 14.2 kDa via ^{1}H NMR; $Đ$ = 1.3).

The polymerization was performed in a 25 mL flame-dried reaction flask containing a Teflon-coated magnetic stir bar. 0.94 g (0.07 mmol of chain transfer end groups) of PI, 11.6 mL (0.10 mol) of styrene, 1.4 mole equivalents of dioxane (0.14 mol, 12.0 mL), and 0.872 mg of AIBN (5.3 μmol) were added to the reaction flask. Once the solids were dissolved completely in the solution, four freeze-pump-thaw cycles were performed. Next, the reaction flask was refilled with argon and the reaction was heated to 60 °C. The reaction was stirred at this temperature for 4.25 days. The mixture was cooled to room temperature, precipitated in methanol three times, and the product (PI-PS) was dried under vacuum for 24 hours (M_n = 45.3 kDa via ^{1}H NMR; $Đ$ = 1.2).

The synthesis of the PDMA block was performed in a 100 mL flame-dried reaction flask containing a Teflon-coated magnetic stir bar. 1 g (22.0 μmol of chain transfer end groups) of the PI-PS macroinitiator, 15.8 mL (0.15 mol) of *N*,*N*-dimethylacrylamide, 3 volume equivalents of THF (47.5 mL) and 0.45 mg (2.8 μmol) of AIBN were added to the reaction flask. Once the solids were dissolved completely in the solution, four freeze-pump-thaw cycles were performed. Next, the reaction flask was refilled with argon and the reaction was heated to 60 °C. The reaction was stirred at this temperature for 1.3 hours. The mixture was cooled to room temperature, precipitated in cold hexanes three times, and the product (PI-PS-PDMA) dried under vacuum for 24 hours (M_n = 68.6 kDa via ^{1}H NMR; $Đ$ = 1.3).

Membranes were cast using the self-assembly and non-solvent induced phase separation (SNIPS) method. The casting solutions were prepared by dissolving the PI-PS-PDMA triblock polymer at a concentration of 15% (by weight) in a 70%-30% (by

weight) mixture of dioxane-tetrahydrofuran. After the triblock polymer was dissolved completely, the solution was allowed to sit unstirred overnight to allow dissolved gases to escape from solution. To prepare a membrane, the solution was drawn into a thin film on a glass substrate using a doctor blade set at a gate height of 254 μm. After casting, the solvent was allowed to evaporate from the film for a period of 75 seconds, and the film was plunged subsequently into a non-solvent (deionized (DI) water) bath to induce polymer precipitation. After fabrication, membranes were stored in DI water to prevent drying of the films.

4.6.3 Preparation of Membrane Samples and Testing

In preparation for scanning electron microscopy (SEM) analysis, 1 cm × 1 cm sections of the membranes were cut from larger sheets, air-dried, and then fixed onto a standard SEM pin stub mount (Ted Pella Inc., Redding, CA) using carbon tape. For cross-sectional micrographs, dried samples were submerged in liquid nitrogen for 15 seconds and then fractured before being taped onto a vertically-walled SEM pin stub. All samples were sputter-coated with 1.5 nm of iridium prior to loading them into a Magellan 400 Field Emission Scanning Electron Microscope. Micrographs were produced using a working distance of 3 mm and an accelerating voltage between 1-3 kV.

To prepare a membrane sample wetted with ionic liquid for SEM imaging, the membrane was fixed on a pin stub and 2-3 drops of ionic liquid were placed on top of the membrane. After allowing the ionic liquid to soak into the membrane for 5 min, the surface was wiped with a Kimwipe to remove the excess liquid. The sample was then

coated with 1.5 nm of iridium, and another 1-2 drops of ionic liquid were added. After the removal of excess liquid, the samples were dried in a vacuum oven to remove residual water.

AFM experiments were carried out as described in previous literature [48]. The characterization was performed in tapping mode (Multimode, Nanoscope IV Controller, Veeco) with a waterproof scanner (J Scanner, Veeco) and a silicon nitride probe (NP, Veeco). The PI-PS-PAA sample was tested in the dry state and in two aqueous buffer solutions, 50 mM acetic acid (pH = 2.98) and 50 mM ammonium acetate (pH = 6.88). The apparatus was washed thoroughly after each image with buffer solutions.

The conversion of the PDMA domain to PAA is based on a previously published protocol [26]. A section of the membrane was submerged in a 6 M HCl aqueous solution at 85 ºC for a predetermined period of time. After removal from the acidic solution, the membrane material was washed repeatedly in DI water. Then the converted membrane was analyzed using ATR-FTIR spectroscopy and transport testing.

Transport tests were performed using a 10 mL Amicon 8010 stirred cell. A 1-inch-diameter circular section of a PI-PS-PDMA membrane was fabricated using a standard hand punch. A 1-inch diameter piece of Crane calendered PP/PE nonwoven microporous substrate was placed in the bottom of the stirred cell for support, and the PI-PS-PDMA membrane was placed on top of this support. The stirred cell was filled with 10 mL of solution, then capped, and pressurized with nitrogen. The permeating solution was recorded in a vial that rested on a balance. The mass of the vial was collected at

regular intervals in order to calculate the water flux. The hydraulic permeability of the membrane was determined by measuring the water flux at various applied pressures.

The hydraulic permeability was measured using solutions of varying acidity and basicity for the PDMA-functionalized and PAA-functionalized membranes. Acidic solutions ($1 < pH < 3$) were prepared using hydrochloric acid, and citric acid was used to prepare solutions from pH ranging from 3 to 5. Basic solutions from pH 7 to pH 10 were made using tris(hydroxymethyl)aminomethane (TRIS), and sodium hydroxide was used to prepare solutions of pH 11 to pH 13. Values for the pH were measured using an Accumet AP115 portable pH meter (Fisher Scientific, Waltham, MA) before adding the solution into the cell.

Polyethylene oxide (PEO) samples with molecular weights of 1.1, 2.1, 4.0, 6.0, 7.8 and 10.0 kDa were purchased from Polymer Source (Montreal, Quebec, Canada), with the dispersity values ($Đ$) of 1.10 or lower for all molecular weights. For the molecular weight cut off (MWCO) tests, a single PEO sample was dissolved in DI water at a concentration of 1 g L^{-1} and added to the stirred cell. During these experiments, the cell was stirred at 400 rpm to prevent concentration polarization. The permeating solution was collected in scintillation vials. The first 1.5 mL of permeate was discarded to eliminate contamination by any residual solution inside the membrane not cleared during washing. Two clean vials were used to collect 1.5 mL each of the permeate samples. The vials were then covered with Parafilm and refrigerated to prevent water evaporation. A 2-mL sample of the feed solution for each experiment was stored in the same manner. The cell was emptied and washed three times with DI water between each test.

The permeate and feed samples from each experimented were diluted by a factor of 20 with DI water, and a Shimadzu TOC-TN Organic Carbon Analyzer was used to quantify the concentration of PEO in the solutions. The percent rejection was calculated according to the following equation.

$$R(\%) = 100 \times \left(1 - \frac{c_p}{c_f}\right) \qquad (4.1)$$

Here, c_p and c_f represent the concentrations of PEO in the permeate and the feed, respectively.

Dynamic mechanical analysis (DMA) experiments of the membrane films were performed in tensile loading mode using a TA Instruments DMA Q800. A length of film (~25 mm by 10 mm) was clamped between the two tensile contacts. All samples were tested at a stress rate of 0.5 N min^{-1}. Wetted film experiments were performed using a humidifier chamber attachment at 35 °C and a relative humidity of 95%

4.7 References

1. Zydney, A. L. *High Performance Ultrafiltration Membranes: Pore Geometry and Charge Effects.* Elsevier: Amsterdam, **2011**; Vol. 14, 333.
2. Hilal, N.; Al-Zoubi, H.; Darwish, N. A.; Mohamma, A. W.; Arabi, M. A. *Desalination* **2004**, 170, 281.
3. Baker, R. W. *Membrane Technology and Applications*. 2nd ed.; J. Wiley: Chichester ; New York, **2004**.
4. Zeman, L. J.; Zydney, A. L. *Microfiltration and Ultrafiltration: Principles and Applications.* Marcel Dekker Inc.: New York, **1996**.
5. Mimoune, S.; Belazzougui, R. E.; Amrani, F. *Desalination* **2007**, 217, 251.
6. Shinde, M. H.; Kulkarni, S. S.; Musale, D. A.; Joshi, S. G. *J. Membr. Sci.* **1999**, 162, 9.
7. Wickramasinghe, S. R.; Stump, E. D.; Grzenia, D. L.; Husson, S. M.; Pellegrino, J. *J. Membr. Sci.* **2010**, 365, 160.
8. Warkiani, M. E.; Bhagat, A. A. S.; Khoo, B. L.; Han, J.; Lim, C. T.; Gong, H. Q.; Fane, A. G. *ACS Nano* **2013**, 7, 1882.
9. Curtin, D. E.; Robert D. Lousenberg; Timothy J. Henry; Paul C. Tangeman; Monica E. Tisack *J. Power Sources* **2002**, 131, 41.
10. Jackson, E. A.; Hillmyer, M. A. *ACS Nano* **2010**, 4, 3548.
11. Phillip, W. A.; Dorin, R. M.; Werner, J.; Hoek, E. M. V.; Wiesner, U.; Elimelech, M. *Nano Lett.* **2011**, 11, 2892.
12. Phillip, W. A.; O'Neill, B.; Rodwogin, M.; Hillmyer, M. A.; Cussler, E. L. *ACS Appl. Mater. Interfaces* **2010**, 2, 847.

13. Yang, S. Y.; Park, J.; Yoon, J.; Ree, M.; Jang, S. K.; Kim, J. K. *Adv. Funct. Mater.* **2008**, 18, 1371.

14. Jung, A.; Filiz, V.; Rangou, S.; Buhr, K.; Merten, P.; Hahn, J.; Clodt, J.; Abetz, C.; Abetz, V. *Macromol. Rapid Commun.* **2013**, 34, 610.

15. Peinemann, K. V.; Abetz, V.; Simon, P. F. W. *Nature Mat.* **2007**, 6, 992.

16. Pendergast, M. T. M.; Dorin, R. M.; Phillip, W. A.; Wiesner, U.; Hoek, E. M. V. *J. Membr. Sci.* **2013**, 444, 461.

17. Yang, S. Y.; Ryu, I.; Kim, H. Y.; Kim, J. K.; Jang, S. K.; Russell, T. P. *Adv. Mat.* **2006**, 18, 709.

18. Jackson, E. A.; Lee, Y.; Hillmyer, M. A. *Macromolecules* **2013**, 46, 1484.

19. Phillip, W. A.; Rzayev, J.; Hillmyer, M. A.; Cussler, E. L. *J. Membr. Sci.* **2006**, 286, 144.

20. Oss-Ronen, L.; Schmidt, J.; Abetz, V.; Radulescu, A.; Cohen, Y.; Talmon, Y. *Macromolecules* **2012**, 45, 9631.

21. Nunes, S. P.; Behzad, A. R.; Hooghan, B.; Sougrat, R.; Karunakaran, M.; Pradeep, N.; Vainio, U.; Peinemann, K. V. *ACS Nano* **2011**, 5, 3516.

22. Rzayev, J.; Hillmyer, M. A. *Macromolecules* **2005**, 38, 3.

23. Querelle, S. E.; Jackson, E. A.; Cussler, E. L.; Hillmyer, M. A. *ACS Appl. Mater. Interfaces* **2013**, 5, 5044.

24. Clodt, J. I.; Filiz, V.; Rangou, S.; Buhr, K.; Abetz, C.; Höche, D.; Hahn, J.; Jung, A.; Abetz, V. *Adv. Funct. Mater.* **2012**, 23, 731.

25. Mastroianni, S. E.; Epps, T. H. *Langmuir* **2013**, 29, 3864.

26. Rzayev, J.; Hillmyer, M. A. *J. Am. Chem. Soc.* **2005**, 127, 13373.

27. Yang, S. Y.; Son, S.; Jang, S.; H., K.; Jeon, G.; Kim, W. J.; Kim, J. K. *Nano Lett.* **2011**, 11, 1032.

28. Gundogan, N.; Okay, O.; Oppermann, W. *Macromol. Chem. Phys.* **2004**, 205, 814.

29. Phillip, W. A.; Hillmyer, M. A.; Cussler, E. L. *Macromolecules* **2010**, 43, 7763.

30. Smolders, C. A.; Reuvers, A. J.; Boom, R. M.; Wienk, I. M. *J. Membr. Sci.* **1992**, 73, 259.

31. Butun, V.; Billingham, N. C.; Armes, S. P. *Chem. Commun.* **1997**, 671.

32. Faraone, A.; Magazu, S.; Maisano, G.; Migliardo, P.; Tettamanti, E.; Villari, V. *J. Chem. Phys.* **1999**, 110, 1801.

33. Meireles, M.; Bessieres, A.; Rogissart, I.; Aimar, P.; Sanchez, V. *J. Membr. Sci.* **1995**, 103, 105.

34. Mehta, A.; Zydney, A. L. *J. Membr. Sci.* **2005**, 249, 245.

35. Zeman, L.; Wales, M. *Sep. Sci. Technol.* **1981**, 16, 275.

36. Song Zhao, X.; Q. Lu, G.; Hu, X. *Chem. Commun.* **1999**, 1391.

37. Hiemenz, P. C.; Lodge, T. P. *Polymer Chemistry 2nd ed.* CRC Press: **2007**.

38. Hamilton, W. A.; Smith, G. S.; Alcantar, N. A.; Majewski, J.; Toomey, R. G.; Kuhl, T. L. *J. Polym. Sci., Part B: Polym. Phys.* **2004**, 42, 3290.

39. Degennes, P. G. *Macromolecules* **1980**, 13, 1069.

40. Dukes, D.; Li, Y.; Lewis, S.; Benicewicz, B.; Schadler, L.; Kumar, S. K. *Macromolecules* **2010**, 43, 1564.

41. Dimitrov, D. I.; Milchev, A.; Binder, K. *J. Chem. Phys.* **2006**, 125, 34905.

42. Bowen, W. R.; Hilmi, M. *J. Membr. Sci.* **1996**, 112, 263.

43. Pieracci, J.; Crivello, J. V.; Belfort, G. *J. Membr. Sci.* **2002**, 202, 1.

44. Bird, B. B.; Stewart, W. E.; Lightfoot, E. N. *Transport Phenomena*. 2nd ed.; John Wiley and Sons: New York, **2002**.

45. Zhang, W.; Shi, L.; An, Y.; Wu, K.; Gao, L.; Liu, Z.; Ma, R.; Meng, Q.; Zhao, C.; He, B. *Macromolecules* **2004**, 37, 2924.

46. Mika, A. M.; Childs, R. F.; West, M.; Lott, J. N. A. *J. Membr. Sci.* **1997**, 136, 221.

47. Jitchum, V.; Perrier, S. *Macromolecules* **2007**, 40, 1408.

48. Jing, B.; Hutin, M.; Connor, E.; Cronin, L.; Zhu, Y. *Chem. Sci.* **2013**, 4, 28.

CHAPTER 5. CHEMICAL FUNCTIONALIZATION OF BLOCK POLYMER-BASED MEMBRANES FOR TARGETED ANALYTE SEPARATION

5.1 Overview

In Chapter 4, it was shown that polyisoprene-*b*-polstyrene-*b*-poly(*N*,*N*-dimethylacrylamide) (PI-PS-PDMA) block polymer templates with PDMA lined pore walls can be deprotected to polyisoprene-*b*-polstyrene-*b*-poly(acrylic acid) (PI-PS-PAA) block polymer nanoporous thin films. From this point, the carboxylic acid chemistry may be exposed for further reaction in the post self assembled state.[1] In this chapter, we demstrate that utilizing facile and selective amidation chemistry, PAA-lined pore walls are able to undergo refuctionalization to a variety of tunable heteroatom chemistries. In this way, the membrane chemstry may be tuned for targeted screening or absorption removal of analytes on the basis of size as well as chemistry.[2, 3]

Specifically, the selective and competitive elution-absorption of copper and nickel in deprotected PI-PS-PAA block polymer membrane templates is shown to have a large and highly reversible sorption capacity of copper (4.1 mmol g^{-1} membrane), with Cu^{2+}:Ni^{2+} permeation selectivities as high as ~10:1 prior to copper saturation.[2]

The chemical versitility of PI-PS-PAA membranes is further demonstrated by facile conversion of the PAA walls to a thiol-functionalized moeity, polyisoprene-*b*-polstyrene-*b*-poly(acrylic acid)-*graft*-thiol (PI-PS-PAA-*g*-thiol). Comparative absorption of membrane samples immersed in lead solutions with refunctionalized thiol pore walls (1.3 mmol g^{-1} Pb^{2+}) vs. carboxylic acid pores (0.2 mmol g^{-1} Cu^{2+}) at sorption selectivities of ~ 24 : 1 (1.18 mmol Pb^{2+}:0.05 mmol Cu^{2+}) demonstrate the highly selective chemistry of PI-PS-PAA membrane templates for targeted separation of analytes as ion exchange resin membrane templates.[2]

5.2 Introduction

In industry, stringent limits may be imposed on permisible concentrations of analytes in products.[4-7] For example, strict limits are imposed on the level of toxic agents in water in accordance with public health and environmental legislation.[8, 9] Such restrictions are low tolerances of metals and and other ions in water purification and wastewater treatment.[10] Traditionally, the use of an ion-selective chromatography technique of a chemsitry selective resin is an effective means for targeted metal separation.[11,12] However, by using packed particles as the sorption medium, diffusive and channeling limits of adsorbtion of target analytes to the selective site can become a rate limiting process, thereby inhibiting efficient removal that requires increased design scale to overcome.[13] On the contrary, the use of reverse osmosis (RO) and nanofiltration membranes are effective for metal ion separation from water, at the comprimise of limited preferential rejection of analytes to achieve target concentration limits.[10, 14]

One such method to achieve targeted separation of between similarly-sized analytes is to utilize their affinity to different chemistries.[15] The use of adsorptive resins facilitate chemistry selective separations between a target analyte via a chelating moiety on a microporous support. To enhance the adsorption and rapid saturation capacity of resins, variation of the geometry of the support from a microporous resin to a membrane support facilitates in convective directed flow to the adsoption sites for high analyte capture efficiency. As such, block polymer membrane devices with tunable lined porous domains represent an ideal architecture to facilitate size and target adsorption capture for removal of trace analytes.[10, 15, 16]

5.3 Results and Discussion

5.3.1 Functionalization of PI-PS-PAA Templates

As previously demonstrated in Chapter 4, the use of polyisoprene-*b*-polstyrene-*b*-poly(*N*,*N*-dimethylacrylamide) (PI-PS-PDMA) templates nanofiltration reigeme membranes for use in the absorptive separation of polyvalent salts.[1] Upon deprotection, the poly(acrylic acid) pores lining the membrane are capable of undergoing chemical transformation as an attachment site for myriad of chemistries. By selection of a funtionality for attchement to the PAA domain, a tunable affinity based adsorptive resin layer may be created for targeted analyte separation. In order to facilitate the functionalization of PAA line pore walls to tunable chelating (-R) groups, the chemsitry for this functilonalization needs to be 1) selective in attachment to PAA lined pore walls

2) tolerant in the chemistry of the of chelate R group 3) non-destructive to the porous architechture, and 4) a facile reaction protocol that is quantitative in conversion.

A reaction chemistry that encompases these requirements is a facile water soluble variation of Steglich esterification.[17-19] By use of a primary amine instead of an alcohol in the presence of a promotor, selective amidation of the activated and promoted carboxylic terminus enables kinetically-controlled addition of the amine to the pore wall (Scheme 5 .1).[20] The resulting amide bond formation is highly chemoselective with respect to binding to the PAA wall.[15] As an additional feature, the strong amide attachement with the exposed chelate R groups are highly resistant to cleavage in the presence of heat and strong acid and base.[15, 16] This increased resistance enables adsorption membranes to be utilized over a diverse range of separation conditions.

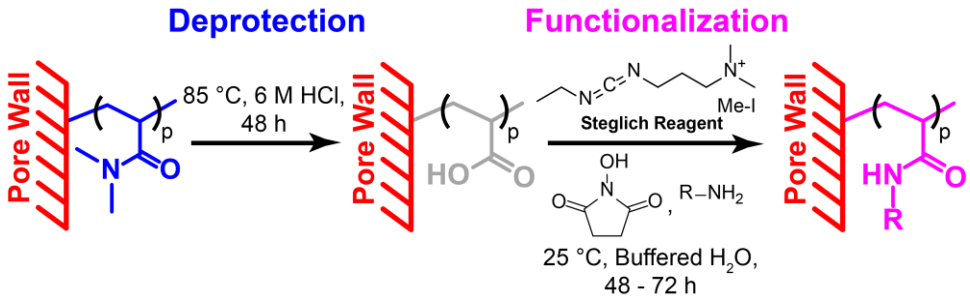

Scheme 5.1. Reaction scheme of tuning the pore chemistry of PI-PS-PDMA block polymer membranes. During the deprotection step, self assembled PI-PS-PDMA membranes consisting of PDMA lined pore walls are hydrolyzed PAA by immersion in 6 M HCl at 85 °C for 48 h. Following quantitative conversion to PAA, the template may be functionalized to a chelating R group pore chemistry. This was achieved by immersion of the membrane in a pH 7 buffered solution containing the R group as a functionalized primary amine ($R\text{-}NH_2$) in the presence of the Steglich reagent 1-Ethyl-3-(3-dimethylamino) propylcarbodiimide methiodide) and N-hydroxysuccinimide (NHS) for 48 to 72 h.

By the use of a ethyl alkyl or phenyl linkage group from the amine terminus, small moelcules that contain the chelating R group on an opposite terminus are readily availible. Common chelating heteoatom functionalities (*e.g.*, alcohol, amine, thiol) as well as the carboxylic acid deprotected intermediate group may be readily attached from PAA lined pore walls to allow for tunable adsorption with of eluting target analytes (Figure 5.1).[16] As a result of using Steglich amidation for functionalization, high conversions (> 95%) with high reaction selectivity are achieveable for maximum grafting density of chelating R groups from the PAA walled substrate.

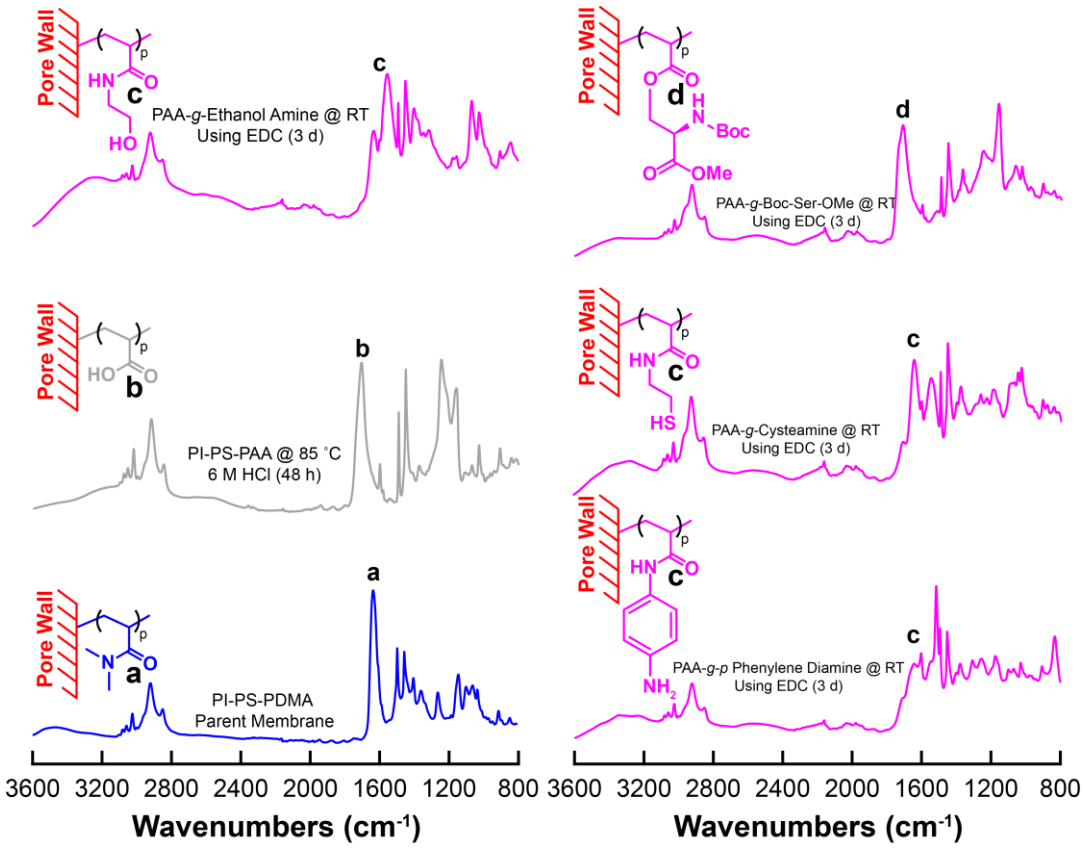

Figure 5.1. Attenuated total internal reflectance-Fourier transform infrared (ATR-FTIR) spectroscopy of block polymer membranes. The characteristic shift of the (a) parent amide C=O stretch at ~ 1630 cm^{-1} in PI-PS-PDMA (shown in blue) is shifted when deprotected in strong acid to (b) polyacrylic acid lined pore walls with the C=O stretch at ~ 1700 cm^{-1} (shown in grey). Following functionalization by immersion in the Steglich Reagent mixture for 3 d, high selective conversions (> 95%) to (c) alcohol, amine and thiol groups are obtained (based on peak area integration. High selective conversions are shown by the uniform shift of the FTIR C=O stretch back to the amide region of ~ 1630 - 1580 cm^{-1} in PI-PS-PDMA. (d) Larger heteroatom groups are possible to be attached, with amine and carboxylic acid protected serine amino acid attached via its -OH group for zwitterionic adsorption applications.[19, 21]

5.3.2 Block Polymers as Adsorptive Membranes for Adsorption of Target Metal Analytes

To affirm that tunable pore chemistry in block polymer templates facilitates in selective absorption, a sorption study of similarly sized copper and nickel ions was performed using a PI-PS-PAA membrane.[2] Elution of equimolar solutions of $CuCl_2$ and $NiCl_2$ demonstrated instantaneous selectivities of the permeate stream to be in excess of 12 to 1 Cu/Ni (Figure 5.2). This demonstrates that copper has a much higher partiality to selectively adsorb and saturate the PAA lined walls. This selectivity has been demonstrated before, which has been attributed to the square planar Cu^{2+} geometry being entropically favored for preferential bidentate chelation of the carboxylic acid over the tetrahedral configuration to the Ni^{2+} geometry.[2]

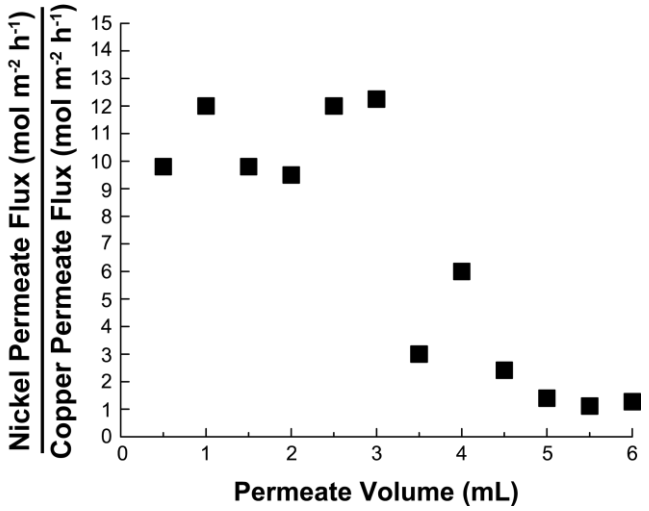

Figure 5.2. Ratio of the nickel permeate flux to the copper permeate flux through a 2 inch PI-PS-PAA membrane. At low saturation of the PAA absorbent at low permeate volumes, preferential binding of Cu^{2+} to free carboxylic acid enables high permeate flux selectivities of nickel to copper to be achieved.[2] This graph produced from data displayed in Reference 2.

5.3.3 Block Polymer Templates as Adsorption Resins for Adsorption of Target Metal Analytes

With a facile method of functionalization available for targeted generation of selective adsorptive membranes, the use of the thiol grafted block polymer membrane, polyisoprene-*b*-polystyrene-*b*-poly(acrylic acid)-*graft*-thiol (PI-PS-PAA-*g*-thiol) (Figure 5.1) is a suitable chemistry for selective adsorption of heavy metals.

To gauge the chemical selectivity of heavy metal adsorption of tunable block polymer membranes, small samples of functionalized PI-PS-PAA-*g*-thiol membrane are immersed in standard solutions for a predetermined period of time before their concentration of the supernatant is measured to determine the sorption capacity. By introduction of a thiol functionality that has a high affinity for myriad of heavy metal salts,[22-25] a modest capacity of 1.3 mmol Pb^{2+} g^{-1} membrane (2 : 1 thiol : lead coordination chemistry)[26, 27] is observed for the PI-PS-PAA-*g*-thiol membrane over the 0.3 mM Pb^{2+} g^{-1} membrane sorption value of the carboxylic acid PI-PS-PAA membrane (square dots in grey). Comparison of competitive adsorption of lead to copper in PI-PS-PAA-*g*-thiol showed a high selectivity ratio of 23.6 to 1, while maintaining a high competitive lead sorption of 1.18 mmol g^{-1} membrane.

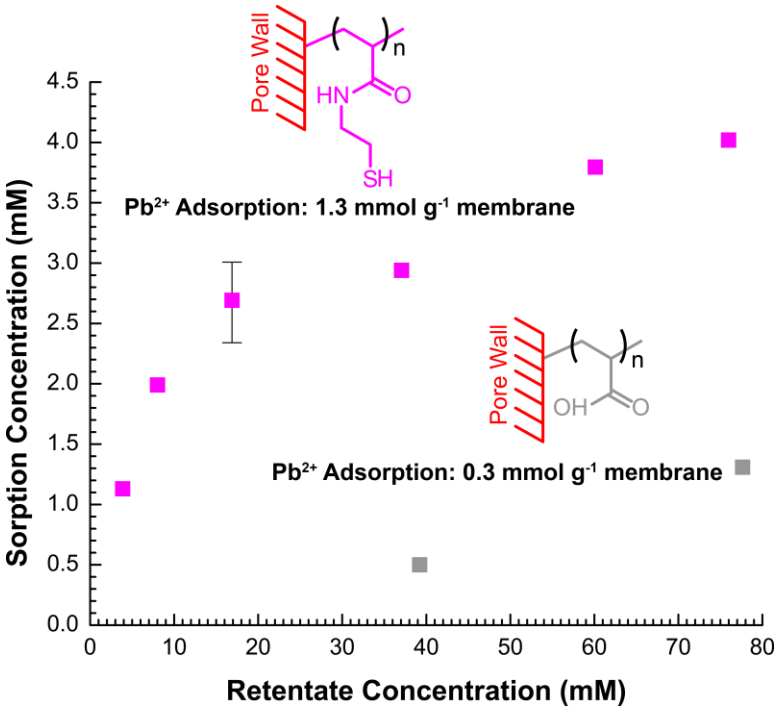

Figure 5.3 Uptake of lead (as $Pb(NO_3)_2$) versus the concentration of retentate supernatant remaining over a distribution of initial solution concentrations from 5 to 80 mM. The lead adsorption capacity of the thiol (PI-PS-PAA-*g*-thiol) functionalized membrane (square dots in magenta) was 1.3 mmol Pb^{2+} g^{-1} membrane, a significant increase over the 0.3 mM Pb^{2+} g^{-1} membrane of the carboxylic acid PI-PS-PAA membrane (square dots in grey).

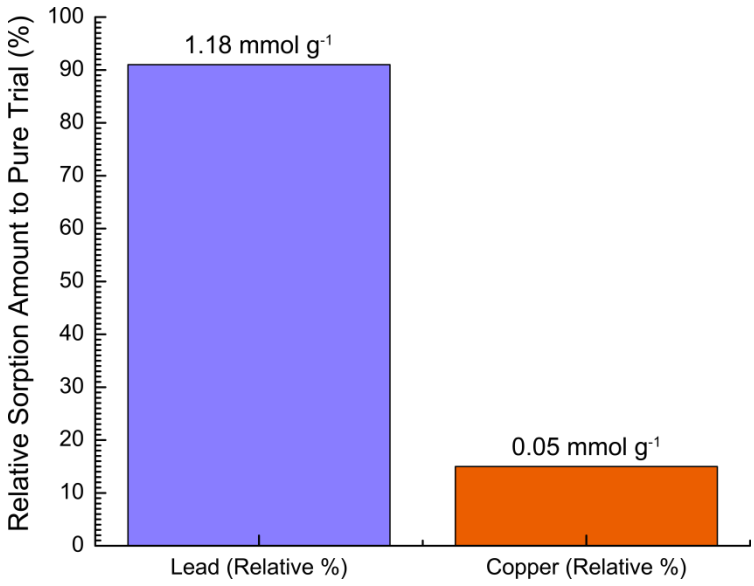

Figure 5.4 Values of competitive lead and copper resin sorption in a 50 mM equimolar PI-PS-PAA-*g*-thiol resin. The axis on the left shows what percentage the competitive sorption value realtive to the value of pure sorption in PI-PS-PAA-*g*-thiol (1.3 mmol g^{-1} membrane for Pb^{2+}, 0.3 mmol g^{-1} membrane for Cu^{2+}). The competitive lead to copper sorption ratio of 23.6 highlights the high utility of these chemically tunable platforms for targeted analyte separation.

5.4 Conclusion

The use of PI-PS-PDMA block polymers as sorption membranes and as resin separation devices serve as a diverse platform for myriad applications into targeted recovery of analytes. The use of PAA chemistry demonstrated competitive membrane sorption values of copper and nickel with the utility of undergoing further reaction chemistry. In addition, functionalization of the PAA lined porous templates to thiol groups demonstrated marked increase for dilute lead adsorption. The myriad tunability of chemistry in PI-PS-PDMA block polymer membrane systems enables whole new

sorption routes to be explored for targeted analyte recovery that extends into all facets of industry.

5.5 Supplementary Information

5.5.1 Steglich Amidation of PI-PS-PAA Block Polymer Templates

In the following example of this functionalization protocol, a PI-PS-PAA membrane has a thiol moiety grafted to the PAA by the use of cysteamine linking group. A 25 mg dried sample of the PI-PS-PAA membrane (11.2 - 20.1 - 12.6 kDa) is first immersed in ~ 0.5 mL of pH 7 phosphate buffered water for 15 minutes. Then, 15 mol equivalents of synthesized 1-Ethyl-3-(3-dimethylamino)propylcarbodiimide methiodide (EDC.MeI)[28] and *N*-Hydroxysuccinimide (NHS) to the number of mols of acrylic acid in the PI-PS-PAA sample are added to the solution (*i.e* EDC.MeI (196 mg, 0.65 mmol), and NHS (136 mg, 0.65 mmol)). Finally, 15 mol equivalents of the heteroatom group (*i.e.*, cysteamine (32.4 mg, 0.65 mmol)) was added to the solution, and stored in the dark for 48 h.

Following the reaction, the piece of the functionalized membrane filtered, immersed, and washed over a Hirsh funnel for 1 h repeatedly with copious amounts of water. The cleaned piece of functionalized membrane was dried in a vacuum oven at room temperature overnight to remove residual water. ATR-FTIR analysis of the sample (Chapter 4 and Figure 5.1) was performed to determine the conversion of the carboxylic acid to the amide by integration of the area under the peak for both shifts. (Conversion: ~ 96 % to PI-PS-PAA-*g*-thiol).

5.5.2 Copper and Lead Block Polymer Adsorption Experiments and Quantification in PI-PS-PAA-*g*-thiol

For sorption studies of lead (as lead nitrate) and copper (as copper nitrate), the solutions for this study in the range 0 - 100 mM were dissolved in DI water for standard calibration using ultraviolet-visible (UV-Vis) light spectrometry in a quartz cuvette. Spectra were taken using a Cary 60 UV-Vis spectrometer, where lead nitrate standard calibration curves measured a max absorbance of Cu at $\lambda_{Cu,\ max}$ = 815 nm, and copper nitrate measured a max absorbance at $\lambda_{Pb,\ max}$ = 300 nm(Figure 5.5a). For competitive sorption of copper and nickel, the contribution of the competitive absorbance peak of Cu (λ^{*}_{Cu}) at $\lambda_{Pb,\ max}$ = 300 nm may be linearly subtracted from the total measured absorbance at 300 nm in order to accurately determine the absorbance of Pb in binary sorption study of with Cu (Figure 5.5b).

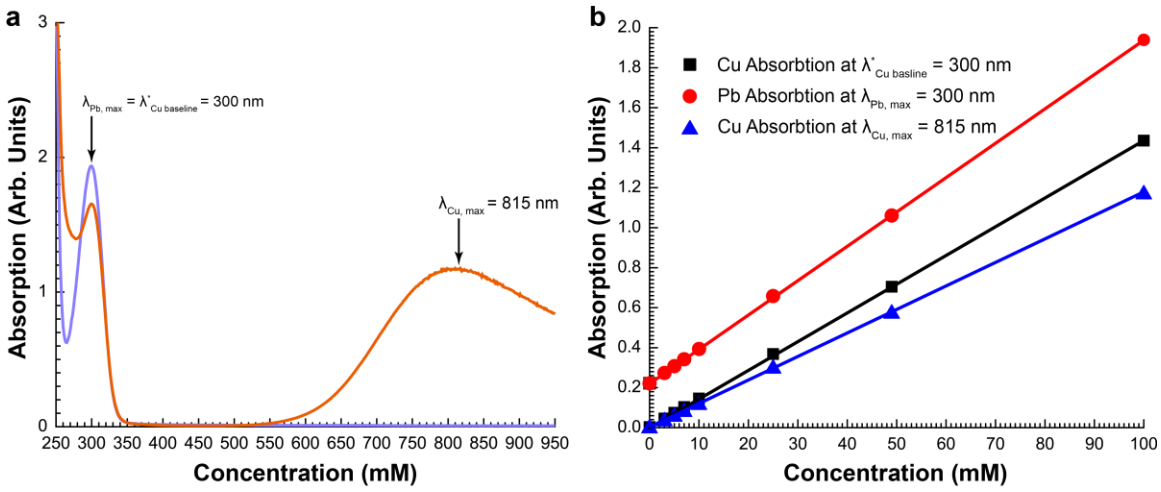

Figure 5.5 (a) Representative UV-Vis absorption spectra of $Cu(NO_3)_2$ (in orange) and $Pb(NO_3)_2$ (in purple) in DI water at 100 mM. (b) Calibrated UV-Vis absorbance curves of Cu (blue line/triangles) at $\lambda_{Cu,\ max}$ = 815 nm and Pb (red line/circles) at $\lambda_{Pb,\ max}$ = 300 nm for determination of the membrane sorption capacity of functionalized membranes. The Cu black line/squares represents the baseline corrected value of competitive copper absorption (λ^*_{Cu}) at the wavelength of Pb absorption ($\lambda_{Pb,\ max}$ = 300 nm). To determine the competitive sorption of Pb, the concentration of copper is first independently determined at $\lambda_{Cu,\ max}$. From the calculated Cu concentration, the experimental value of Pb concentration at may be evaluated by subtracting the contributing Cu sorption (λ_{Cu}^*) at 300 nm.

For a sorption study, a sample of a ~ 3.4 mg piece of PI-PS-PAA-*g*-thiol or PI-PS-PAA is completely immersed in 1.25 mL of a Cu/Pb DI water standard solution, and allowed to statically adsorb for 12 hours. Upon completion of the sorption study, the membrane piece was removed from the supernatant and dipped in deionized (DI) water three times rapidly to remove any surface unbound metal analyte solution. Next, the membrane piece was immersed in a 1.25 mL solution of pH 1 HCl solution for 3 h to desorb the bound Cu/Pb analyte from the thiol functionalized pore walls. Upon

completion of the desorption, a 1 mL acidic desorbed solution was analyzed using the calibrated UV-Vis spectroscopy curves to determine the concentration of reversible sorption. Using this measured sorption value, the sorption capacity per unit mass of the membrane (*i.e.* membrane sorption capacity) may be calculated.

5.6 References

1. Mulvenna, R. A.; Weidman, J. L.; Jing, B.; Pople, J. A.; Zhu, Y.; Boudouris, B. W.; Phillip, W. A. *J. Membr. Sci.* **2014**, 470, 246.

2. J. L. Weidman; R. A. Mulvenna; B. W. Boudouris; Phillip, W. A. *Langmuir* **2015**, 31, 11113.

3. Zhang, Y.; Sargent, J. L.; Boudouris, B. W.; Phillip, W. A. *J. Appl. Polym. Sci.* **2015**, 132, 41683.

4. Yang, H.; Xu, Z.; Fan, M.; Gupta, R.; Slimane, R. B.; Bland, A. E.; Wright, I. *J. of Env. Sci.* **2008**, 20, 14.

5. Ravanchi, M. T.; Kaghazchi, T.; Kargari, A. *Desalination* **2009**, 235, 199.

6. Bernardo, P.; Drioli, E.; Golemme, G. *Ind. Eng. Chem. Res.* **2009**, 48, 4638.

7. Humphrey, J. L.; Koort, R. *Separation technologies: Advances and priorities*; Humphrey (JL) and Associates, Austin, TX (USA): **1991**.

8. Beman, J. M.; Arrigo, K. R.; Matson, P. A. *Nature* **2005**, 434, 211.

9. Oliver, S. P.; Jayarao, B. M.; Almeida, R. A. *Foodbourne Pathogens & Disease* **2005**, 2, 115.

10. Fu, F.; Wang, Q. *J. Env. Managment* **2011**, 92, 407.

11. Shannon, M. A.; Bohn, P. W.; Elimelech, M.; Georgiadis, J. G.; Marinas, B. J.; Mayes, A. M. *Nature* **2008**, 452, 301.

12. Bashir, W.; Paull, B. *J. Chromatog. A* **2002**, 942, 73.

13. Ghosh, R. *J. Chromatogr. A* **2002**, 952, 13.

14. Rautenbach, R.; Gröschl, A. *Desalination* **1990**, 77, 73.

15. Brown, R.; Bennet, A.; Slebocka-Tilk, H. *Acc. Chem. Res.* **1992**, 25, 481.

16. Mackie, J.; Meares, P. In *The diffusion of electrolytes in a cation-exchange resin membrane. I. Theoretical*, Proc. of Royal Society of London A: Math., Physical and Eng. Sci., The Royal Society: **1955**; pp 498.

17. Neises, B.; Steglich, W. *Angewandte Chemie International Edition in English* **1978**, 17, 522.

18. Rzayev, J.; Hillmyer, M. A. *J. Am. Chem. Soc.* **2005**, 127, 13373.

19. Hadidi, M.; Zydney, A. L. *J. Membr. Sci.* **2014**, 452, 97.

20. Rzayev, J.; Hillmyer, M. A. *Macromolecules* **2005**, 38, 3.

21. Liu, J.; Xu, T.; Fu, Y. *J. Membr. Sci.* **2005**, 252, 165.

22. Buck, M.; Grunze, M.; Eisert, F.; Fischer, J.; Träger, F. *J. Vac. Sci. Tech. A* **1992**, 10, 926.

23. Nakayama, M.; Chikuma, M.; Tanaka, H.; Tanaka, T. *Talanta* **1983**, 30, 455.

24. Tanco, M. A. L.; Tanaka, D. A. P.; Flores, V. C.; Nagase, T.; Suzuki, T. M. *React. Funct. Poly.* **2002**, 53, 91.

25. Monier, M.; Abdel-Latif, D. *J. of Hazard. Mat.* **2012**, 209, 240.

26. Claudio, E. S.; Goldwin, H.; Magyar, J. S. *Prog. Inorg. Chem* **2003**, 51, 1.

27. Flora, S. J.; Pachauri, V. *Int. J. Env. Res. Public Health* **2010**, 7, 2745.

28. Sheehan, J. C.; Cruickshank, P. A. *Org. Synth*. **1968**, 83.

CHAPTER 6. BLOCK POLYMER ARCHITECTURES FOR SUB-NANOMETER SEPARATION

6.1 Overview

As shown previously in Chapter 4, changing the chemical identity of block polymer membranes significantly affects the final pore size of the separation device. In addition to tuning block polymer chemistry, changing the pore size of a given block polymer provides an additonal parameter by which to tune pore size.[1] However, physical limits apply to the lower scale of pore size tunablility obtainable on the basis of block polymer size alone. In the case of polyisoprene-*b*-polstyrene-*b*-poly(*N*,*N*-dimethylacrylamide) (PI-PS-PDMA) block polymer templates, a limit of low total block polymer molecular weight of ~ 50 kDa applies due to the degradation of the size selective pores during acid deprotection at elevated temperatures to polyisoprene-*b*-polstyrene-*b*-poly(acrylic acid) (PI-PS-PAA).[2, 3]

In this chapter, new PI-PS-Poly(acrylate) chemitries consisting of poly(tetrahydro-2H-pyran-2-yl acrylate) (PTHPA)[4-7] or poly(*tert*-butyl acrylate) (PtBA) are proposed.[8] The use of these new chemistries serves to enable more facile generation of PI-PS-PAA block polymer templates with lower pore sizes for application in reverse osmosis (RO) (< 1 nm) purification of water.

6.2 Introduction

As the demand for natural resources increases, a particularly high stress exists on the availability for fresh water. Since the implementation of reverse osmosis (RO) membranes with pore sizes of less than 1 nm for high flux desalination in the 1960s,[9, 10] the use of this technology has been able to curb the increasing demand with the worlds growing population for increased access to drinking and potable water.[11]

The most common materials used in RO membranes in industry today are primarily interfacial polymerized anisotropic condensation polymer films[11-15] or phase inverted membranes from cellulose acetate.[16, 17] While these materials demonstrate high flux and rejection of salt in brackish and seawater, the ever present accumulation of membrane fouling in the form of accumulation of microorganisms and pathogens, organic matter and scale hinders their performance. Unfortunately, even after mitigation of fouling by water pretreatment prior to RO, the long term use of cleaning materials are destructive to the porous architecture of these films.[18 19-23]

With the emergence of nanotechnology, new controlled architectures from hierarchical structured materials have led to the development of RO membranes from zeolites, mixed matrix and organic/inorganic composites, electrospun fibers as well as carbon nanotube membranes.[24] Of these new methodologies and materials for next generation separation devices, the use of block polymers represents yet another attractive route for achieving high flux, chemically resistant templates with inherent anti-fouling properties for long service life by mere tuning of the block domains.

6.3 Results and Discussion

The use of ~ 70 kDa PI-PS-PDMA enables pore radii of sizes less than 1 nm upon deprotection to PAA.[3] During the deprotection step (Figure 6.1), no change in the porous structure was observed, making these templates a viable candidates for robust RO membranes with high chemical tolerance.[3] The cast membranes resistance to changes in sturcture with heat may be attributed to the hindered motion[24] from the high molecular weight polymers utilized in this 70 kDa cast block polymer membrane.

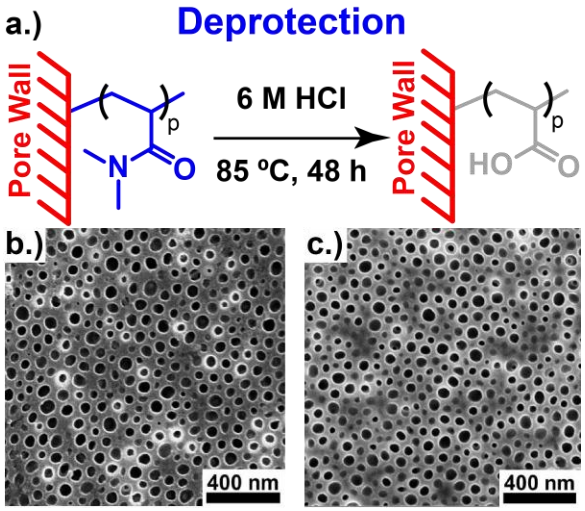

Figure 6.1. Deprotection of (higher) ~ 70 kDa molecular weight PI-PS-PDMA block polymer membranes in the presence of (a) 6 M HCl for 48 h at 85°C result in successful deprotection of (b) PDMA lined pores to (c) PAA lined pores without the compromise of pore degradation.[3] SEM micrographs in (b) and (c) are Reproduced from Reference 3.

By variation of the total molecular weights of block polymers for membrane templates, the size of the porous surface is tunable (Figure 6.2). In an effort to create

lower pore sizes from block polymer templates, low molecular weight PI-PS-PDMA block polymers of 48 kDa total molecular weight were created. However, when low molecular weight PI-PS-PDMA block polymers are deprotected using strong acid to PI-PS-PAA, degradation of the size selective porous surface occurs (Figure 6.3).

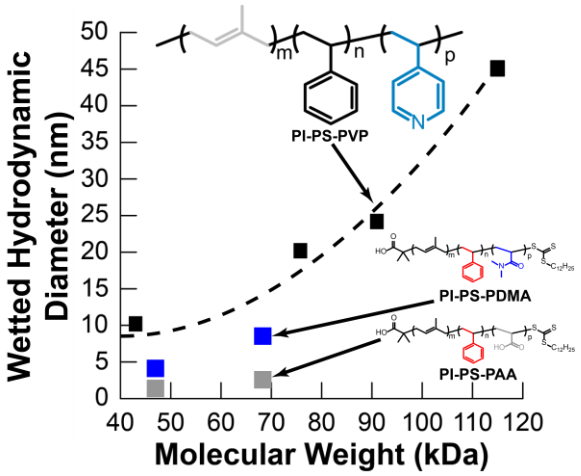

Figure 6.2. Comparison of wetted hydrodynamic pore diameter through polyisoprene-*b*-polystyrene-*b*-poly(4-vinyl pyridine) (PI-PS-PVP)[1] membranes (shown in black), versus 48 and 68 kDa PI-PS-PDMA (shown in blue) and deprotected PI-PS-PAA templates (shown in grey). The use of PI-PS-PDMA and PA-PS-PAA enables block polymer membrane sizes to approach sub nanometer pore sizes for application into reverse osmosis.

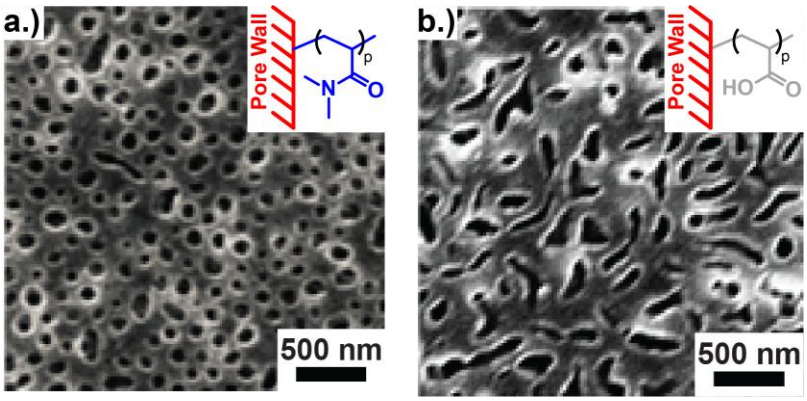

Figure 6.3. SEM of the deprotection of (low) ~ 48 kDa molecular weight (a) PI-PS-PDMA block polymer membrane before deprotection and (b) PI-PS-PAA after deprotection by immersion of 6 M HCl for 48 h at 85°C result in successful deprotection of (b) PDMA lined pores to (c) PAA lined pores at the compromise of size selectivity. Casting and SEM micrographs courtesy of Jacob Weidman.

Unfortunately, the modification of the deprotection conditions of PI-PS-PDMA to PI-PS-PAA using a milder protocol with 100% conversion is not possible without comprimising the porous architecture. Regardless of the presence of a lewis acid catalyst,[26] a stronger acid (trifluroacetic acid (TFA)),[27] or prolonged periods of exposure at a lower temperature, the deprotection of PDMA to PAA is thermally activated and is dependent on temperature. A temperature of ≥80 °C is required for quantitative conversion of PDMA to PAA, with deprotection temperatures above 45 °C for extended periods resulting in the degradation of the size selective porous surface. As such, the use of polyacrylate chemistries that require milder low temperature conditions to generate the PAA functionality for subsequent functionalization (Chapter 5) is highly desireable to create and maintain (sub) nanometer pores for RO applications.

In order to achieve a PI-PS-Polyacrylate architecture for lower pore sized templates, differing the chemistry of the parent polyacrylate block itself may change its native range of pore size. Similarly, by designing the parent polyacrylate ester protecting group to facily convert to PAA at low temperature, membrane pore degradation may be inhibited. This will enable lower pore sizes to be obtained by using the swellability of PAA to template sub nanometer pores for RO membranes.[3, 28, 29]

For this study, the use of poly(*tert*-butyl acrylate) (PtBA) and poly(tetrahydro-2H-pyran-2-yl acrylate) (PTHPA) polyacrylate domains were considered to allow facile deprotection to PAA with potentially lower pore-sizes. Firstly, their required conditions of conversion to PAA by hydrolysis were measured by immersing the synthesized homopolymer analogs in deprotecting solutions. Monitoring the conversion of the carbonyl peak shift from the parent homopolymer to PAA, the mildest conditions required for quantitative conversion of PtBA to PAA was achieved in a 1 M trifluroacetic acid (TFA) solution after 24 h., and the mildest conditions required for complete conversion of PTHPA was achieved in a 0.1 M HCl solution after 24 h (Figure 6.4).

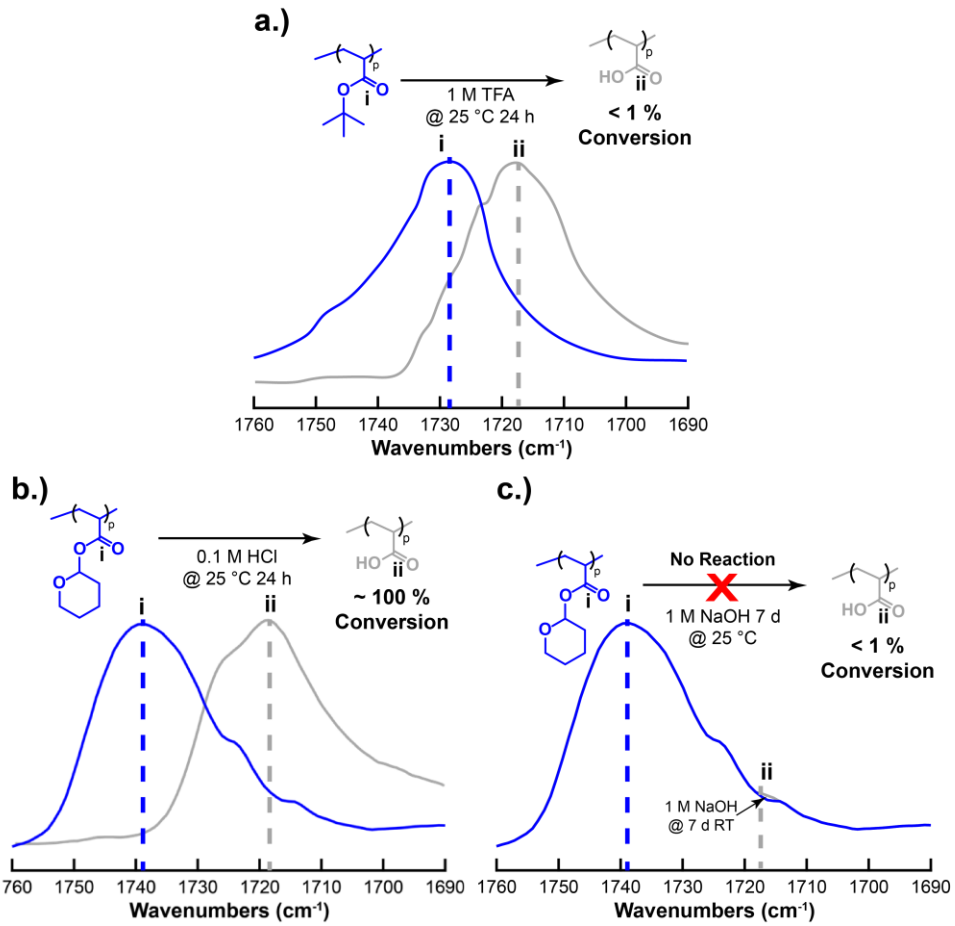

Figure 6.4. Attenuated total internal reflectance-Fourier transform infrared (ATR-FTIR) spectroscopy of samples immersed in deprotective solutions. Immersion of (a) PtBA in 1 M TFA solubilizes in solution as it hydrolyses the polymer to be 100 % converted to PAA after 24 h by the complete characteristic carbonyl stretch shift between i and ii. Similarly, the reaction of (b) PTHPA in 0.1 M HCl for 24 h completely deprotects to PAA. The immersion of (c) PTHPA in 1 M sodium hydroxide (NaOH) does not detail any conversion to PAA after 7 days. This is indicative that PTHPA deprotection to PAA is only acid labile, with the presence of strong basic conditions inhibiting this impulsive reaction.

By incorporation of these facile polyacrylate deprotection chemistries, block polymers of comparable molecular weight to PI-PS-PDMA studied samples were

synthesized (refer to Section 6.4 Supplementary Information for more details). Casting polyisoprene-*b*-polystyrene-*b*-poly(*tert*-butyl acrylate) (PI-PS-PtBA) and polyisoprene-*b*-polystyrene-*b*-poly(tetrahydro-2H-pyran-2-yl acrylate) (PI-PS-PTHPA) from selective solvents as thin films using the self-assembly and non-solvent induced phase separation (SNIPS) process yields pore sizes in the dried-state significantly below tested PI-PS-PDMA samples of similar molecular weight (Figure 6.5).

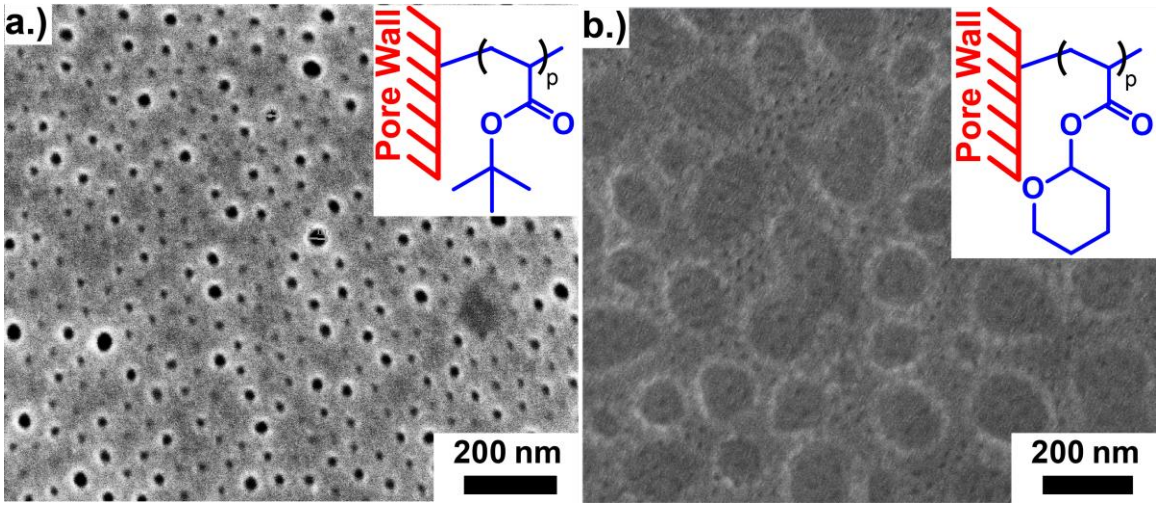

Figure 6.5. Scanning Electron Microscopy (SEM) of SNIPS membranes of (a) a 67 kDa PI-PS-PtBA block polymer cast as a 15% (by weight) polymer solution in a 70/30 (w/w) mixture of tetrahydrofuran (THF) and dimethylformamide (DMF), and (b) a 44 kDa PI-PS-PTHPA block polymer cast as a 18% (by weight) polymer solution in a 80/20 (w/w) mixture of tetrahydrofuran (THF) and dimethylformamide (DMF). Using Fast Fourier Transform (FFT) of the images, a pore feature size of (a) 28 nm and (b) 12 nm is calculated. Casting and SEM images courtesy of Jacob Weidman and Chris Zhang.

The substantially reduced pore sizes observed in the dried-state for PI-PS-PtBA (67 kDa, 28 nm) and PI-PS-PTHPA (44 kDa, 12 nm) block polymer membranes versus PI-PS-PDMA candidates (48 kDa, 40 nm, 68 kDa, 53 nm) demonstrate that changing the chemistry of the system significantly affects the potential outcome of the final pore size. As such, this significantly changes their solvation and chain extension into a more confined pore, which greatly affects their final solvated pore size of separation.

6.4 Conclusion

In conclusion, the use of either PI-PS-PtBA or PI-PS-PTHPA polyacrylate chemistries for generating new block polymer membrane candidates have been demonstrated. As a result of their different chemistry, these new native parent bock polymer membranes demonstrate potential for significantly lower pore sizes than the established PI-PS-PDMA architecture.[3, 30] Their facile deprotection chemistry at room temperature enables low total molecular weight materials to undergo conversion to PI-PS-PAA intermediates for functionalization for potential generation of sub nanometer pores for RO membrane applications.

6.5 Supplementary Information.

6.5.1 Synthesis of THPA Monomer

The synthesis of tetrahydro-2H-pyran-2-yl acrylate (THPA) for polymerization to poly(tetrahydro-2H-pyran-2-yl acrylate) has been described in literature previously,[4] and is summarized in Scheme 6.1.

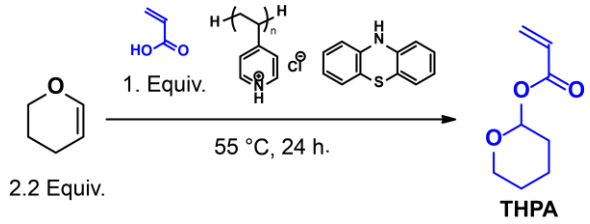

Scheme 6.1 Variation of the literature synthetic method used for the synthesis of THPA monomer.[4]

Briefly, 35 mL (0.31 mol) of 3,4-dihydro-2H-pyran is added to a 100 mL sealed three neck vessel with a stirbar that has been previously purged with argon for 30 minutes containing 0.56 g of crosslinked poly(4-vinylpyridine hydrochloride) and 0.06 g of phenothiazine. 11.2 ml (0.16 mol) of acrylic acid was then added dropwise until complete addition, before immersing on a hotplate to stir at 60 °C for 24 hours. The vessel was cooled in a water bath before filtering. 0.1 g of phenothiazine and calcium hydride (CaH_2) was then added to the permeate in a round bottom flask before removal of the excess 3,4-dihydro-2H-pyran under vacuum. The temperature was then increased for vacuum distillation of fresh tetrahydro-2H-pyran-2-yl acrylate (THPA) (50 °C, 1 mm Hg).

6.5.2 Polyisoprene-*b*-Polystyrene-*b*-Poly(tetrahydro-2H-pyran-2-yl acrylate) Synthesis

The PI-PS-PtBA triblock polymer was synthesized from a macroinitiation of a RAFT PI-PS block polymer. The synthetic scheme for PI-PS RAFT synthetic has been described previously. In this reaction, 1.05 g (35.4 μmol) of the PI-PS macroinitiator was mixed with 5.0 mL (0.03 mol) of freshly distilled THPA monomer, 0.47 mg (2.8 μmol) of azobisisobutyronitrile (AIBN), and 14.9 mL of inhibitor free tetrahydrofuran (THF). The mixture was combined into a 100 mL round bottom flask containing a Teflon-coated stir bar under an argon blanket. The vessel underwent four freeze-pump-thaw cycles, refilled and stirred in a stirred oil bath at 60 ºC for 2.25 h. After the reaction, the mixture was cooled in a water bath and quickly precipitated twice in methanol from THF. The solid material was then dried under vacuum overnight. (10.1-21.1-12.0 kDa PI-PS-PTHPA)

6.5.3 Polyisoprene-*b*-Polystyrene-*b*-Poly(*tert*-butyl acrylate) Synthesis

The PI-PS-PtBA triblock polymer was synthesized from a macroinitiation of a RAFT PI-PS block polymer. The synthetic scheme for PI-PS RAFT synthesis has been described previously.[3, 30] For the PtBA block addition reaction, 0.60 g (1.84 μmol) of the PI-PS macroinitiator was mixed with 1.7 mL (0.01 mol) of twice basic alumina column purified *tert*-butyl acrylate monomer, 0.30 mg (1.8 μmol) of azobisisobutyronitrile (AIBN), and 5.1 mL of inhibitor free tetrahydrofuran (THF). The mixture was combined into a 100 mL round bottom flask containing a Teflon-coated stir bar under an argon blanket. The vessel underwent four freeze-pump-thaw cycles, refilled and stirred in a

stirred oil bath at 60 ºC for 3.5 h. After the reaction, the mixture was precipitated three times into methanol from THF. The solid material was then dried under vacuum overnight (17.0 -34.0-16.1 kDa PI-PS-PtBA).

6.6 References

1. Dorin, R. M.; Phillip, W. A.; Sai, H.; Werner, J.; Elimelech, M.; Wiesner, U. *Polymer* **2014**, 55, 347.

2. J. L. Weidman; R. A. Mulvenna; B. W. Boudouris; Phillip, W. A. *Langmuir* **2015**, 31, 11113

3. Mulvenna, R. A.; Weidman, J. L.; Jing, B.; Pople, J. A.; Zhu, Y.; Boudouris, B. W.; Phillip, W. A. *J. Membr. Sci.* **2014**, 470, 246.

4. Hertler, W. R. *US Patent 5,072,029,* **1991**.

5. Petzetakis, N.; Dove, A. P.; O'Reilly, R. K. *Chemical Science* **2011**, 2, 955.

6. O'Reilly, R. K.; Joralemon, M. J.; Hawker, C. J.; Wooley, K. L. *Chem.-A Euro. J.* **2006**, 12, 6776.

7. Petzetakis, N.; Walker, D.; Dove, A. P.; O'Reilly, R. K. *Soft Matter* **2012**, 8, 7408.

8. Stewart, S.; Liu, G. *Chemistry of materials* **1999**, 11, 1048.

9. Loeb, S.; Sourirajan, S. *Adv. Chem. Series* **1962**, 38.

10. Sidney, L.; Srinivasa, S. *Sea Water Demineralization by Means of an Osmotic Membrane*. American Chemical Society: **1963**; Vol. 38, 117.

11. Vörösmarty, C. J.; Green, P.; Salisbury, J.; Lammers, R. B. *Science* **2000**, 289, 284.

12. Chai, G.-Y.; Krantz, W. B. *J. Membr. Sci.* **1994**, 93, 175.

13. Petersen, R. J. *J. Mem. Sci.* **1993**, 83, 81.

14. Freger, V. *Langmuir* **2003**, 19, 4791.

15. Jeong, B.-H.; Hoek, E. M.; Yan, Y.; Subramani, A.; Huang, X.; Hurwitz, G.; Ghosh, A. K.; Jawor, A. *J. Membr. Sci.* **2007**, 294, 1.

16. Achilli, A.; Childress, A. E. *Desalination* **2010**, 261, 205.

17. Hirose, M.; Ito, H.; Kamiyama, Y. *J. Membr. Sci.* **1996**, 121, 209.

18. Xu, P.; Drewes, J. E.; Kim, T.-U.; Bellona, C.; Amy, G. *J. Membr. Sci.* **2006**, 279, 165.

19. Lee, S.; Ang, W. S.; Elimelech, M. *Desalination* **2006**, 187, 313.

20. Al-Ahmad, M.; Aleem, F. A.; Mutiri, A.; Ubaisy, A. *Desalination* **2000**, 132, 173.

21. Tessaro, I.; Da Silva, J.; Wada, K. *Desalination* **2005**, 181, 275.

22. Soice, N. P.; Greenberg, A. R.; Krantz, W. B.; Norman, A. D. *J. Membr. Sci.* **2004**, 243, 345.

23. Simon, A.; Nghiem, L. D.; Le-Clech, P.; Khan, S. J.; Drewes, J. E. *J. Mem. Sci.* **2009**, 340, 16.

24. Odian, G. 2004. *Principles of Polymerization*. Wiley.

25. Lee, K. P.; Arnot, T. C.; Mattia, D. . *J. Mem. Sci.* **2011**, 370, 1.

26. Suh, J. *Acc. Chem. Res.* **1992**, 25, 273.

27. Williams, A. *J. Am. Chem. Soc.* **1976**, 98, 5645.

28. Maschmann, M. R.; Franklin, A. D.; Amama, P. B.; Zakharov, D. N.; Stach, E. A.; Sands, T. D.; Fisher, T. S. *Nanotechnology* **2006**, 17, 3925.

29. Lu, Z.; Liu, G.; Phillips, H.; Hill, J. M.; Chang, J.; Kydd, R. A. *Nano letters* **2001**, 1, 683.

30. Mulvenna, R. A.; Prato, R. A.; Phillip, W. A.; Boudouris, B. W. *Macro. Chem. Phys.* **2015**, 216, 1831.

CHAPTER 7. FUTURE WORK

7.1 Overview

First, preliminary work into further exploration of different block polymer systems is presented by changing the chemical thermoplastic backbone architecture of block polymers for membranes by incorporating polyacrylonitrile (PAN). Incorporation of the moieity enables mechanically robust diblocks of PAN-*b*-polyacrylate without the need to synthesize triblock templates. The insertion of a PAN domain enables the system to potentially undergo complementary chemistry with polyacrylate pore wall chemistry for ultimate size and chemistry separation with the PAN support undergoing 'click' chemistry for the additionional capacity of the membrane having tunable membrane antifouling properties for futher enhanced separation of salts.[1, 2] Secondly, the utilization of a network of chemistry selective block-polymer templates are proposed as a potential future project. By the use of a system of parallel and series configurations of memrbranes, a multicomponent separation system with process control may be utilized for intelligent and controllable separation of multiple analytes.

7.2 Introduction of Polyacrylonitrile (PAN) Support Block Polymer Membranes

In industry, the utilization of PAN is commonplace in the creation of ultrafiltration and microfiltration membranes using the phase inversion method for

membrane films.[3] The material is tolerant to mild acidic and basic conditions, where such conditions are used in the clenaning of membranes from fouling (Figure 7.1).[3, 4]

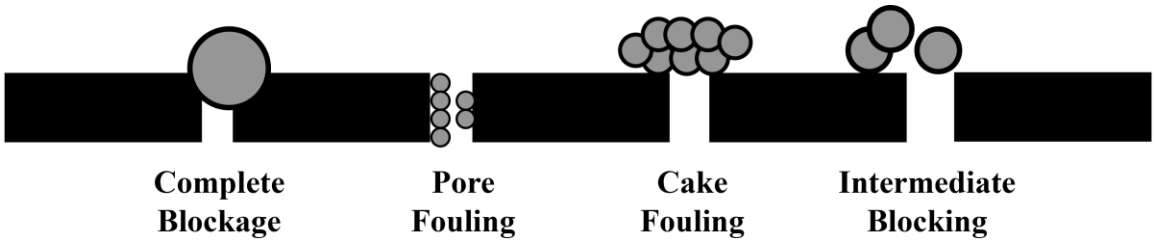

Figure 7.1. Common fouling mechanisms of membranes.[5] Reproduced from Reference 5.

In addition, the mechanical strength of this inexpensive and abundant thermoplastic arises from its low entanglement molecular weight,[6] further making it an ideal material for use in membranes. The mechanically robust thermoplastic PAN enables this material to be used to replace the exisitng PI-*b*-PS diblock thermoplastic elastomer support for more facile diblock block polymer synthesis for low pore sized applications.

Recently, developments of the creation of living polymeriation methods of PAN have enabled the creation of highly tunable molcular weights with low dispersity. In particular, the use of ATRP or RAFT polymerization methods have taken center stage in the creation of PAN-*b*-P(acrylate) polymers.[6-9] By utilizing RAFT polymerization techniques, mechanically robust PAN-*b*-PDMA block polymer systems may be synthesized (Scheme 7.1 and 7.2).

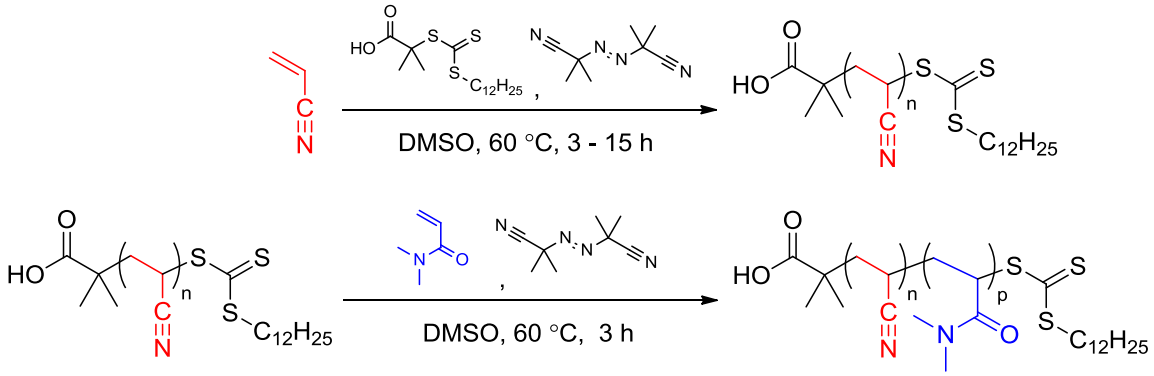

Scheme 7.1. Synthesis scheme of PAN-*b*-PDMA for mechanically robust diblock polymer membranes.

In addition to its mechanical stength, the material is able to undergo chemical transformation. The presence of the cyano group enables the material to undergo chemical transformation by utilizing 'click' chemistry, This synthetic concept, defined by K. B. Sharpless in 2001,[10] are reactions that are chemo and regiospecific with facile and high yielding conversions with limited and easily separable (side) products.[11, 12] As the seminal example that exemplifies this concept, the use of a copper catalyzed 1,3-dipolar addition between an cyano group and a azide is a cornerstone concept of this chemical methodology.[13, 14] With the complementary use of Steglich[15] reaction chemistry of carboxylic acids with complementary click chemsitry of cyano groups,[10] functionalization of the PAN-*b*-Polyacrylate templates may be made to facily tune the pore chemistry and support. More specifically, the use of copper catalyzed 1,3-dipolar addition 'click' chemsitry of the PAN nitrile groups with azide ($-N_3$) terminated R groups enables tunable functionalization of the thermoplastic support for antifouling capabilities,

[16, 17] while the use of one-pot use of Steglich chemsitry enables simultaneous functionalization for targeted analyte purification.

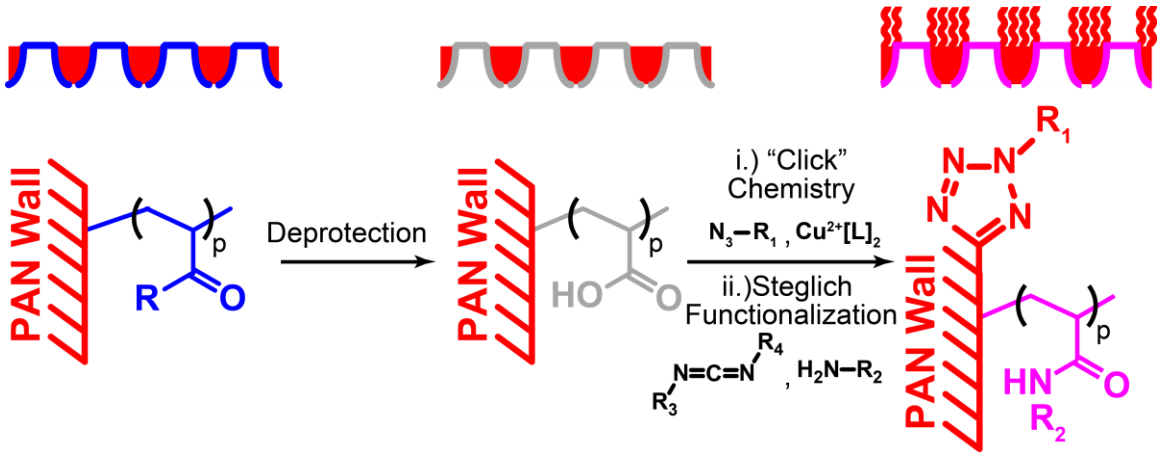

Scheme 7.2. Synthetic scheme for utilizing complimentary 'click' and Steglich chemistry for functionalization of a proposed self assembled PAN-*b*-Polyacrylate membrane for chemistry specific separation of target analytes (R_1) with antifouling coatings (R_2).

In this preliminary work, 6 mL (0.06 mol) of twice basic alumina column purified acrylonitrile was mixed with 14 mL of inhibitor free dimethylsulfoxide (DMSO), 24.3 mg (64.8 µmol) of 2-(dodecylthiocarbonothioylthio)-2-methylpropanoic acid RAFT agent, and 2.13 mg (12.96 µmol) of azobisisobutyronitrile (AIBN) and injected into an air free vessel under argon. Following four freeze pump thaw cycles, the vessel was refilled with argon and stirred under heat at 60 °C for 15 h.. Upon completion of the reaction, the vessel was cooled in a water bath to room temperature and exposed to air. The RAFT terminated PAN was then precipitated from DMSO three times in methanol before washing thoroughly with water and methanol over a Hirsh funnel. The yellow powder was placed in a vacuum over overnight to remove the residue. 18% conversion (gravimetric analysis) 29%, M_n = 18.0 kDa.

The PAN-*b*-PDMA diblock polymer was synthesized through the macroinitiation of the RAFT terminated PAN. Specifically, 0.5 g (27.8 μmol, 18.0 kDa) of PAN-RAFT macroinitiator was mixed with 2.6 mL (0.06 mol) of twice basic alumina column purified *N*,*N*-dimethylacrylamide, 7.9 mL of of inhibitor free dimethylsulfoxide (DMSO), and 0.91 mg (5.5 μmol) of azobisisobutyronitrile (AIBN) in a argon sealed vessel. Upon four freeze-pump-thaw cycles and being refilled with argon under temperature at 60 ºC for 3 h.. Upon completion of the reaction, the vessel was cooled in a water bath to room temperature and exposed to air. The polyacrylonitrile was then precipitated three times in methanol before washing thoroughly with water and methanol over a Hirsh funnel. The yellow powder was placed in a vacuum over overnight to remove the residue. 9% conversion (gravimetric analysis) 9%, M_n = 18.0-8.9 kDa.

As an important prerequisite for complementary functionalization of PAN block polymers, the deprotection conditions must not interfere with the functionality of the PAN support prior to reaction with azide containing R_2 groups for 'click' chemistry functionalization (Scheme 7.2). To test if the deprotection conditions affect the polyacrylonitrile chemistry, PAN homopolymers cast as thin films from DMSO were immersed in acid agents utilized in the deprotection of acrylates to polyacrylic acid previously mentioned in Chapters 3-6 (Figure 7.1). Unfortunately, the use of elevated temperatures in the presence of strong acid hydrolyzes PAN to PAN-*co*-PAA, making the use of PAN-*b*-PDMA block polymers limited in their complementary functionalization capacity for chemistry selectivity and anti fouling properties. However, the use of strong acids (TFA, HCl) at room temperatures for extended periods of time do not hydrolyze PAN to PAA (Figure 7.2)

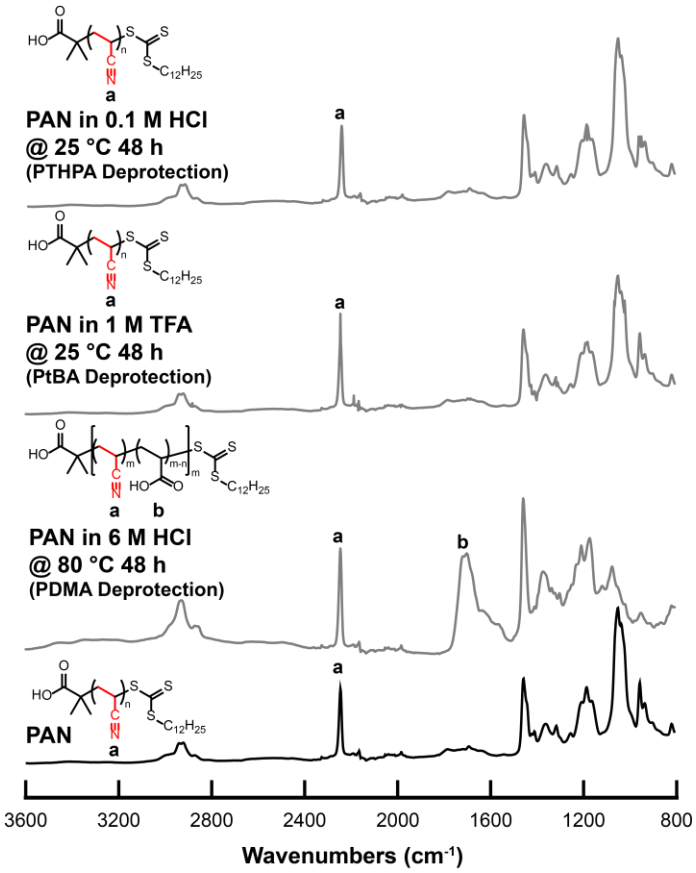

Figure 7.2. ATR-FTIR of PAN films immersed in acidic deprotection conditions of protected acrylates (*i.e.*, poly(*N*,*N*-dimethylacrylamide) (PDMA), poly(*tert*-butyl acrylate) (PtBA), and poly(tetrahydopyran acrylate) PTHPA). The stretch at ~ 2300 cm^{-1} represents the nitrile stretch of PAN. In the required presence of heat for quantitative PDMA deprotection, the emergence of the broad peaks at ~ 1600 cm^{-1} indicate the onset of hydrolysis of PAN to PAA. The coexistence of the nitrile stretch at ~ 2300 cm^{-1} after 48 hours using the PDMA deprotection protocol indicate degradation of PAN to PAN-*co*-PAA. However, in the presence of strong acid at room temperature for the deprotection, no chemical change has occurred. As such, the use of PtBA and PTHPA are viable acrylate block chemistries for selective deprotection to PAA. This allows for subsequent conjugate functionalization of the pore chemistry for targeted separation and functionalization of the PAN support for fouling resistance.

To evaluate the casting performance of PAN-b-Polyacrylate block polymers as films, PAN-*b*-PDMA templates of 18.0-8.9 kDa were dissolved (18 w.t. %) by stirring in a 80/20 DMSO/THF vol. % solution for 72 h. Onto a clean glass microscope substrate, a small volume of the solution was spread onto the surface then cast with a doctor blade (250 μm gate height). The film was then dried in a fumehood for 150 seconds before immersing in a water bath. The resulting film (Figure 7.2) afforded a smooth, flexible and tough film for its low molecular weight (*i.e.* compared to PI-PS-PDMA films of ~40 kDa). Unfortunately, SEM microscopy of the film did not show any indication of self-assembly and non-solvent induced phase separation (SNIPS) at the surface of pores. To facilitate in the creation of block polymer membranes, further optimization of the acrylate solvent selective system (THF in DMSO or dimethylformamide (DMF)) is required for successful self-assembly into size selective pores for high flux anisotropic membrane templates.

7.3 Proposed Networking of Chemistry Selective Block Polymers for Multicomponent Separation

Previously in Chapter 5, successful post modification of PI-PS-PAA block polymer membrane templates were shown by refunctionalizing the PAA pore walls to a vaiety of chemistries for targeted metal salt purification. The work presented in Chapter 5 only considered single and binary separations of components. In industry, mutiple components from an industrial procees are requried to be separated, thus requiring multiple stages utilizing multiple separation techniques.

As these tunable block polymer template films have demonstrated high selectivity and tunability in the separation of analytes, these materials have the potential to be similarly utilized in a multple stage configuration. By combination of multiple separation devices as single process unit, tunable block polymer templates have the potential for exploration into replacing unit operations and multiple separation stages for both targeted capture, separation, retention and multicomponent separation of analytes (Figure 7.3).

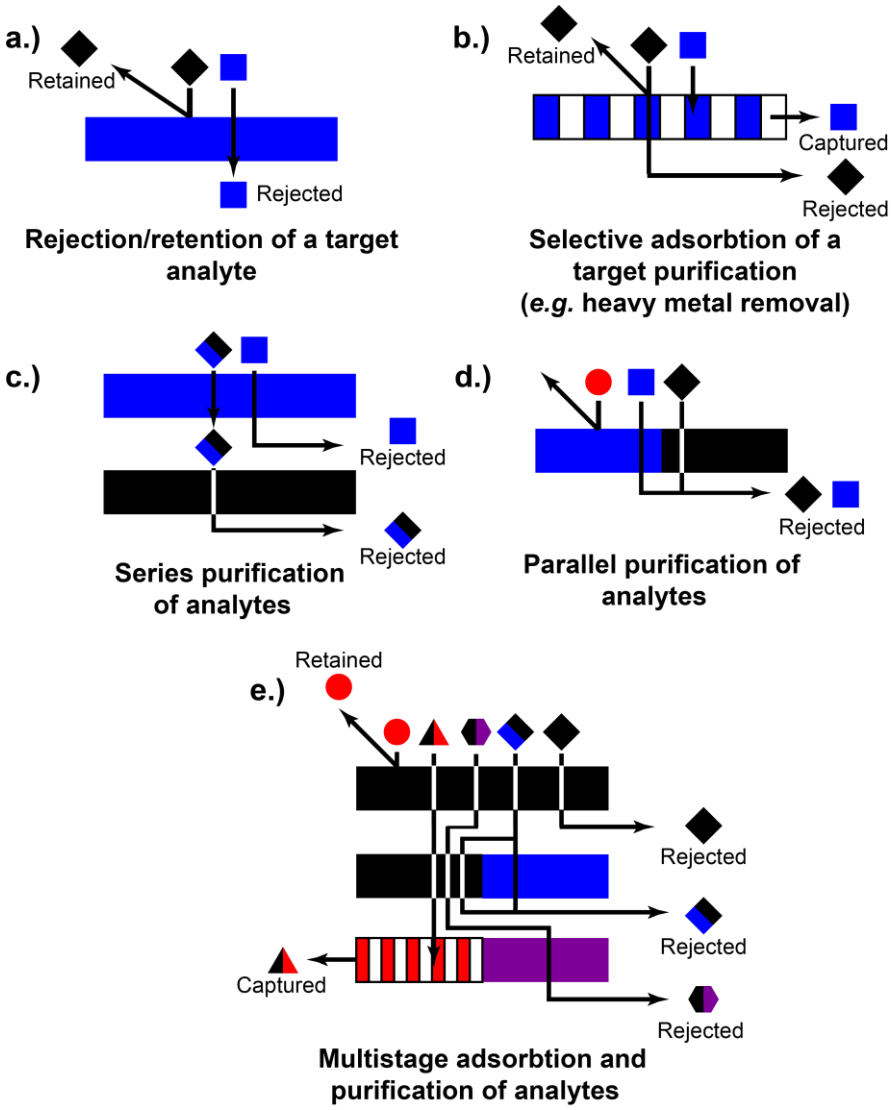

Figure 7.3. Utilizing the (a) (size) rejection (b) absorption configuration of these templates, multiple separation devices may be utilized in (c) series and (d) parallel for (e) multi-component separation and collection of analytes on the basic of size as well as chemistry.

A prime example for the application use of multi-stage purification is in the pharmaceutical industry for the separation of bio-derived products following fermentation from similar bio products. [73, 74 18, 19]Figure 7.4 details a industrial scale

pharmaceutical process for producing a therapeutic protein product. Upon initial cell lysis to final formulation, a bio-product needs to undergo a labyrinth of purification processes resulting in increased cost of the final material.[75-77 20-22] Consolidation of these processes into a size and chemo-specific transporting material would greatly reduce the complexity and cost of purification of target analytes by simple modification of the cast pore size and pore functionality in the post self-assembled state[20, 23-27]

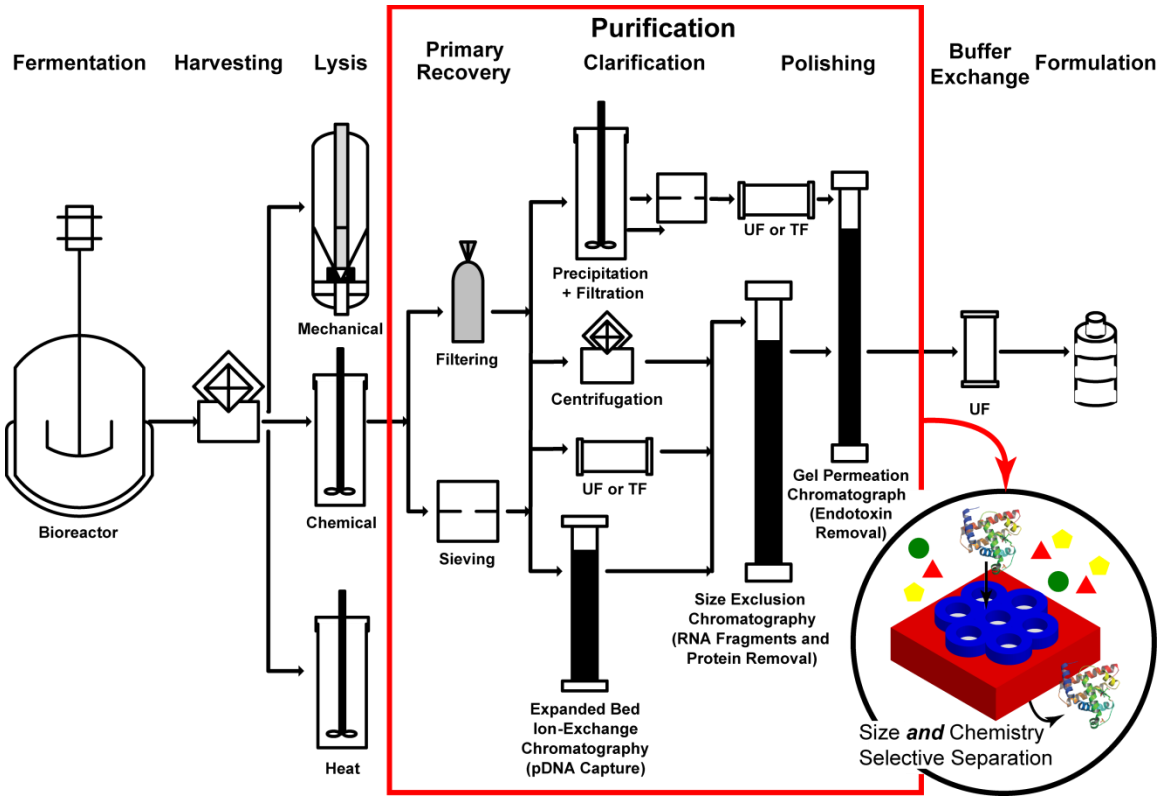

Figure 7.4. Process flow diagram of biomolecule production in the bio-pharmaceutical industry.[28] Figure reproduced from Reference 28. (Inset) Process intensification of the purification process (red box) from a series of selective waste and solvent exchange processes to a multi-component separation system using concerted steps of size and chemistry selective elution is an attractive option to greatly reduce the complexity and cost of purification.

By expansion of the block polymer chemistries available using facile controlled radical polymerization techniques, this work will focus on the new synthetic methods for expanding the use of chemically tunable block polymer materials for diversifying targeted separations of analytes.

7.4 Block Polymer Membranes - Outlook

By modification of existing block polymer membrane material architectures, significant progress has been made in greatly expanding the range of size selective separations towards nanofiltration and RO memrbranes (Chapters 4 and 6). The unique chemistry of this block polymer system has enabled for tunable chemistry of self assembled memrbranes for target capture of salts and the observation RAFT kinetic phenomenon in dilute block polymerization reaction environment. However, these new findings have only glimpsed on a small subset of block polymer chemistries. With further expansion and more thorough exploration of block polymer chemistry, additonal fundamental structure-property relationships and further progress for block polymer separation devices can be made to expand their application for use in industry.

7.5 References

1. Mulvenna, R. A.; Prato, R. A.; Phillip, W. A.; Boudouris, B. W. *Macro. Chem. Phys.* **2015**, 216, 1831.
2. Mulvenna, R. A.; Weidman, J. L.; Jing, B.; Pople, J. A.; Zhu, Y.; Boudouris, B. W.; Phillip, W. A. *J. Membr. Sci.* **2014**, 470, 246.
3. Vrijenhoek, E. M.; Hong, S.; Elimelech, M. *j. Membr. Sci.* **2001**, 188, 115.
4. Field, R.; Wu, D.; Howell, J.; Gupta, B. *J. Membr. Sci.* **1995**, 100, 259.
5. Radjenović, J.; Matošić, M.; Mijatović, I.; Petrović, M.; Barceló, D. *Membrane bioreactor (MBR) as an advanced wastewater treatment technology*. Springer: **2008**; 37.
6. Rangarajan, P.; Yang, J.; Bhanu, V.; Godshall, D.; McGrath, J.; Wilkes, G.; Baird, D. *J. App. Poly. Sci.* **2002**, 85, 69.
7. Dong, H.; Tang, W.; Matyjaszewski, K. *Macromolecules* **2007**, 40, 2974.
8. Tang, C.; Kowalewski, T.; Matyjaszewski, K. *Macromolecules* **2003**, 36, 8587.
9. Cai, J. Y. *US Patent 20,140,271,442,* **2014**.
10. Kolb, H. C.; Finn, M.; Sharpless, K. B. *Angewandte Chemie Int. Eng.* **2001**, 40, 2004.
11. Kolb, H. C.; Sharpless, K. B. *Drug Discovery Today* **2003**, 8, 1128.
12. Wu, P.; Feldman, A. K.; Nugent, A. K.; Hawker, C. J.; Scheel, A.; Voit, B.; Pyun, J.; Frechet, J. M.; Sharpless, K. B.; Fokin, V. V. *Angewandte Chemie Int. Eng.* **2004**, 43, 3928.
13. Huisgen, R. *Angewandte Chemie Int. Eng.* **1963**, 2, 565.
14. Huisgen, R. *Angewandte Chemie Int. Eng.* **1963**, 2, 633.
15. Neises, B.; Steglich, W *Angewandte Chemie Int. Eng.* **1978**, 17, 522.

16. Binder, W. H.; Sachsenhofer, R. *Macromol. Rapid Commun.* **2007**, 28, 15.

17. Tsarevsky, N. V.; Bernaerts, K. V.; Dufour, B.; Du Prez, F. E.; Matyjaszewski, K. *Macromolecules* **2004**, 37, 9308.

18. Berkowitz, S. A.; Engen, J. R.; Mazzeo, J. R.; Jones, G. B. *Nature Rev. Drug Dis.* **2012**, 11, 527.

19. Rzayev, J.; Hillmyer, M. A. *Macromolecules* **2005**, 38, 3.

20. van Reis, R.; Zydney, A. *J. Membr. Sci.* **2007**, 297, 16.

21. Ainsworth, S. J. *Chem. Eng. News* **2005**, 83, 21.

22. Erickson, B. E. *Chem. Eng. News.* **2010**, 88, 25.

23. Roberts, M. W. H.; Ongkudon, C.; Forde;, G. M.; Danquah, M. K. *J. Separation Sci.* **2009**, 32, 2485.

24. Ghose, S.; Forde, G. M.; Slater, N. K. *Biotech. Prog.* **2004**, 20, 841.

25. Han, Y.; Forde, G. M. *J. of Chromat. B* **2008**, 874, 21.

26. Han, Y.; Liu, S.; Ho, J.; Danquah, M. K.; Forde, G. M. *Chem. Eng. Res. Design* **2009**, 87.

27. Danquah, M. K.; Forde, G. M. *Chem. Eng. Res. Design* **2009**, 87, 343.

28. Shamlou, P. A. *Biotechnology and Applied Biochemistry* **2003**, 37, 207.

BIBLIOGRAPHY

BIBLIOGRAPHY

Achilli, A. & A. E. Childress *Desalination* **2010**, 261, *3*, 205-211.

Ainsworth, S. J. *Chem. Eng. News* **2005**, 83, *23*, 21.

Al-Ahmad, M., F. A. Aleem, A. Mutiri & A. Ubaisy *Desalination* **2000**, 132, *1*, 173-179.

Apel, P. *Rad. Meas.* **2001**, 34, 559-566.

Baker, R. W. 2004. *Membrane Technology and Applications*. Chichester ; New York: J. Wiley.

Baker, R. W. & K. Lokhandwala *Ind. Eng. Chem. Res.* **2008**, 47, 2109-2121.

Barner-Kowollik, C. 2008. *Handbook of RAFT Polymerization*. John Wiley & Sons.

Barner-Kowollik, C., M. Buback, B. Charleux, M. L. Coote, M. Drache, T. Fukuda, A. Goto, B. Klumperman, A. B. Lowe, J. B. McLeary, G. Moad, M. J. Monteiro, R. D. Sanderson, M. P. Tonge & P. Vana *J. Polym. Sci., Part A: Polym. Chem.* **2006**, 44, *20*, 5809.

Barner-Kowollik, C., M. L. Coote, T. P. Davis, L. Radom & P. Vana *J. Polym. Sci., Part A: Polym. Chem.* **2003**, 41, *18*, 2828.

Bashir, W. & B. Paull *J. of Chromatog. A* **2002**, 942, *1*, 73-82.

Bates, F. S. *MRS Bulletin* **2005**, 30, 525-532.

Bates, F. S. & G. H. Fredrickson *Physics Today* **1999**, 52, 32-38.

Beman, J. M., K. R. Arrigo & P. A. Matson *Nature* **2005**, 434, *7030*, 211-214.

Berkowitz, S. A., J. R. Engen, J. R. Mazzeo & G. B. Jones *Nature Rev. Drug Dis.* **2012**, 11, 527-540.

Bernardo, P., E. Drioli & G. Golemme *Ind. Eng. Chem. Res.* **2009**, 48, *10*, 4638-4663.

Binder, W. H. & R. Sachsenhofer *Macromolecular Rapid Communications* **2007**, 28, *1*, 15-54.

Bird, B. B., W. E. Stewart & E. N. Lightfoot. 2002. *Transport Phenomena.* New York: John Wiley and Sons.

Bowen, W. R. & M. Hilmi *J. Membr. Sci.* **1996**, 112, 263-274.

Braunecker, W. A. & K. Matyjaszewski *Prog. Polym. Sci.* **2007**, 32, *1*, 93.

Brown, R., A. Bennet & H. Slebocka-Tilk *Acc. Chem. Res.* **1992**, 25, *11*, 481-488.

Buback, M., T. Junkers & P. Vana *Macromol. Rapid Commun.* **2005**, 26, *10*, 796.

Buck, M., M. Grunze, F. Eisert, J. Fischer & F. Träger *J. Vac. Sci. Tech. A* **1992**, 10, *4*, 926-929.

Butun, V., N. C. Billingham & S. P. Armes *Chem. Commun.* **1997**, 671-672.

Cai, J. Y. *US Patent 20,140,271,442*, **2014**.

Calitz, F. M., J. B. McLeary, J. M. McKenzie, M. P. Tonge, B. Klumperman & R. D. Sanderson *Macromolecules* **2003**, 36, *26*, 9687.

Chai, G.-Y. & W. B. Krantz *J. Membr. Sci.* **1994**, 93, *2*, 175-192.

Chernikova, E., V. Golubev, A. Filippov, C. Y. Lin & M. L. Coote *Polym. Chem.* **2010**, 1, *9*, 1437.

Chiefari, J., Y. Chong, F. Ercole, J. Krstina, J. Jeffery, T. P. Le, R. T. Mayadunne, G. F. Meijs, C. L. Moad & G. Moad *Macromolecules* **1998**, 31, *16*, 5559-5562.

Chong, Y. K., T. P. T. Le, G. Moad, E. Rizzardo & S. H. Thang *Macromolecules* **1999**, 32, *6*, 2071.

Claudio, E. S., H. Goldwin & J. S. Magyar *Prog. Inorg. Chem* **2003**, 51, 1-144.

Clodt, J. I., V. Filiz, S. Rangou, K. Buhr, C. Abetz, D. Höche, J. Hahn, A. Jung & V. Abetz *Adv. Funct. Mater.* **2012**, 23, *6*, 731-738.

Cochran, E. W., C. J. Garcia-Cervera & G. H. Fredrickson *Macromolecules* **2006**, 39, 2449.

Coessens, V., T. Pintauer & K. Matyjaszewski *Prog. Polym. Sci.* **2001**, 26, *3*, 337-377.

Coote, M. L. *Macromolecules* **2004**, 37, *13*, 5023.

Coote, M. L. & L. Radom *J. Am. Chem. Soc.* **2003**, 125, *6*, 1490.

Curtin, D. E., Robert D. Lousenberg, Timothy J. Henry, Paul C. Tangeman & Monica E. Tisack *J. Power Sources* **2002**, 131, *1-2*, 41-48.

D. H. Solomon, E. Rizzardo & P. Cacioli *US patent 4,581,429*, **1986**.

Danquah, M. K. & G. M. Forde *Chem. Eng. Res. Design* **2009**, 87, 343-348.

Degennes, P. G. *Macromolecules* **1980**, 13, *5*, 1069-1075.

Dimitrov, D. I., A. Milchev & K. Binder *J. Chem. Phys.* **2006**, 125, 34905.

Dong, H., W. Tang & K. Matyjaszewski *Macromolecules* **2007**, 40, *9*, 2974-2977.

Dorin, R. M., W. A. Phillip, H. Sai, J. Werner, M. Elimelech & U. Wiesner *Polymer* **2014**, 55, *1*, 347-353.

Dorin, R. M., H. Sai & U. Wiesner *Chem. of Mat.* **2014**, 26, 339-347.

Dukes, D., Y. Li, S. Lewis, B. Benicewicz, L. Schadler & S. K. Kumar *Macromolecules* **2010**, 43, 1564-1570.

Erickson, B. E. *Chem. Eng. News.* **2010**, 88, 25-27.

Faraone, A., S. Magazu, G. Maisano, P. Migliardo, E. Tettamanti & V. Villari *J. Chem. Phys.* **1999**, 110, 1801-1806.

Feldermann, A., M. L. Coote, M. H. Stenzel, T. P. Davis & C. Barner-Kowollik *J. Am. Chem. Soc.* **2004**, 126, *48*, 15915.

Field, R., D. Wu, J. Howell & B. Gupta *J. Membr. Sci.* **1995**, 100, *3*, 259-272.

Fissell, W. H., A. Dubnisheva, A. N. Eldridge, A. J. Fleischman, A. L. Zydney & S. Roy *J. Membr. Sci.* **2009**, 326, 58-63.

Flora, S. J. & V. Pachauri *Int. J. Env. Res. Public Health* **2010**, 7, *7*, 2745-2788.

Freger, V. *Langmuir* **2003**, 19, *11*, 4791-4797.

Fritzmann, C., J. Löwenberg, T. Wintgens & T. Melin *Desalination* **2007**, 216, *1*, 1-76.

Fu, F. & Q. Wang *J. Env. Managment* **2011**, 92, *3*, 407-418.

Gaucher, G., M.-H. Dufresne, V. P. Sant, N. Kang, D. Maysinger & J.-C. Leroux *J. Membr. Sci.* **2005**, 109, *1*, 169.

Geise, G. M., H. B. Park, A. C. Sagle, B. D. Freeman & J. E. McGrath *J. Membr. Sci.* **2011**, 369, 130-138.

Gennes, P.-G. d. 1979. *Scaling Concepts in Polymer Physics*. Cornell University.

Germack, D. S., S. Harrisson, G. O. Brown & K. L. Wooley *J. Polym. Sci., Part A: Polym. Chem.* **2006**, 44, *17*, 5218.

Germack, D. S. & K. L. Wooley *J. Polym. Sci., Part A: Polym. Chem.* **2007**, 45, *17*, 4100-4108.

Ghose, S., G. M. Forde & N. K. Slater *Biotech. Prog.* **2004**, 20, 841-850

Ghosh, R. *J. Chromatogr. A* **2002**, 952, *1*, 13-27.

Gody, G., T. Maschmeyer, P. B. Zetterlund & S. Perrier *Macromolecules* **2014**, 47, *10*, 639–649.

Guerrier, B., C. Bouchard, C. Allain & C. Bénard *AlChE J.* **1998**, 44, 791-798.

Gundogan, N., O. Okay & W. Oppermann *Macromol. Chem. Phys.* **2004**, 205, 814-823.

Hadidi, M. & A. L. Zydney *J. Membr. Sci.* **2014**, 452, 97-103.

Hadjichristidis, N., H. Iatrou, S. Pispas & M. Pitsikalis *J. Polym. Sci., Part A: Polym. Chem.* **2000**, 38, *18*, 3211-3234.

Hadjichristidis, N., S. Pispas & G. Floudas. 2002. *Block Copolymers: Synthetic Strategies, Physical Properties, and Applications*. Wiley.

Hahn, J., J. I. Clodt, V. Filiz & V. Abetz *RSC Adv.* **2014**, 4, *20*, 10252.

Hamilton, W. A., G. S. Smith, N. A. Alcantar, J. Majewski, R. G. Toomey & T. L. Kuhl *J. Polym. Sci., Part B: Polym. Phys.* **2004**, 42, 3290-3301.

Hamley, I. 1999. *The Physics of Block Copolymers*. Oxford Science.

Han, J., J. Fu & R. B. Schoch *Lab on a Chip* **2008**, 8, 23-33.

Han, Y. & G. M. Forde *J. of Chromat. B* **2008**, 874, 21-26.

Han, Y., S. Liu, J. Ho, M. K. Danquah & G. M. Forde *Chem. Eng. Res. Design* **2009**, 87.

Hawker, C. J. & K. L. Wooley *Science* **2005**, 309, *5738*, 1200-1205.

Hawthorne, D. G., G. Moad, E. Rizzardo & S. H. Thang *Macromolecules* **1999**, 32, *16*, 5457.

He, Y. & E. L. J. Cussler *J. Membr. Sci.* **1992**, 68.

Hertler, W. R. *US Patent 5,072,029,* **1991**.

Hiemenz, P. C. & T. P. Lodge. 2007. *Polymer Chemistry 2nd ed.*: CRC Press.

Hilal, N., H. Al-Zoubi, N. A. Darwish, A. W. Mohamma & M. A. Arabi *Desalination* **2004**, 170, 281-308.

Hirose, M., H. Ito & Y. Kamiyama *J. Membr. Sci.* **1996**, 121, *2*, 209-215.

Ho, W. S. W. & K. K. Sirkar. 2001. *Membrane Handbook*. Boston: Kluwer Academic Publishing.

Hong, S. & M. Elimelech *J. Membr. Sci.* **1997**, 132, *2*, 159.

Hsieh, H. & R. P. Quirk. 1996. *Anionic polymerization: principles and practical applications*. CRC Press.

Huisgen, R. *Angew. Chem., Int. Ed. Engl.* **1963**, 2, *10*, 565-598.

Humphrey, J. L. & R. Koort. 1991. Separation technologies: Advances and priorities. Humphrey (JL) and Associates, Austin, TX (USA).

Ikkala, O. & G. ten Brinke *Science* **2002**, 295, *5564*, 2407.

Iovu, M. C., C. R. Craley, M. Jeffries-El, A. B. Krankowski, R. Zhang, T. Kowalewski & R. D. McCullough *Macromolecules* **2007**, 40, *14*, 4733.

J. L. Weidman, R. A. Mulvenna, B. W. Boudouris & W. A. Phillip *Langmuir* **2015**, 31, *40*, 11113 - 11123.

Jackson, E. A. & M. A. Hillmyer *ACS Nano* **2010**, 4, *7*, 3548-3553.

Jackson, E. A., Y. Lee & M. A. Hillmyer *Macromolecules* **2013**, 46, *4*, 1484-1491.

Jeong, B.-H., E. M. Hoek, Y. Yan, A. Subramani, X. Huang, G. Hurwitz, A. K. Ghosh & A. Jawor *J. Membr. Sci.* **2007**, 294, *1*, 1-7.

Jeong, B. & A. Gutowska *Trends Biotechnol.* **2002**, 20, *7*, 305.

Jing, B., M. Hutin, E. Connor, L. Cronin & Y. Zhu *Chem. Sci.* **2013**, 4, 2818-3826.

Jitchum, V. & S. Perrier *Macromolecules* **2007**, 40, *5*, 1408-1412.

Jung, A., V. Filiz, S. Rangou, K. Buhr, P. Merten, J. Hahn, J. Clodt, C. Abetz & V. Abetz *Macromol. Rapid Commun.* **2013**, 34, *7*, 610-615.

Jung, A., S. Rangou, C. Abetz, V. Filiz & V. Abetz *Macromol. Mater. Eng.* **2012**, 297, *8*, 790-798.

Junkers, T., C. Barner-Kowollik & M. L. Coote *Macromol. Rapid Commun.* **2011**, 32, *23*, 1891.

Junkers, T., G. Delaittre, R. Chapman, F. Günzler, E. Chernikova & C. Barner-Kowollik *Macromol. Rapid Commun.* **2012**, 33, *11*, 984-990.

Karniadakis, G. & S. Sherwin. 2013. *Spectral/HP Element Methods for Computational Fluid Dynamics*. Oxford University Press.

Khandpur, A. K., S. Foerster, F. S. Bates, I. W. Hamley, A. J. Ryan, W. Bras, K. Almdal & K. Mortensen *Macromolecules* **1995**, 28, *26*, 8796-8806.

Kim, E., H. Ahn, S. Park, H. Lee, M. Lee, S. Lee, T. Kim, E.-A. Kwak, J. H. Lee, X. Lei, J. Huh, J. Bang, B. Lee & D. Y. Ryu *ACS Nano* **2013**, 7, *3*, 1952.

Kim, H., S. Park & W. D. Hinsberg *Chem. Rev.* **2009**, 110, *1*, 146.

Kolb, H. C., M. Finn & K. B. Sharpless *Angew. Chem., Int. Ed. Engl.*, **2001**, 40, *11*, 2004-2021.

Kolb, H. C. & K. B. Sharpless *Drug Discovery Today* **2003**, 8, *24*, 1128-1137.

Konkolewicz, D., B. S. Hawkett, A. Gray-Weale & S. Perrier *Macromolecules* **2008**, 41, *17*, 6400.

Konkolewicz, D., B. S. Hawkett, A. Gray-Weale & S. Perrier *J. Polym. Sci., Part A: Polym. Chem.* **2009**, 47, *14*, 3455.

Kwak, Y., A. Goto & T. Fukuda *Macromolecules* **2004**, 37, *4*, 1219.

Lee, K. P., T. C. Arnot & D. Mattia *J. Membr. Sci.* **2011**, 370, *1–2*, 1.

Lee, S., W. S. Ang & M. Elimelech *Desalination* **2006**, 187, *1*, 313-321.

Leibler, L. *Macromolecules* **1980**, 13, *6*, 1602-1617.

Li, M. & C. K. Ober *Materials Today* **2006**, 9, *9*, 30-39.

Lind, M. L., A. K. Ghosh, A. Jawor, X. F. Huang, W. Hou, Y. Yang & E. M. V. Hoek *Langmuir* **2009**, 25, *17*, 10139-10145.

Liu, J., T. Xu & Y. Fu *J. Membr. Sci.* **2005**, 252, *1*, 165-173.

Lodge, T. P. *Macromolecular Chem. Phys.* **2003**, 204, *2*, 265-273.

Loeb, S. & S. Sourirajan *Adv. Chem. Series* **1962**, 38, 117-132.

Lu, Z., G. Liu, H. Phillips, J. M. Hill, J. Chang & R. A. Kydd *Nano Lett.* **2001**, 1, *12*, 683-687.

Mackie, J. & P. Meares. 1955. The diffusion of electrolytes in a cation-exchange resin membrane. I. Theoretical. In *Proc. of Royal Society of London A: Math., Physical and Eng. Sci.*, 498-509. The Royal Society.

Marques, D. S., U. Vainio, N. M. Chaparro, V. M. Calo, A. R. Bezahd, J. W. Pitera, K.-V. Peinemann & S. P. Nunes *Soft Matter* **2013**, 9, *23*, 5557-5564.

Marshall, A., P. Munro & G. Trägårdh *Desalination* **1993**, 91, *1*, 65.

Maschmann, M. R., A. D. Franklin, P. B. Amama, D. N. Zakharov, E. A. Stach, T. D. Sands & T. S. Fisher *Nanotechnology* **2006**, 17, *15*, 3925.

Mastroianni, S. E. & T. H. Epps *Langmuir* **2013**, 29, *12*, 3864-3878.

Matsen, M. & F. S. Bates *Macromolecules* **1996**, 29, *4*, 1091-1098.

Matyjaszewski, K. *Macromolecules* **2012**, 45, *10*, 4015-4039.

Matyjaszewski, K. & J. Xia *Chem. Rev.* **2001**, 101, *9*, 2921-2990.

Mayadunne, R. T., E. Rizzardo, J. Chiefari, Y. K. Chong, G. Moad & S. H. Thang *Macromolecules* **1999**, 32, *21*, 6977.

McLeary, J., F. Calitz, J. McKenzie, M. Tonge, R. Sanderson & B. Klumperman *Macromolecules* **2004**, 37, *7*, 2383.

Mehta, A. & A. L. Zydney *J. Membr. Sci.* **2005**, 249, 245-249.

Meireles, M., A. Bessieres, I. Rogissart, P. Aimar & V. Sanchez *J. Membr. Sci.* **1995**, 103, 105-115.

Mika, A. M., R. F. Childs, M. West & J. N. A. Lott *J. Membr. Sci.* **1997**, 136, 221-232.

Miller, S. J., W. J. Koros & D. Q. Vu *Catalysis* **2007**, 170B, 1590-1596.

Millipore, E. 2012. Millipore Express® PLUS Membrane Filters Catalogue. EMD Millipore: Millipore.

Mimoune, S., R. E. Belazzougui & F. Amrani *Desalination* **2007**, 217, 251-259.

Moad, G. *Macromol. Chem. Phys.* **2014**, 215, *1*, 9.

Moad, G., M. Chen, M. Haussler, A. Postma, E. Rizzardo & S. H. Thang *Polym. Chem.* **2011**, 2, *3*, 492.

Moad, G., E. Rizzardo & S. H. Thang *Aust. J. Chem.* **2006**, 59, *10*, 669.

Moad, G., E. Rizzardo & S. H. Thang *Polymer* **2008**, 49, *5*, 1079-1131.

Moad, G., E. Rizzardo & S. H. Thang *Aust. J. Chem.* **2009**, 62, *11*, 1402-1472.

Moad, G. & D. H. Solomon. 2006. *The Chemistry of Radical Polymerization*. Elsevier.

Monier, M. & D. Abdel-Latif *J. of Hazard. Mat.* **2012**, 209, 240-249.

Monteiro, M. J. *J. Chem. Phys.* **2005**, 43, *22*, 5643-5651.

Monteiro, M. J. & H. de Brouwer *Macromolecules* **2001**, 34, *3*, 349.

Mulvenna, R. A., R. A. Prato, W. A. Phillip & B. W. Boudouris *Macro. Chem. Phys.* **2015**, 216, *17*, 1831-1840.

Mulvenna, R. A., J. L. Weidman, B. Jing, J. A. Pople, Y. Zhu, B. W. Boudouris & W. A. Phillip *J. Membr. Sci.* **2014**, 470, 246.

Nakayama, M., M. Chikuma, H. Tanaka & T. Tanaka *Talanta* **1983**, 30, *7*, 455-458.

Neises, B. & W. Steglich *Angew. Chem., Int. Ed. Engl.* **1978**, 17, *7*, 522-524.

Nunes, S. P., A. R. Behzad, B. Hooghan, R. Sougrat, M. Karunakaran, N. Pradeep, U. Vainio & K. V. Peinemann *ACS Nano* **2011**, 5, *5*, 3516-3522.

O'Reilly, R. K., M. J. Joralemon, C. J. Hawker & K. L. Wooley *Chem.-A Euro. J.* **2006**, 12, *26*, 6776-6786.

Odian, G. 2004. *Principles of Polymerization*. Wiley.

Oh, J. K., R. Drumright, D. J. Siegwart & K. Matyjaszewski *Prog. Polym. Sci.* **2008**, 33, *4*, 448.

Oliver, S. P., B. M. Jayarao & R. A. Almeida *Foodbourne Pathogens & Disease* **2005**, 2, *2*, 115-129.

Oss-Ronen, L., J. Schmidt, V. Abetz, A. Radulescu, Y. Cohen & Y. Talmon *Macromolecules* **2012**, 45, 9631-9642.

Peinemann, K.-V., V. Abetz & P. F. W. Simon *Nat. Mater.* **2007**, 6, *12*, 992-996.

Peinemann, K. V., V. Abetz & P. F. W. Simon *Nature Mat.* **2007**, 6, 992-996.

Pendergast, M. T. M., R. M. Dorin, W. A. Phillip, U. Wiesner & E. M. V. Hoek *J. Membr. Sci.* **2013**, 444, *0*, 461-468.

Pepy, G., P. Boesecke, A. Kuklin, E. Manceau, B. Schiedt, Z. Siwy, M. Toulemondeg & C. Trautmanne *J. App. Crystal.* **2007**, 40, 388-392.

Perrier, S., C. Barner-Kowollik, J. F. Quinn, P. Vana & T. P. Davis *Macromolecules* **2002**, 35, *22*, 8300.

Petersen, R. J. *J. Membr. Sci.* **1993**, 83, *1*, 81.

Petzetakis, N., A. P. Dove & R. K. O'Reilly *Chemical Science* **2011**, 2, *5*, 955-960.

Petzetakis, N., D. Walker, A. P. Dove & R. K. O'Reilly *Soft Matter* **2012**, 8, *28*, 7408-7414.

Phillip, W. A., R. M. Dorin, J. Werner, E. M. V. Hoek, U. Wiesner & M. Elimelech *Nano Lett.* **2011**, 11, 2892-2900.

Phillip, W. A., M. A. Hillmyer & E. L. Cussler *Macromolecules* **2010**, 43, 7763-7770.

Phillip, W. A., B. O'Neill, M. Rodwogin, M. A. Hillmyer & E. L. Cussler *ACS Appl. Mater. Interfaces* **2010**, 2, *3*, 847-853.

Phillip, W. A., J. Rzayev, M. A. Hillmyer & E. L. Cussler *J. Membr. Sci.* **2006**, 286, *1-2*, 144-152.

Pieracci, J., J. V. Crivello & G. Belfort *J. Membr. Sci.* **2002**, 202, 1-16.

Qiu, X., H. Yu, M. Karunakaran, N. Pradeep, S. P. Nunes & K.-V. Peinemann *ACS Nano* **2012**, 7, *1*, 768.

Querelle, S. E., E. A. Jackson, E. L. Cussler & M. A. Hillmyer *ACS Appl. Mater. Interfaces* **2013**, 5, *11*, 5044-5050.

Radjenović, J., M. Matošić, I. Mijatović, M. Petrović & D. Barceló. 2008. *Membrane bioreactor (MBR) as an advanced wastewater treatment technology*. Springer.

Rangarajan, P., J. Yang, V. Bhanu, D. Godshall, J. McGrath, G. Wilkes & D. Baird *J. App. Poly. Sci.* **2002**, 85, *1*, 69-83.

Ranieri, K., G. Delaittre, C. Barner-Kowollik & T. Junkers *Macromol. Rapid Commun.* **2014**, 35, *23*, 2023.

Rautenbach, R. & A. Gröschl *Desalination* **1990**, 77, 73-84.

Ravanchi, M. T., T. Kaghazchi & A. Kargari *Desalination* **2009**, 235, *1*, 199-244.

Rizzardo, E. & D. H. Solomon *Aust. J. Chem.* **2012**, 65, 945.

Roberts, M. W. H., C. Ongkudon, G. M. Forde; & M. K. Danquah *J. Separation Sci.* **2009**, 32, 2485-2494.

Rostro, L., A. G. Baradwaj & B. W. Boudouris *ACS Appl. Mater. Interfaces* **2013**, 5, *20*, 9896.

Runge, M. B. & N. B. Bowden *J. Am. Chem. Soc.* **2007**, 129, *34*, 10551.

Rzayev, J. & M. A. Hillmyer *J. Am. Chem. Soc.* **2005**, 127, 13373.

Rzayev, J. & M. A. Hillmyer *Macromolecules* **2005**, 38, 3-5.

Rzayev, J. & J. Penelle *Angewandte Chemie* **2004**, 116, *13*, 1723.

Schilli, C., M. G. Lanzendörfer & A. H. Müller *Macromolecules* **2002**, 35, *18*, 6819.

Segalman, R. A. *Mater. Sci. Eng., R* **2005**, 48, *6*, 191.

Semsarilar, M. & S. Perrier *Nat. Chem.* **2010**, 2, *10*, 811.

Shamlou, P. A. *Biotechnology and Applied Biochemistry* **2003**, 37, 207-218.

Shannon, M. A., P. W. Bohn, M. Elimelech, J. G. Georgiadis, B. J. Marinas & A. M. Mayes *Nature* **2008**, 452, *7185*, 301.

Sheehan, J. C. & P. A. Cruickshank *Organic Syntheses* **1968**, 83-83.

Shefelbine, T. A., M. E. Vigild, M. W. Matsen, M. A. H. D. A. Hajduk, E. L. Cussler & F. S. Bates *J. Am. Chem. Soc.* **1999**, 121, 8457-8465.

Shinde, M. H., S. S. Kulkarni, D. A. Musale & S. G. Joshi *J. Membr. Sci.* **1999**, 162, 9-22.

Sidney, L. & S. Srinivasa. 1963. *Sea Water Demineralization by Means of an Osmotic Membrane*. American Chemical Society.

Simon, A., L. D. Nghiem, P. Le-Clech, S. J. Khan & J. E. Drewes *J. Membr. Sci.* **2009**, 340, *1*, 16-25.

Smolders, C. A., A. J. Reuvers, R. M. Boom & I. M. Wienk *J. Membr. Sci.* **1992**, 73, 259-275.

Soice, N. P., A. R. Greenberg, W. B. Krantz & A. D. Norman *J. Membr. Sci.* **2004**, 243, *1*, 345-355.

Song Zhao, X., G. Q. Lu & X. Hu *Chem. Commun.* **1999**, *15*, 1391-1392.

Spohr, R. *Rad. Meas.* **2005**, 40, *2*, 191-292.

Stenzel, M. H. *Chem. Commun.* **2008**, *30*, 3486-3503.

Stewart, S. & G. Liu *Chemistry of materials* **1999**, 11, *4*, 1048-1054.

Suh, J. *Acc. Chem. Res.* **1992**, 25, *7*, 273-279.

Szwarc, M. *Nature* **1956**, 178, 1168.

Szwarc, M. 1983. *Living polymers and mechanisms of anionic polymerization*. Springer.

Szwarc, M., M. Levy & R. Milkovich *J. Am. Chem. Soc.* **1956**, 78, *11*, 2656.

Tanco, M. A. L., D. A. P. Tanaka, V. C. Flores, T. Nagase & T. M. Suzuki *React. Funct. Poly.* **2002**, 53, *2*, 91-101.

Tang, C., T. Kowalewski & K. Matyjaszewski *Macromolecules* **2003**, 36, *23*, 8587-8589.

Tang, C., E. M. Lennon, G. H. Fredrickson, E. J. Kramer & C. J. Hawker *Science* **2008**, 322, *5900*, 429-432.

Tessaro, I., J. Da Silva & K. Wada *Desalination* **2005**, 181, *1*, 275-282.

Ting, S. R. S., T. P. Davis & P. B. Zetterlund *Macromolecules* **2011**, 44, *11*, 4187.

Tsarevsky, N. V., K. V. Bernaerts, B. Dufour, F. E. Du Prez & K. Matyjaszewski *Macromolecules* **2004**, 37, *25*, 9308-9313.

van den Dungen, E. T. A., H. Matahwa, J. B. McLeary, R. D. Sanderson & B. Klumperman *J. Polym. Sci., Part A: Polym. Chem.* **2008**, 46, *7*, 2500.

van Reis, R. & A. Zydney *J. Membr. Sci.* **2007**, 297, *1-2*, 16-50.

Vana, P. 2007. Kinetic aspects of RAFT polymerization. In *Macromol. Symp.*, 71. Wiley Online Library.

Vana, P., T. P. Davis & C. Barner-Kowollik *Macromol. Theory Simul.* **2002**, 11, *8*, 823.

Vörösmarty, C. J., P. Green, J. Salisbury & R. B. Lammers *Science* **2000**, 289, *5477*, 284-288.

Vrijenhoek, E. M., S. Hong & M. Elimelech *j. Membr. Sci.* **2001**, 188, *1*, 115-128.

Wang, J.-S. & K. Matyjaszewski *J. Am. Chem. Soc.* **1995**, 117, *20*, 5614-5615.

Warkiani, M. E., A. A. S. Bhagat, B. L. Khoo, J. Han, C. T. Lim, H. Q. Gong & A. G. Fane *ACS Nano* **2013**, 7, 1882-1904.

Wickramasinghe, S. R., E. D. Stump, D. L. Grzenia, S. M. Husson & J. Pellegrino *J. Membr. Sci.* **2010**, 365, 160-169.

Williams, A. *J. Am. Chem. Soc.* **1976**, 98, *18*, 5645-5651.

Wu, P., A. K. Feldman, A. K. Nugent, C. J. Hawker, A. Scheel, B. Voit, J. Pyun, J. M. Frechet, K. B. Sharpless & V. V. Fokin *Angew. Chem., Int. Ed. Engl.*, **2004**, 43, *30*, 3928-3932.

Wulkow, M. *Macromol. Theory Simul.* **1996**, 5, *3*, 393.

Wulkow, M., M. Busch, T. P. Davis & C. Barner-Kowollik *J. Polym. Sci., Part A: Polym. Chem.* **2004**, 42, *6*, 1441.

Xu, P., J. E. Drewes, T.-U. Kim, C. Bellona & G. Amy *J. Membr. Sci.* **2006**, 279, *1*, 165-175.

Yang, H., Z. Xu, M. Fan, R. Gupta, R. B. Slimane, A. E. Bland & I. Wright *J. Enviro. Sci.* **2008**, 20, *1*, 14-27.

Yang, S. Y., J. Park, J. Yoon, M. Ree, S. K. Jang & J. K. Kim *Adv. Funct. Mater.* **2008**, 18, *9*, 1371-1377.

Yang, S. Y., I. Ryu, H. Y. Kim, J. K. Kim, S. K. Jang & T. P. Russell *Adv. Mat.* **2006**, 18, *6*, 709-712.

Yang, S. Y., S. Son, S. Jang, K. H., G. Jeon, W. J. Kim & J. K. Kim *Nano Lett.* **2011**, 11, 1032-1035.

Yoon, J., W. Lee & E. L. Thomas *Adv. Mat.* **2006**, 18, *20*, 2691.

York, A. W., S. E. Kirkland & C. L. McCormick *Adv. Drug Delivery Rev.* **2008**, 60, *9*, 1018.

Yu, K. & A. Eisenberg *Macromolecules* **1998**, 31, *11*, 3509-3518.

Zeman, L. & M. Wales *Sep. Sci. Technol.* **1981**, 16, 275-290.

Zeman, L. J. & A. L. Zydney. 1996. *Microfiltration and Ultrafiltration: Principles and Applications.* New York: Marcel Dekker Inc.

Zetterlund, P. B., G. Gody & S. Perrier *Macromol. Theory Simul.* **2014**, 23, *5*, 331.

Zhang, L. & A. Eisenberg *Science* **1995**, 268, *5218*, 1728-1731.

Zhang, W., L. Shi, Y. An, K. Wu, L. Gao, Z. Liu, R. Ma, Q. Meng, C. Zhao & B. He *Macromolecules* **2004**, 37, 2924-2929.

Zhang, Y., J. L. Sargent, B. W. Boudouris & W. A. Phillip *J. Appl. Polym. Sci.* **2015**, 132, *21*, 41683.

Zhu, L., S. Z. Cheng, P. Huang, Q. Ge, R. P. Quirk, E. L. Thomas, B. Lotz, B. S. Hsiao, F. Yeh & L. Liu *Adv. Mat.* **2002**, 14, *1*, 31-34.

Zhu, L., P. Huang, W. Y. Chen, Q. Ge, R. P. Quirk, S. Z. Cheng, E. L. Thomas, B. Lotz, B. S. Hsiao & F. Yeh *Macromolecules* **2002**, 35, *9*, 3553-3562.

Zydney, A. L. 2011. *High Performance Ultrafiltration Membranes: Pore Geometry and Charge Effects.* Amsterdam: Elsevier.

APPENDIX

APPENDIX

The material in Chapter 3 was originally published in Macromolecular Chemistry and Physics as:

"Polymerization Rate Considerations for High Molecular Weight Polyisoprene-b-Polystyrene-b-Poly(N,N-dimethylacrylamide) Triblock Polymers Synthesized Via Sequential Reversible Addition-Fragmentation Chain Transfer (RAFT) Reactions", by Ryan A. Mulvenna, Rafael A. Prato, William A. Phillip, Bryan W. Boudouris, Macromol. Chem. Phys. 2015, 216, 1831−1840.

Wiley guidelines for permissions and reprints for use in a dissertation are detailed at wqw.wiley.com/WileyCDA/Section/id-403426.html, where permission may be granted through RightsLink®, as per the recommendation of this site. A copy for the use of this publication for using RightsLink® has previously been submitted to the Purdue Graduate school for record.

The material in Chapter 4 was originally published in the Journal of Membrane Science as:

"Tunable Nanoporous Membranes with Chemically-Tailored Pore Walls from Triblock Polymer Templates", by Ryan A. Mulvenna, Jacob L. Weidman, Benxin Jing, John A. Pople, Yingxi Zhu, Bryan W. Boudouris and William A. Phillip, J. Membr. Sci. 2014, 470, 246–256.

Elsevier guidelines for permissions and reprints for use in a dissertation are at https://www.elsevier.com/about/companyinformation/policies/copyright/permissons#SD, where permission may be granted through RightsLink®, as per the recommendation of this site. A copy for the use of this publication for using RightsLink® has been submitted to the Purdue Graduate school for record.

VITA

VITA

Ryan Andrew Mulvenna was born in Frankston, Victoria, Australia. He completed a double degree from Monash University as a Bachelor Science (Chemistry and Applied Mathematics, both as First Class Honors) in 2009 and as a Bachelor of Chemical Engineering (First Class Honors) in 2010. Following graduation, Ryan entered the Graduate School at Purdue University in August 2011.